Novel Thermodynamic Cycles involving Ferrofluids displaying Temporary Magnetic Remanence

R. O. Cornwall MSc(Lon) BSc(UMIST) AMInstP MIET
School of Engineering and Material Science
Queen Mary, University of London
May 2013

Abstract

The objective of the research is to utilise the massive amount of low grade heat energy, for instance which exists in the worlds oceans, by a new type of magnetic cycle. Developed herein are methods based on 2nd order phase changes that make it possible to achieve high efficiency despite small temperature differences with the reservoir. Ferrofluids displaying temporary magnetic remanence are an almost perfect embodiment of the working substance for these cycles. Standard Kinetic Theory, Thermodynamic and Electrodynamic analysis validates the new cycle. Experiment, both physical and by numerical solution have laid the foundations for this work showing: that a property of the system is a strong function of temperature, that a temporary independent flux remains after magnetisation and that a cancellation scheme is required to achieve energy transduction in excess of the magnetisation energy input. This research shows that a new type of heat engine/refrigerator/heat pump is possible.

Foreword and Acknowledgments

Many thanks to Professor Peter Dobson of the University of Oxford Engineering Department for his moral support and diplomacy through all the years that this project has germinated and come to fruition.

I am indebted to my supervisor Professor Dongsheng Wen and indirectly, Professor Theo Alexander of Queen Mary University of London (QMUL), Materials Science and Engineering Department. They gave the bulk of important thermodynamic criticism of my work (T-S diagrams) leading me to seal the arguments and define the subject, whilst allowing a fair amount of "hands-off" guidance that gave me time to think and develop my own ideas.

I wish to thank Richard Balding who as a business angel has kept me in clover through the difficult years of the inception of this and other projects. His input not only provided a stipend but initially paid for materials, experiments and the intellectual property for the project. It was because of his foresight that this (and other) projects survived. Richard has also been a stalwart friend.

Also I thank Andrea Mica who introduced me to Professor Peter Dobson. I'd like to thank Andrea Mica again and his wife Vanda who've often played the role of confidant.

Martin Colborne as business manager originally introduced me to Richard and has also found other sources of funding. Martin too has been a stalwart friend and has managed to shield me from most of the more boring aspects of business management.

Finally I'd like to thank mine and everyone's parents, without whose fundamental contributions, no project would ever be initiated.

Table of Contents

(The method of citing references in this document is to use square brackets with the number of the reference.)

Table of Figures

Table of Important Equations or Concepts

Notation

Vectors are in **bold** (**B**, **E**)

Differentials as: $\dfrac{dy}{dx}$, partial differentials as $\dfrac{\partial y}{\partial x}$ and $\left(\dfrac{\partial y}{\partial x}\right)_{a,b,c}$ when quantities held constant

Differentiation w.r.t time, e.g. $\dot{\theta}$ or $\theta' = \dfrac{d\theta}{dt}$

Divergence: $div = \nabla \cdot$

Infinitesimal circulation: $curl = \nabla \times$

Laplacian: ∇^2

Integral around a closed path e.g. $\oint F(x,y)\,dl$

"Defined as equal to": $\triangleq$
"Approximately equal to": $\approx$

Quantity	Symbol	Name/approximate value, defined value or definition	Common Unit	SI base
Angle	θ	degree, radian	degree, radian	degree, radian
Area	A			m^2
Boltzmann's constant	k, k_B	$\approx 1.381 \times 10^{-23}$	$J\ K^{-1}$	$kg\ m^2\ s^{-2}\ K^{-1}$
Fundamental Charge	e	$\approx 1.602 \times 10^{-19}$	Coulomb (C)	C
Charge	Q	Coulomb	Coulomb	C
Electrical Capacitance	C	$Q = \dfrac{C}{V}$, $i = C\dfrac{dV}{dt}$ Farad	Farad $C\ V^{-1}$	$kg^{-1}\ m^{-2}\ s^4\ A^2$
Charge density	ρ, ρ_E	$Q = \int \rho\,dV$	$C\ m^{-3}$	$C\ m^{-3}$
Density	ρ		$kg\ m^{-3}$	$kg\ m^{-3}$
Efficiency	η			1
Electrical Current	I, i	$i = \dfrac{dQ}{dt}$ Ampere	A	A
Electrical Current Density	**j**	$I = \int \mathbf{j}\cdot\mathbf{dA}$	$A\ m^{-2}$	$A\ m^{-2}$
Electric Field Strength	**E**	$\mathbf{E} = \dfrac{\mathbf{F}}{Q} = -grad(V)$	V/m	$A^{-1}\ kg\ m\ s^{-3}$
Energy,Work, internal energy, (specific energy)[†], (energy, work density)[‡]	E, U, (u)[†], W, (u, w)[‡]	Joules(J) $\triangleq 10^7\,erg$ (J/kg)[†], (J/m³)[‡]	Joule(J) (J/kg)[†], (J/m³)[‡]	$kg\ m^2\ s^{-2}$ $(m^2\ s^{-2})$[†] $(kg\ m^{-1}\ s^{-2})$[‡]
Entropy, (specific entropy)	S, (s)	$\delta Q = T\,dS$ $\delta q = T\,ds$	$J\ K^{-1}\ (kg^{-1})$	$(kg)\ m^2\ s^{-2}\ K^{-1}$
Heat, (specific heat)	Q, (q)		Joules, (J/kg)	$(kg)\ m^2\ s^{-2}$
Heat capacity (specific.)	$C_x\ c_x$	$\left(\dfrac{\partial Q}{\partial T}\right)_x, T\left(\dfrac{\partial S}{\partial T}\right)_x$ $\left\{\left(\dfrac{\partial q}{\partial T}\right)_x, T\left(\dfrac{\partial s}{\partial T}\right)_x\right\}$	Joules/Kelvin (J/K/kg)	$(kg)\ m^2\ s^{-2}\ K^{-1}$
Electrical Inductance	L	$L = \dfrac{\lambda}{i}$, $V = -L\dfrac{di}{dt}$	Henries $V\ A^{-1}\ s$	$A^{-2}\ kg\ m^2\ s^{-2}$
Electrical Impedance	Ω		Ohm $V\ A^{-1}$	$m^2\ kg\ s^{-3}\ A^{-2}$

Electric Permittivity of free space	ε_0	Farad m^{-1} $\approx 8.854 \times 10^{-12}$	F m^{-1}	A^2 kg^{-1} m^{-3} s^4
Magnetic "Charge"	q_m	$q_m = -\oint_S \mathbf{M} \cdot \mathbf{dA}$	A m	A m
Magnetic Field Density	**B**	$\mathbf{F} = Q\mathbf{v} \times \mathbf{B}$ Tesla(T)	Tesla(T), Vs m^{-2} $1\,T \triangleq 10,000\,\text{Gauss(G)}$ $\approx 796,000$ A/m	A^{-1} kg s^{-2}
Magnetic Field Strength	**H**	$\mathbf{B} = \mu_0 \mu_r \mathbf{H}$ A m^{-1}	A m^{-1} $1\,T \triangleq 10,000\,\text{Oersted(Oe)}$ $\approx 796,000$ A/m	A m^{-1}
Magnetic Flux (flux linkage)	Φ, λ	$\Phi = \int \mathbf{B} \cdot d\mathbf{A}$ $\lambda = n\Phi$ Weber(Wb)	Weber(Wb), Vs	A^{-1} kg m^2 s^{-2}
Magnetic Moment	$\mathscr{M}$	$E = \mathscr{M} \cdot \mathbf{B}$ $\mathscr{M} = \mathbf{M}V$ $\mathscr{M} = \int I d\mathbf{A}$ $\mathscr{M} = q_m \mathbf{d}$	J/T, A m^2 (T m^3)	A m^2 (A^{-1} kg m^3 s^{-2})
Magnetisation (Magnetic moment per unit volume)	**M**	$\mathbf{M} = \dfrac{\mathbf{B}}{\mu_0} - \mathbf{H}$	A m^{-1}	A m^{-1}
Magnetic Permeability of free space	μ_0	Henries m^{-1} $\approx 4\pi \times 10^{-7}$	Henries m^{-1}	A^{-2} kg m s^{-2}
Magnetic Relative Permeability	μ_r	$\mu_r = \chi + 1$		1
Bohr Magneton	μ_B	$\mu_B = \dfrac{e\hbar}{2m_e}$ $\approx 9.274 \times 10^{-24}\,\text{JT}^{-1}$	J/T, A m^2	A m^2
Electron Rest Mass	m_e	$m_e \approx 9.109 \times 10^{-31}$ kg	kg	kg
Planck's Constant	$h, \hbar$	$h \approx 6.626 \times 10^{-34}\,\text{Js}$ $\hbar = h/2\pi$	J s	kg m^2 s^{-1}
Pressure	P	Pascal(Pa)	Pascal, N m^{-2}	kg m^{-1} s^{-2}
Speed of Light $\left(c = 1/\sqrt{\varepsilon_0 \mu_0} \right)$	c	$\approx 2.997 \times 10^8$		m s^{-1}
Susceptibility	χ	$\chi = \mu_r - 1$		1
Temperature	T	Kelvin		K
Thermal Conductivity (of "x" i.e. k_{h_2o})	k_x	$k_{h_2o} \approx 0.0471$	W m^{-1} K^{-1}	kg m s^{-3} K^{-1}
Dynamic viscosity	η_0	Poise	Pa s, N s m^{-2}	kg m^{-1} s^{-1}
Volume	V	$\text{Litre}(1) \triangleq 10^{-3} m^3$		m^3

1. Introduction

Current heat engines in all their forms essentially take the working substance, between two reservoirs, an upper and lower with a portion of the heat transferred being converted to work subject to Carnot's limit.

$$\eta \leq \frac{T_H - T_L}{T_H}$$

<div align="right">eqn. 1</div>

Refrigeration and Heat Pumping follow similar principles and have their coefficients of performance (COP) as follows:

$$COP_{pump} \leq \frac{T_H}{T_H - T_C}$$

<div align="right">eqn. 2</div>

$$COP_{cool} \leq \frac{T_C}{T_H - T_C}$$

<div align="right">eqn. 3</div>

The thermodynamic identity allows us to model the working substance thus:

$$dU = \delta Q - \delta W$$
$$= TdS - \delta W$$

<div align="right">eqn. 4</div>

And around a closed cycle we can relate changes in entropy of the working substance to the work converted, that is, to form a heat engine there must be a property that is a strong function of temperature over the operating temperature range.

Properties of thermofluids are well known and have been the staple of thermo-engineering for at least two centuries and arguably into antiquity (Hero's steam engine). However there is interest in magnetic materials for the possibility of greater temperature range[1, 2], fewer moving parts to an engine, less toxic materials (in the case of magnetic refrigeration [3]) and intriguingly as this thesis will show, direct conversion of heat into electricity and highly efficient operation by means of a new Temporary Remanence cycle.

First we must understand how entropy changes in magnetic materials relate to their usefulness as conventional heat engines before we undertake the purpose of the thesis, the exposition of the new Temporary Remanence cycle.

1.1. Simple Magneto-caloric effect heat engines

Magnetic heat engines need a variation of magnetisation with temperature and two effects are noted: the force experienced by magnetic materials in an external field[4-6] ($\mathcal{M}$ is the volume magnetisation or dipole moment, eqn. 5) and the magneto-caloric effect (appendix 1).

$$F = -\nabla \left(\mathcal{M} \cdot \mathbf{B} \right)$$

<div align="right">eqn. 5</div>
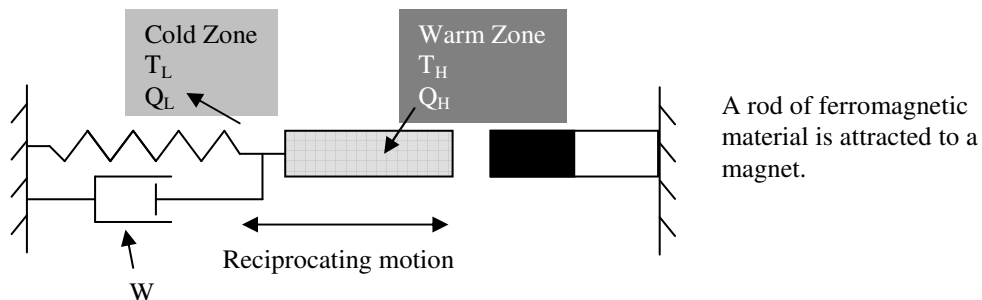
Figure 1 – A Simple Reciprocating Magnetic Motor

Figure 1 shows a means to convert heat energy to work by a simple reciprocating motor. A rod of ferromagnetic material is attracted to a magnet and does work against a spring. However at the same time near the magnet it is heated, absorbing heat Q_H, above its Curie temperature (the temperature above which the material becomes paramagnetic, appendix 2) with the result that its moment, μ, becomes smaller. Consequently the force on rod diminishes and it is retracted into the cold zone rejecting heat Q_L into the lower reservoir. Useful work is shown as being merely dissipated in the dashpot.

Thermodynamic analysis can be quickly performed by analysing this heat engine as two adiabatic processes alternated with isothermal processes (figure 2) and we can compare this to figure 50 (appendix 1).
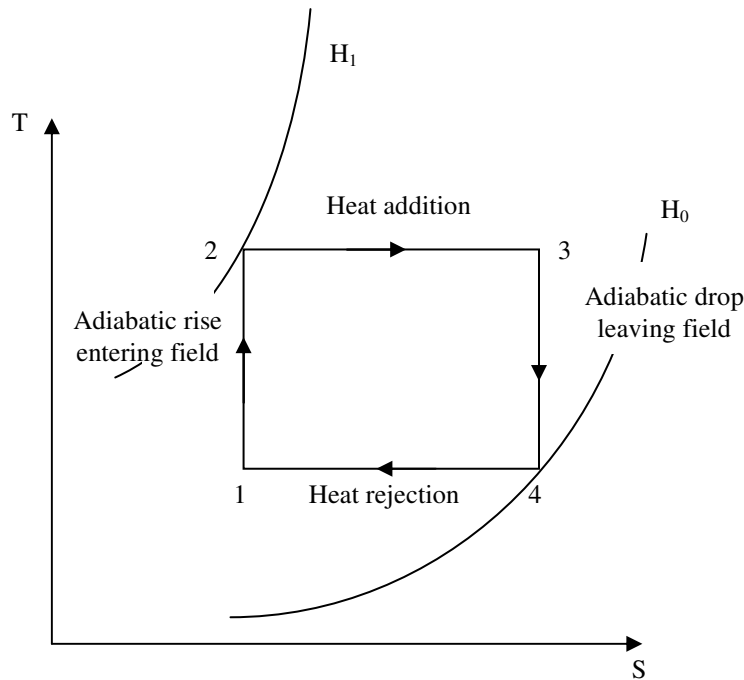
Figure 2 – T-S diagram for the Magnetic Heat Engine

The Thermodynamic Identity (eqn. 4) equates the change in heat to the work around a cycle and thus the area on the T-S diagram is equivalent to the work performed by equations eqn. 48 and eqn. 52 (appendix 1). This equates to:

$$W = \int_{H_0}^{H_1} \frac{\mu_0 T}{C_H} \left(\frac{\partial \mathscr{m}}{\partial T} \right)_H dH \cdot \int_{H_0}^{H_1} \mu_0 \left(\frac{\partial \mathscr{m}}{\partial T} \right)_H dH \qquad \text{eqn. 6}$$

Or approximately,

$$W \approx \frac{\mu_0^2 T}{C_H} \left(\frac{\partial \mathscr{m}}{\partial T} \right)_H^2 (\Delta H)^2 \qquad \text{eqn. 7}$$

1.1.1. A Simple Magnetic Refrigerator

Figure 3 and 4 show a magnetic refrigerator and how the working substance is placed in contact with upper and lower reservoirs to cool the lower reservoir. The steps are:

1:      Working substance is in thermal equilibrium with lower reservoir
2:      Working substance enters field and warms
2-3:   Working substance achieves thermal equilibrium with the upper reservoir and rejects heat
4:      Working substance leaves field and cools
4-1:   Working substance achieves thermal equilibrium with the lower reservoir and absorbs heat

Figure 4 shows the T-S diagram for the process.
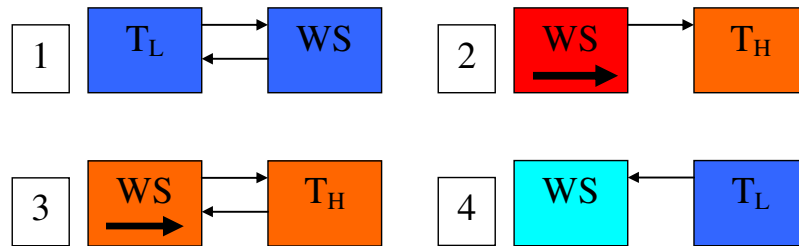
Figure 3 – Process steps for the Magnetic Refrigerator
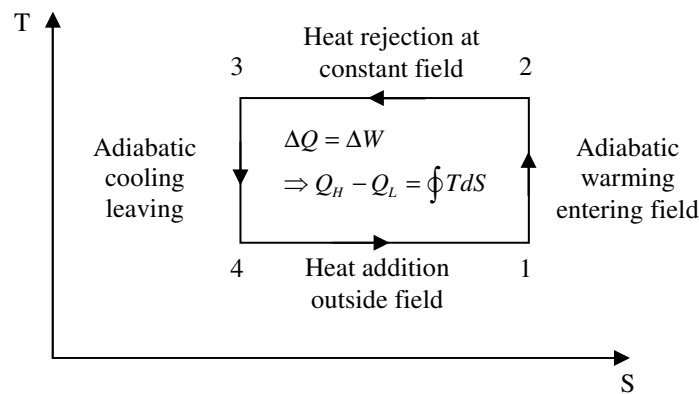
Figure 4 – T-S diagram for the Magnetic Refrigerator

The reversible nature of the Carnot cycle allows us to use the work figure (eqn. 7) to compute the coefficients of performance for refrigeration or an heat pump:

$$COP_{ref} \leq \frac{T_H}{T_H - T_C} = \frac{Q_H}{W}$$

And

$$COP_{pump} \leq \frac{T_C}{T_H - T_C} = \frac{Q_C}{W}$$

1.2. Literature Review on Magneto-caloric Effect research

The magnetic heat pump discussed previously is more practically realised by heat transfer at constant magnetic intensity ("Magnetic Enthalpy", appendix 3) in the magnetic analogy of Brayton and Ericsson cycles[7, 8] (figures 5 and 6). The former cycle performs heat transfer when the magnetic intensity is higher and thus achieves a higher temperature range and heat transfer between the magneto-caloric material and the heat transfer fluid. Figure 5 shows this as two adiabatic processes and two constant intensity processes. Process 2a-3 is an additional cooling caused by a regenerator that exchanges heat with process 4a-1. The Ericsson cycle heat pump (figure 6) features isothermal magnetisation and demagnetisation processes with regeneration at processes 2-3 and 4-1. Since the heat exchange process of regeneration in both cases requires a finite temperature difference, this is an irreversible process and so is a decrease in the efficiency of both cycles compared to the Carnot cycle.

As shown in appendix 1, the magneto-caloric effect is centred on a transition temperature (this is applicable to 1st order transitions too) and wide temperature range of operation is not as easy as with other heat engines. Figure 7 shows a cascaded Ericsson cycle where two materials with different transition temperature are used; the outflow from the higher temperature cycle latterly impinges on the lower temperature material.
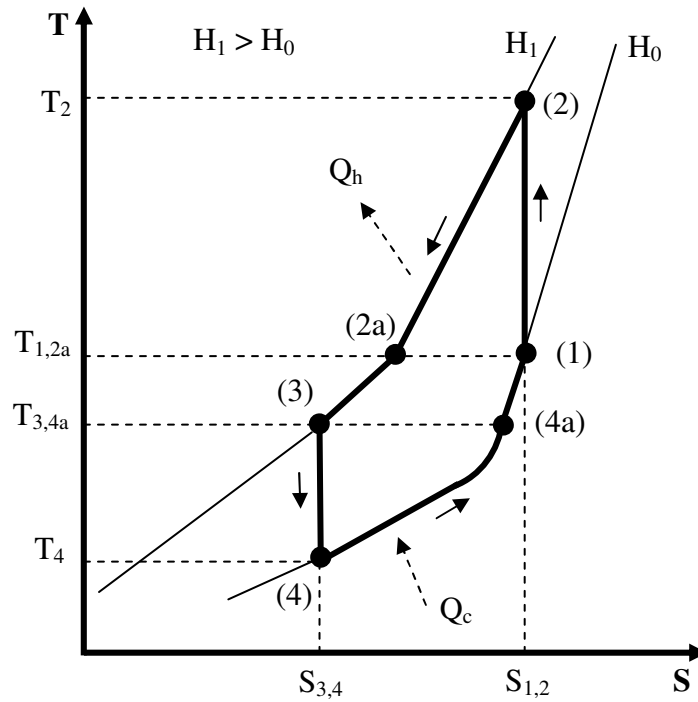
Figure 5 – Magnetic Brayton cycle
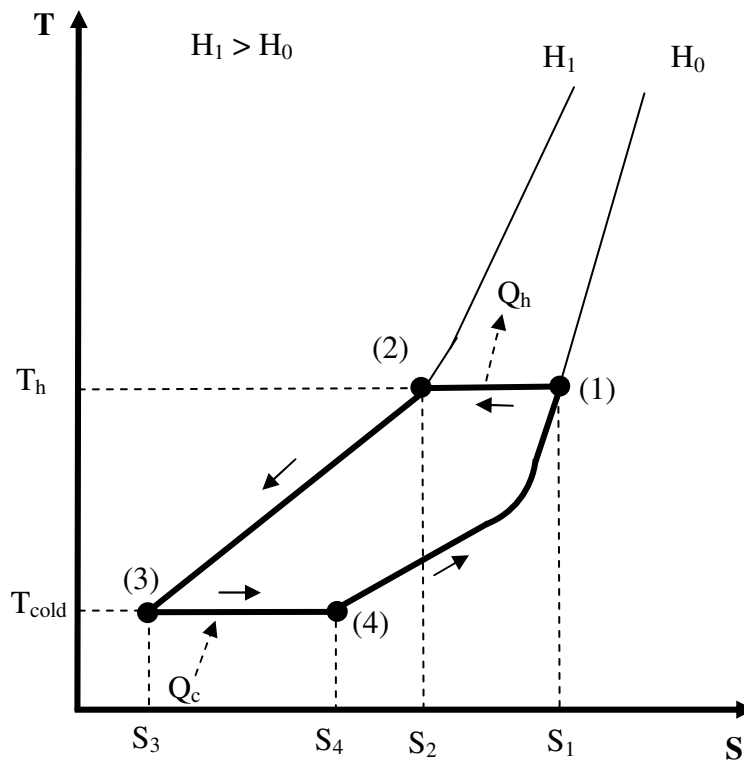
Figure 6 – Magnetic Ericsson cycle

Yet another cycle is the "Active Magnetic Regenerator" (AMR) cycle. Allegedly this cycle cannot be illustrated with a T-S diagram[7] and researchers are still struggling to classify it into the categories of cycle already discussed. It seems that the problem of description is one of multiple nested, coupled thermodynamic cycles. Nethertheless its operation is conceptually simple to understand (figure 8).

The AMR consists of five essential components:

1. Magnet
2. The Regenerator (MCE material in high surface area matrix that lets fluid pass through it)
3. The cold heat exchanger
4. The hot heat exchanger
5. The pump
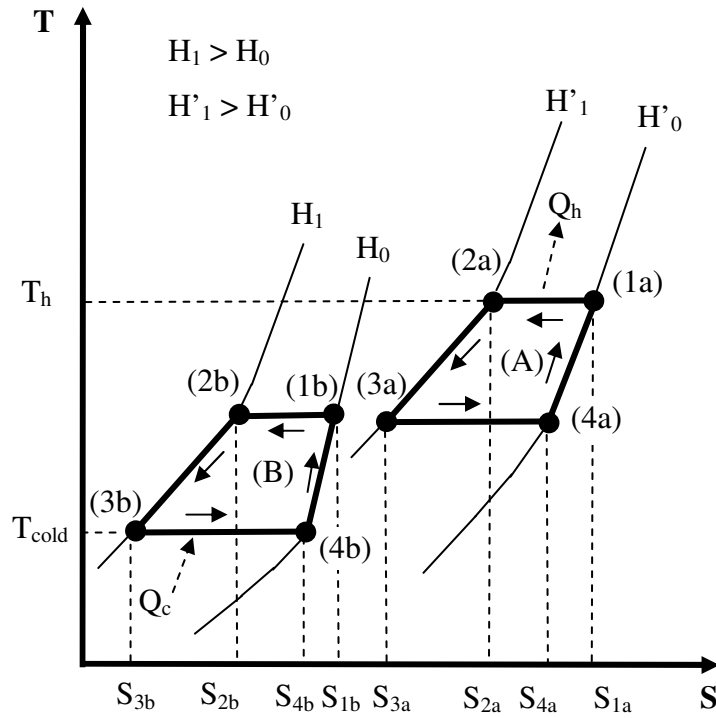
Figure 7 – Magnetic Cascade Ericsson cycle
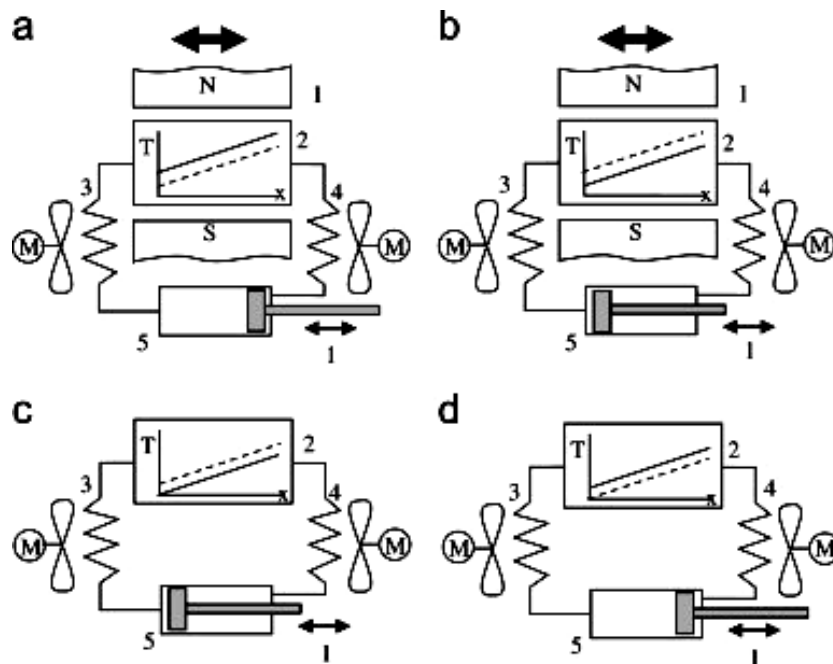
Figure 8 – Active Magnetic Regenerator cycle

In a nutshell the process is one of, a "warm blow" and "cold blow", that is, the exchanging fluid is moved by the pump between the two heat exchangers in synchronisation with the following cycle:

a. Field on and magneto-caloric rise in temperature and exchange of heat to the fluid
b. (Field still on) Fluid passed over cold heat exchanger
c. Field off and magneto-caloric fall in temperature and cooling of the fluid
d. (Field still off) Fluid passed over hot heat exchanger

To summarise the various cycle merits and disadvantages of all the cycles we note,

The Carnot cycle is:

- Restricted by the adiabatic temperature change
- Must operate near the Curie temperature and is not really suitable for cooling cycles
- Uses large magnetic fields varied at each point in the cycle which typically requires an electromagnet

By the addition of a regenerator to the cycle (a heat exchanger) the heat change from the change in lattice entropy (appendices 1 and 6) in one part of the cycle can be returned in another part of the cycle and this is the basis of the increased temperature range of the magnetic Brayton, Ericsson and Active Magnetic Regenerator (AMR) cycles. The differences between these cycles are:

- The theoretical Brayton cycle has lower cooling capacity but greater heat rejection than the Ericsson cycle[7]
- A multi-staged system with materials of different Curie temperatures can further increase the temperature range
- The AMR cycle is, allegedly, not fully theoretically understood[7] but is the most popular of the cycles being researched.

On the magneto-caloric effect itself, it is evident[3, 7, 9] (appendix 1) that the magneto-caloric effect will be large if the magnetic field variation is large, the magnetisation changes rapidly with temperature and that the material has a low specific heat capacity. Gschneidner[3] and Rómero[7] list a number of desirable material features:

- Low Debye temperature[10] values
- Curie temperature near working temperature
- Large temperature difference in the vicinity of the phase transition
- No thermal or magnetic hysteresis to enable high operating frequency and consequently a large cooling effect
- Low specific heat and high thermal conductivity
- High electrical resistance to avoid Eddy currents

Gadolinium alloys and Lanthanum-Iron-Colbalt-Silicon alloys, $La(Fe_{1-x}Co_x)_{11.9}Si_{1.1}$ with their "giant magneto-caloric effect"[7] are the focus for materials research due to their inherent high MCE although traditional ferromagnetic materials enter the scene again in the form of colloidal suspensions called ferrofluids.

1.3. Literature Review on the use of Ferrofluids

It would seem obvious that the immersion of high surface area magneto-caloric materials in a liquid phase would lend itself to a more refined magneto-caloric heat engine or refrigeration. Ferrofluids and magneto-rheological fluids (MR) are very fine to colloidal suspensions of magnetic materials in a carrier fluid which is commonly water[2]. The suspension in the medium is assisted by long surfactant molecules with one end bonded to the magnetic particle and the other having more of an affinity to the liquid medium (figure 9). Ferrofluids have core particles ranging in the 5-100nm range whilst MR fluids range from microns to almost a millimetre.

Applied science and engineering interest developed in the fluids from about the start of the 1960s as more efficient and pure chemical methods of preparation became available over the traditional ball milling. This interest has been driven by the aforementioned magneto-caloric and interesting hydrodynamic effects, most of which are beyond the scope of this presentation; MR fluids have slightly different hydrodynamic properties too.
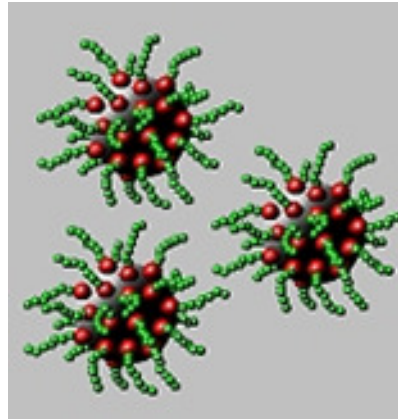
Figure 9 – Depiction of Ferrofluid particles and their surfactant chains in a suspending medium

1.3.1. The Magneto-caloric pump and Energy Conversion with Ferrofluids

Rosensweig[1, 2, 11] presents the key element in power conversion with ferrofluids as a key component of the magneto-caloric pump (figure 10). It is able to change variation in magnetisation by heat input directly to pressure volume-work.
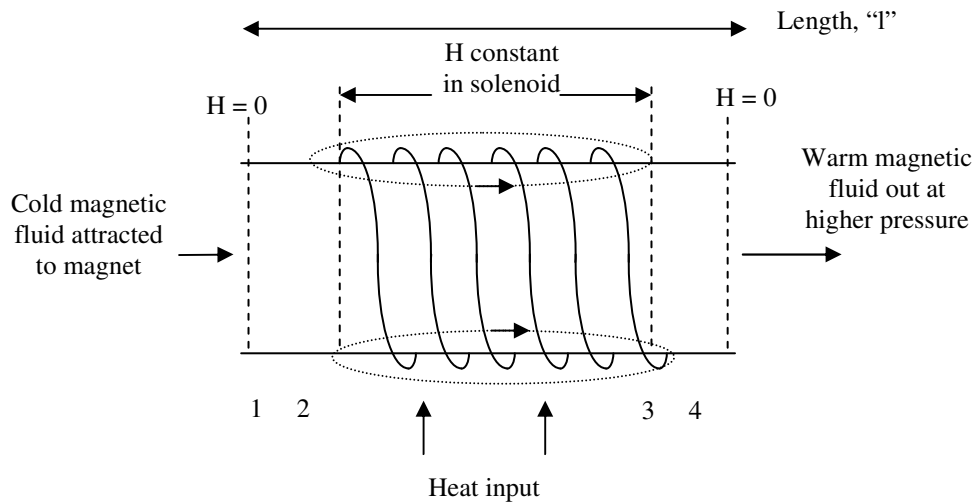
Figure 10 – The Magneto-caloric Pump

The pressure differential across the device follows from eqn. 5:

In one dimension, if M(x,T) is the magnetisation, V = Al the volume, A is area, l is length, then:

$$\int_0^l F dx = -\int_1^4 \frac{\partial \left[M\left(x,T\right) V \mu_0 H \right]}{\partial x} dx$$

integrals **1**-**2** and **3**-**4** negligible as M $\propto$ H and dipole field falls x^{-3} so at least x^{-6} at ends

$$\Rightarrow \frac{\Delta F}{A} = -\mu_0 \left[\int_1^2 \frac{\partial \left[M\left(x,T\right) H\left(x\right) \right]}{\partial x} dx + H \int_2^3 \frac{\partial M\left(x,T\right)}{\partial x} dx + \int_3^4 \frac{\partial \left[M\left(x,T\right) H\left(x\right) \right]}{\partial x} dx \right]$$

if regions **1**-**2** and **3**-**4** are small, $M\left(2\right) = M$ and $M\left(3\right) \approx 0$ and if $\frac{\partial M\left(x\right)}{\partial x} \approx \frac{\Delta M}{l}$ then

$$\Rightarrow \Delta P = \mu_0 H \Delta M \qquad \text{eqn. 8}$$

The pressure change can be substantial[2]; the reference has a table where for an applied field of 1T and ΔM of about 630G a value of 1atm pressure difference is obtained. Figure 11 shows a plant diagram for a heat engine with this pump: the pressure volume work is converted at the turbine and heat is rejected to the lower reservoir at the heat exchanger.

Solenoid Magneto-calorific pump
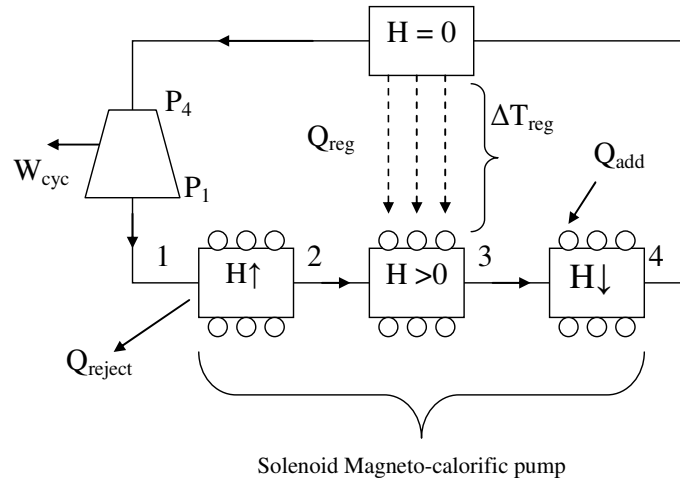
Figure 11 – Complete plant diagram for Magneto-caloric conversion with Ferrofluids

Rosensweig[2] supplies a complete cycle analysis of this scheme and is able to derive a figure for the efficiency which tends to the Carnot limit by the addition of the regenerator[11]. The regenerator merely acts to stop heat used to warm the fluid, in excess of that converted to work, being rejected and wasted at the cold sink.

Other applications for ferrofluids somewhat dependent on their thermodynamic properties are: ore and scrap metal separation (from different hydrodynamic effects on magnetic and non-magnetic materials), printer inks and magnetic character recognition (on cheques and postal franking). One other application of note is diathermy where rapid cycling of the magnetising field beyond their relaxation rate leads to irreversible heat generation (appendix 5).

1.4. Research Objective and Layout of thesis

Contrary to current thought is the notion that ferrofluids can be used for *cooling* as well as power generation. It has been found at least theoretically at this stage by the author that a new type of cycle is possible exploiting a hither-to unused property of ferrofluids, temporary remanence[2]. The objective of this research is to rigorously underpin the nascent subject area with the necessary physics and engineering techniques to lead to a new method of heat engine construction for the canon of engineering sciences.

This thesis shall layout the steps to operation of the cycle in section 2, which comprises subsections on: A Kinetic Theory analysis which leads to an analytical proof of direct lowering of the average ensemble kinetic energy (hence the temperature) in an adiabatic step by the "dipole-work" (appendix 4); A Thermodynamic 2nd Law analysis giving the energy balance for the cycle and directly relating the changes in magnetic entropy of the working substance to the work; Identification of two levels of nested thermodynamic cycle called the "Micro-cycle" and "Macro-cycle".

The next section 3 recounts early experiments in rapid cycling of magnetic fields by electronic means to measure relaxation rate, observe the temperature variation of relaxation rate and early energy conversion experiments. The observations made in section 3 lead to the development of an Electrodynamic Model and computer simulation in section 4 as it was found that electrical loading had a severe effect on cycle time. The loading problem seemed to indicate that the temporary remnant process could only ever return the magnetisation energy, however a solution was found to this by non-linear electrical loads from the computer simulation and semi-analytic methods.

2. A New Temporary Remanence Cycle

Aside from the magneto-caloric effect, which is related to changes in the magnetic moment with temperature, ferrofluids have other temperature dependent properties that we shall see can be used for power conversion and refrigeration. Appendix 2 shows how various aspects of magnetism relate to one another, from paramagnetism to super-paramagnetism to ferromagnetism. In the appendix it can be seen that super-paramagnetism is ferromagnetism in a sense, as each paramagnetic moment in the particle is at saturation, for the temperature it experiences by the exchange force.

The magnetic system will configure itself to achieve the lowest possible energy by breaking up into domains so the net magnetic field of the ensemble can cancel. An energy barrier be it shape anisotropy, crystalline anisotropy or other phenomena acts against this randomisation and thermal agitation perturbs the system over this barrier such that a probability and hence a relaxation rate can be calculated.

Ferrofluids behave super-paramagnetically, that is they have features pertaining to paramagnetism i.e. potentially no hysteresis or permanent moment in a magnetising cycle. However they show a large response to the magnetising field, similar to ferromagnetism, due to the large spin moment of the magnetic entity. The distinction between super-paramagnetism and ferromagnetism is one of timescale. Two mechanisms contribute to the super-paramagnetism dependent on the size of the core particle, Brownian or Néel relaxation[2, 12-14]:

$$\text{Brownian:} \quad \tau_B = \frac{3V\eta_0}{kT} \qquad \text{eqn. 9}$$

$$\text{Néel:} \quad \tau_N = \frac{1}{f_0} e^{\frac{KV}{kT}} \qquad \text{eqn. 10}$$

- Brownian type fluids are modelled as an ensemble of domain or greater sized particles where the magnetic moment is constant (on the time scale of other relaxation processes) and large (spin in excess of 10,000 Bohr magneton). The relative constancy of this moment is related to the energy barrier provided by the shape or crystalline anisotropy constant and the size of the particle (KV, eqn. 10) so that $\tau_N \gg \tau_B$. The ensemble behaves super-paramagnetically to an applied field H, a Langèvin type equation describes M(H) and the energy barrier to randomisation is $3V\eta_0$ (volume, viscosity, eqn. 9) which is a purely fluid dynamical effect ("a paddlewheel swishing in a fluid").

- Néel type fluids are sub-domain sized so that the *internal* moment of the particle is being randomised by thermal energy against the energy barrier KV ($f_0 \approx 10^9$ Hz is the Néel frequency). Compared to any tendency for the particle to rotate wholesale, the energy barrier for the Néel process is much lower than a Brownian process so that $\tau_B \approx \tau_N$. Once again the ensemble behaves super-paramagnetically.

Both eqn. 9 and eqn. 10 show these phenomena as strong functions of temperature, however if the magnetising field is switched on and off slowly relative to the relaxation rate, the process is reversible. In appendix 5 the irreversible losses from magnetising faster than the relaxation rate are quantified. Also if the ferrofluid is magnetised and then the magnetising field is removed abruptly, so that the magnetic work is not returned to the magnetising apparatus (as it would if the magnetisation is removed slowly), the magnetic work become dissipated as internal energy in the fluid and this is practically complete after 5τ time constants.

The above description of a magnetising cycle doesn't sound like a very good prescription for making a heat engine as there appears to be purely dissipative processes in operation. We believe that for this reason temporary remanence heat engines have been overlooked. An extensive literature search and indeed patent searches (even to the PCT level required for patent granting) has turned up no prior art[15]. However we can make our first observation – if the rate of magnetisation is slow compared to the relaxation rate, this irreversible loss can practically be avoided.

We require a work step in our putative magnetisation de-magnetisation cycle and unlike the magneto-caloric pump discussed earlier, we propose direct conversion of heat energy to electrical energy by Faraday induction. This step would return both the magnetisation energy and extra work of thermal conversion called "dipole-work" (appendix 4) and this is manifested as an extra term on the thermodynamic identity.

It is pertinent to point out the similarities and differences between our cycle and the plant diagram for the magneto-caloric pump based cycle of figure 11, these are (figure 12):

- There is a net circulation of ferrofluid around the circuit.

- There is a zone of magnetisation and demagnetisation similar to the existing cycle (the solenoid figs. 10 and 11) and the "power extraction area" (fig. 12) which is also a solenoid.

- Pressure volume work is negligible/irrelevant and/or can be made so in this cycle (we can turn off the solenoid for a short while and pump a new volume of fluid into it). Direct electrical energy conversion is achieved on the demagnetisation part of the new cycle in the solenoid by Faraday induction.

- There is a component that interfaces to an external heat source (regions C to D fig. 12).

- There is no lower sink. It forms its own virtual cold reservoir by the dipole-work (section 2.1.2, appendix 4).

- For the new cycle there is rapid temporal variation of the magnetising field as the ferrofluid transits the region A to B (fig. 12). Many times in this region the ferrofluid is subject to a magnetising field which switches on relatively slowly (compared to its relaxation rate) which is then switched off abruptly leaving a temporary remnant flux for dipole-work. This is not just an inductor but is able to do excess work because there is a flux existing independently of a magnetising current that can convert micro-mechanical motions of heat into electricity.

- The new cycle has a wider temperature range of operation than the magneto-caloric process (section 2.2) which isn't just centred around the Curie temperature, as for super-paramagnetic materials there is extended temperature variation in several parameters (magnetisation *and* relaxation rate).

- The new cycle is both an heat engine and a refrigerator/heat pump.
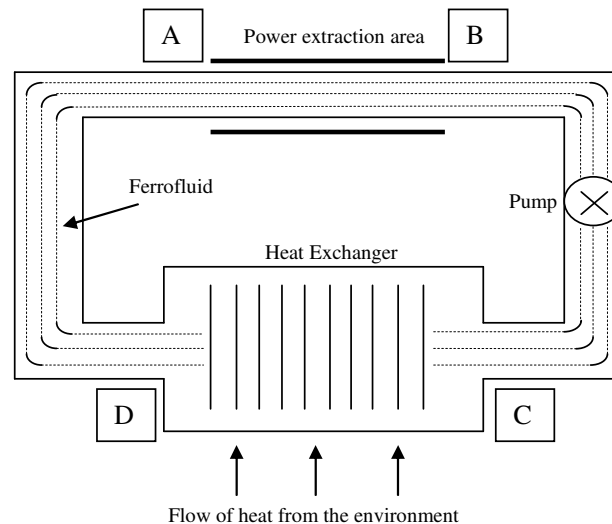
Figure 12 – Plant diagram and *Macro-cycle* for the Temporary Remanence Heat Engine

We stress again that in the region of the power extraction area, the magnetising solenoid *temporally* provides many magnetisation-demagnetisation cycles as the fluid transits the region. Only two cycles are shown in the figures below (fig. 13) where two cases of a ferrofluid with a small response (M = χH, susceptibility $0 < \chi < 1$) and one with a larger response ($\chi > 1$) is exhibited.
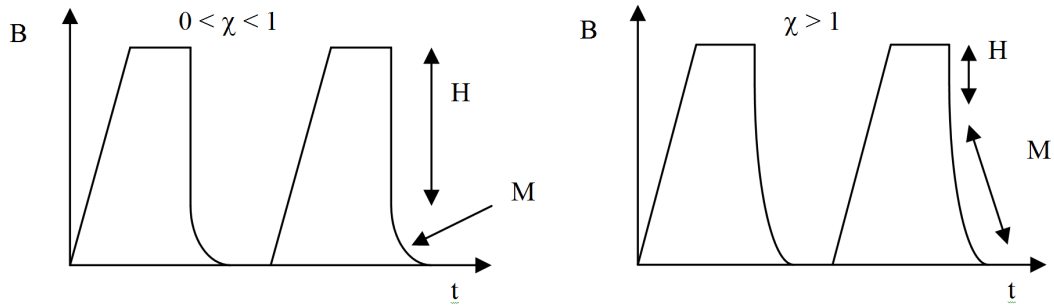
Figure 13 – A depiction of only two trains of magnetising pulses in the ***Micro-cycle*** in the power extraction region for $0 < \chi < 1$ and then $\chi > 1$

As discussed before, we show the feature of slow switch on of the field relative to the relaxation rate, to minimise irreversible magnetising losses.

The next section shall conduct a Kinetic theory analysis of the dipole-work term and show how each dipole, randomising as the magnetising field is switched off, is able to do electrical work via Faraday induction; each dipole experiences a virtual drag force, meaning that energy is directly transferred from the internal energy of the ferrofluid to electrical energy. This explains the feature of the cycle having only one reservoir, only the external source of heat and no cold reservoir; it forms a virtual cold reservoir in its operation so that heat energy flows from the ambient reservoir to the device. The section after the Kinetic theory analysis is a Thermodynamic analysis (of both the Macro-cycle, fig. 12 and Micro-cycle, fig. 13) and will back up these claims. We shall see that the micro-cycles bear a relation to the magneto-caloric effect of figures 57 and 58.

2.1. Kinetic Theory Analysis

We shall now show that dipole-work, on the demagnetisation step of the micro-cycle of the temporary remanence new cycle, manifests itself as a cooling effect; energy is directly transferred from the internal energy of the working substance to the external electrical power circuit. In the section after this the magneto-caloric effect is revisited and an enhanced cooling occurs on the demagnetisation step, from this dipole-work term, such that an asymmetric magneto-caloric effect results.

N.B. this is not just an inductor in a magnetise-demagnetise cycle but it is able to do excess work into the electrical load R.
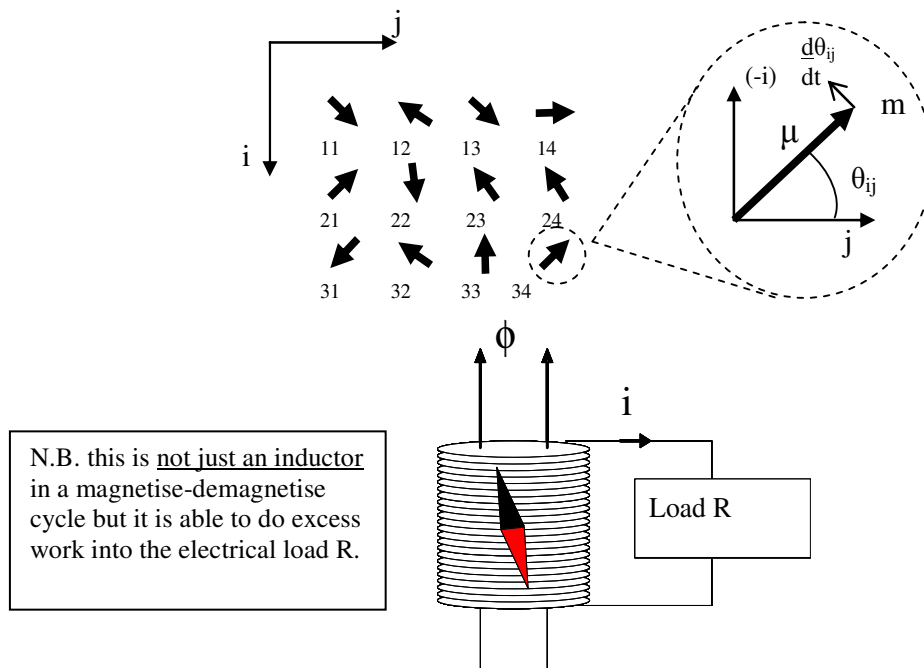
Figure 14 – The Kinetic Theory Model

There is no mystery to heat energy – it is random microscopic motion. Figure 14 models a 2-D array ensemble of magnetic dipoles, in analogy to the ferrofluid core particles, with Newtonian Dynamics; it is a simple kinetic

model of a super-paramagnetic system. The fact that they are lain out in a regular lattice is irrelevant and in fact models the innards of a Néel type fluid rather than a Brownian fluid, where they are not constrained to fixed sites. However both models would display the same feature of seeking minimal energy configuration in the total field of the ensemble by the well known expedient of multi-pole fields falling off with distance more rapidly than a polar inverse square field (the potential falls as $\frac{1}{r^{1+n}}$ where n is the number of poles[4-6]). This results purely from the least energy principle and superposition of fields.

A popular misconception in molecular dynamic modelling is that a randomizing input is required to model relaxation or "heat" in general. The multi-particle dynamics (i.e. the Three Body Problem[6, 16]) is the *sine qua non* of Brownian motion/Ergodic Theorem.

The model is made as simple as possible but is able to derive some important results. Physics is necessarily a science of approximation but enough features are introduced to simulate the 'mechanical' and magnetic aspects of the system such that the system entropy and temperature can be defined. Some acceptable caveats shall be given.

- Use of Newtonian Mechanics is justified because the energy and time scale of the process (the 'action') $kT\tau \gg h\tau$, where 'k' is Boltzmann's constant, T is temperature, 'h' is Planck's constant and τ is the time scale of the ferrofluid relaxation processes. We shall see in the experimental section that these are much greater than 10^{-13}s, the time of heat relaxation/phonon processes.

- No energy barrier in the form of anisotropy is included to simulate the ferrofluid relaxation equations (eqn. 9 and eqn. 10). In computer simulation form (rather than the analytical working out we shall do here) all that happens is that, the relaxation proceeds rather quickly at some rate limited by the moment of inertia of our dipoles. An energy barrier simply slows the process until a perturbation takes it over the barrier.

- The induction of electrical work into the external circuit by the dipole-work term does not model the external circuit's dynamics and the consequent need for electrical non-linearities to achieve the objective of energy transfer greater than the magnetisation energy (sections 4 and 4.3)

2.1.1. Dipole-work as the mechanism of energy conversion

Note, this is not just an inductor in a magnetise-demagnetise cycle but it is able to do work in excess of the magnetising energy, we have a temporary remnant flux which acts just like a dynamo transferring shaftwork to the external electrical system. Here we are drawing an analogy with the microscopic dipoles rotating via the randomisation process and the "micro-shaftwork" of heat energy. In fact, considering the energy of a dipole in a field[4-6]:-

$$E = +\mathcal{M} \cdot \mathbf{B} + const \qquad \text{eqn. 11}$$

It matters not whether the magnetic moment is rotated wholesale or randomised between the maximum and minimum energy configuration, it is the same result:

$$\Delta E \big|_{max}^{min} = \mathcal{M} B \cos\theta \big|_{0}^{\pi/2} \text{ or } \mathcal{M} \big|_{\mu_{max}}^{0} B \cos\theta \qquad \text{eqn. 12}$$

In this Kinetic Theory section we concern ourselves with what happens on the demagnetisation part of the new micro-cycle. One would ask "just what is the field B in eqn. 11 if the magnetising field is off?" The putative mechanism for energy conversion is the change in energy experienced by each dipole in figure 14. It seems perverse to say that it is the self-field of the ensemble as they induce a current in the solenoid but this just follows from Faraday's law of induction:-

The solenoidal field (application of Ampère's Law) [4, 6] is given by $\mathbf{B}_{ext} = \mu_0 ni$ where n is the turns per unit length. Substitute $i = -\frac{N}{R} \partial\Phi/dt$ where N is the number of turns, Φ is the flux from the dipole field collapse and $\Phi = Area \times \mu_0 \sum_{ii,jj} \frac{\mathbf{m}_{ii,jj}}{vol} \cdot \mathbf{e_j}$ the sum of the nanoscopic dipole moments (of volume "vol") in direction $\mathbf{e_j}$:

$$\Rightarrow B_{ext} = -\mu_0^2 k_\lambda n^2 \frac{1}{R} \sum_{ii,jj} \frac{\partial}{\partial t} \left(\frac{\mathbf{m}_{ii,jj}}{vol} \cdot \mathbf{e_j} \right) \qquad \text{eqn. 13}$$

Where

        $\mathbf{m}$ is the value of the dipole moment

        k_λ is a dimensionless constant

        R is the resistance of the electrical load

        e_j is a unit vector along axis j, only the flux down this axis causes the induction

2.1.2. The Dynamical Model

The basic equation describing the system is a system of coupled dipoles in a lattice, whose components couple to their nearest neighbours' dipole-dipole interaction torques[5, 6] $\tau\left(\theta_{ij}, \theta_{ii,jj}, \mathbf{m}, \mathbf{r}\right) = -\mathbf{m}_{ij} \times \overline{\mathbf{B}_{local.neighbour}}$.

$$\ddot{\theta}_{ij} = \frac{1}{I} \left(-k_{dip} \sum_{\substack{ii=i-1, \\ jj=j-1 \\ ii\neq i \wedge jj\neq j}}^{\substack{ii=i+1 \\ jj=j+1}} \tau\left(\theta_{i,j}, \theta_{ii,jj}, \mathbf{m}, \mathbf{r}\right) - \mathbf{m}_{ij} \times \mathbf{B}_{ext} \right) \qquad \text{eqn. 14}$$

The matrix of dipoles (i, j) of moment of inertia I, is represented by a state vector $\ddot{\theta}_{ij}, \dot{\theta}_{ij}, \theta_{ij}$ giving the angular acceleration, velocity and position respectively; motion is constrained in a flat plane with torques $k_{dip}\tau(..)$ and $\mathbf{m} \times \mathbf{B}_{ext}$. In the second half of the temporary remanence cycle the collapse of the net field of the dipoles, as they become randomised, induces a current in a surrounding coil which dumps its power into a resistance, R. The Boltzmann relation[10, 17] gives the entropy $S = k_B \ln(w)$ which is related to the number of states, the magnetic positional and magnetic angular velocity entropy of the array of dipoles in this classical setting is:

$$S_{pos} = const \times \ln\left(\text{standard deviation } \theta_{ij}\right)$$
$$S_{vel} = const \times \ln\left(\text{standard deviation } \dot{\theta}_{ij}\right) \qquad \text{eqn. 15}$$
$$T = const \times \text{average}\left(\dot{\theta}_{ij}^2\right)$$

We shall see these two entropy terms for the magnetic system (as distinct from the mechanical system, figs. 57 and 58) is important in the next section as we derive temperature-entropy diagrams for the new cycle.

On substituting eqn. 13 into eqn. 14 and unpacking the last term this expression is developed:

$$\overline{I\ddot{\theta}_{ij} = -k_v m_{ij} \sum_{ii,jj} \frac{\partial}{\partial t}\left(m_{ii,jj} \cos\theta_{ii,jj}\right)\sin\theta_{ij}} \rightarrow I\ddot{\theta}_{ij} = -k_v \left(m_{ij} \sin\theta_{ij}\right)^2 \dot{\theta}_{ij} \qquad \text{eqn. 16}$$

That is, the average angular acceleration cancels the uncorrelated terms and tends to a simple expression which can be understood as a velocity damping term for each dipole. Clearly the average kinetic energy of the ensemble – the temperature, is decreasing. This is a reflection of the micro-mechanical work being turned to external electrical work which is then dissipated in the resistance R (fig. 14), so the magnetic system acts as a virtual cold sink as it cools and heat energy flows from the surrounding mechanical system (fig. 58); obviously this effect won't happen when there is zero resultant flux from the working substance, as B_{ext} (eqn. 14) must be greater than zero – it is hence reliant on the symmetry breaking of an order-disorder phase transition.

2.1.3. Energy conversion only results in a slight modification to the Boltzmann barrier

Fast operation of the new magnetise-demagnetise cycle leads to more power output (dipole-work, appendix 4). For reasons regarding electrical engineering and the speed of switching components, we set a lower limit on ferrofluid relaxation rates of 100kHz. If our goal is to extract 1kW from 1 litre per second (say), it is informative to look at what modification this makes to the energy barrier and the relaxation rate.

Considering a Néel type fluid, the energy barrier per particle to achieve a fluid relaxation rate of 100kHz must be of the order of 3.5 x 10^{-20}J at S.T.P. The number of particles per litre of ferrofluid suspension is of the order 1 x 10^{20} (Rosensweig [2]) and the extraction of 1kW (or 10mJ per 10µs, i.e. 100kHz) would increase the energy barrier by 10mJ/10^{20} = 10^{-22}J. We can see that there is hardly any modification to the intrinsic relaxation barrier by the energy conversion process and conclude that it is dynamically feasible.

2.2. Thermodynamic Analysis of the New Cycle

Appendices 3 and 4 split the magnetised working substance, coil and electrical load depicted in figure 14 into three sub-systems. Indubitably, once the magnetising current has been switched off, a remnant flux decays into the electrical load which introduces an extra third term[†] onto the thermodynamic identity:

$$dU = TdS + \mu_0 Hd\mathcal{M} + \mu_0 K_e Md\mathcal{M} \qquad \text{(eqn. 97, appendix 4)}$$

Clearly once the magnetising energy $\mu_0 Hd\mathcal{M}$ is recouped, the third term is negative and directly causes the internal energy to decrease. Note that this term results from the independent flux (there is no "H field" and expenditure of energy from the magnetising source) and reflects the collapsing flux reacting against its own induced current in the coil (it's own H field in a way) as energy is repartitioned from the internal energy to the electrical load (sec. 2.1.1 and appendix 4). Our thermodynamic analysis will, of course, account for the change in internal energy around a cycle by the thermodynamic identity.

> A slight digression is made now concerning dissipation terms. Appendix 5 shows us how to account for irreversible losses on magnetising the ferrofluid onto which we can add further dissipation terms:

$$\delta Q_{irr} = f_{irr}(\omega)\mu_0 Hd\mathcal{M} + \delta Q_{irr.other} \qquad \text{eqn. 17}$$

$$\delta W_{mag} = f(\omega)\mu_0 Hd\mathcal{M} \qquad \text{eqn. 18}$$

> Where $f_{irr}(\omega)$ and $f(\omega)$ are fractions that are functions of frequency components of ω of the magnetising field such that:

$$f_{irr}(\omega) + f(\omega) = 1 \qquad \text{eqn. 19}$$

$$f_{irr}(\omega) \to 0 \text{ as } \omega \to 0 \qquad\qquad f(\omega) \to 1 \text{ as } \omega \to 0$$
$$f_{irr}(\omega) \to 1 \text{ as } \omega \to \infty \qquad\qquad f(\omega) \to 0 \text{ as } \omega \to \infty$$

> The form of these functions is given in the appendix. They simply state that, if the magnetising field is applied slowly $(\omega \to 0)$ then magnetisation is a reversible process but if done quickly, only dissipation results leaving no magnetisation - the achieved magnetisation at higher frequency is lower than at low. We shall not let this point of pedantry interfere with the following arguments where we'd have to write the thermodynamic identity as:

$$dU = TdS + f_{irr}(\omega)\mu_0 Hd\mathcal{M} + f(\omega)\mu_0 Hd\mathcal{M} + f(\omega)\frac{\mu_0}{V}K_e \mathcal{M}d\mathcal{M}$$

So, proceeding on the same tact as the appendix 1 without superfluous detail, the double differentiation procedure of the last two terms is rapidly derived:

$$\left(\frac{\partial}{\partial S}\right)_H \left(\frac{\partial U}{\partial H}\right)_S = -\left(\frac{\partial}{\partial S}\right)_H \frac{\mu_0 \mathcal{M}\partial H}{\partial H} - \left(\frac{\partial}{\partial S}\right)_H \left\{\mu_0 K_e \frac{\mathcal{M}_{rem}\partial M_{rem}}{\partial H}\right\}$$

$$\Rightarrow \quad -\mu_0\left(\frac{\partial \mathcal{M}}{\partial S}\right)_H - \mu_0\left(\frac{\partial \mathcal{M}_{rem}}{\partial S}\right)_H \left(\frac{\partial M_{rem}}{\partial H}\right) \quad \equiv \quad \left(\frac{\partial T}{\partial H}\right)_S \quad \text{the other cross product}$$

[†] Section 4.3 will show the method to ensure the third term is greater than the second and any other dissipation.

and since $\left(\dfrac{\partial \mathcal{M}}{\partial S}\right)_H = \left(\dfrac{\partial \mathcal{M}}{\partial T}\right)_H \left(\dfrac{\partial T}{\partial S}\right)_H$

and also $\left(\dfrac{\partial \mathcal{M}_{rem}}{\partial T}\right)_H = \left(\dfrac{\partial \mathcal{M}}{\partial T}\right)_H$

$$\Rightarrow \Delta T = -\mu_0 \frac{T}{C_H}\left(\frac{\partial \mathcal{M}}{\partial T}\right)_H \left[\Delta H + K_e \Delta M_{rem}\right] \qquad \text{eqn. 20}$$

We discover:

- That the dipole-work term will lead to a <u>greater asymmetrical negative swing</u> on the demagnetisation step if there is remnant flux.
- Appendix 2 derived a relation (eqn. 67) between magnetisation (M) and the applied magnetic field (H) for super-paramagnetic materials (m is the dipole moment of the core particle):

$$M = 0.9 M_S(0)\, tanh\left(\frac{m_{nano} H}{3kT}\right) \qquad \text{(eqn. 67, page 59)}$$

$$\Rightarrow \left(\frac{\partial M}{\partial T}\right)_H = 0.9 M_S(0)\left(\frac{m_{nano} H}{3kT^2}\right)\left[tanh^2\left(\frac{m_{nano} H}{3kT}\right) - 1\right] \qquad \text{eqn. 21}$$

And we note that super-paramagnetic materials display a magneto-caloric effect (provided they are not saturated) <u>even well below the Curie temperature</u> of the material from which they are made.

Straightaway we can say that a temporary remanence cycle with super-paramagnetic materials will have a greater range of operation over temperature than just the magneto-caloric effect. Even if $\left(\dfrac{\partial \mathcal{M}}{\partial T}\right)_H$ is small, it will be enhanced by the dipole-work term. Indeed we could operate around the Curie point of the core particle to enhance the effect; for instance we might construct the temporary remanence cycle from a fine suspension of Gadolinium near Curie point and have the relaxation rate controlled by the rate of heat flow instead of magnetic least action/thermal disruption mechanism of super-paramagnetism.

2.2.1. <u>The Method of Thermodynamic Analysis of the Temporary Remanence Cycle</u>

It is not easy to define a thermodynamic cycle for the new scheme as easily as say as Carnot, Brayton, Ericsson and other cycles. There are elements of widely differing time scales and length scales (the micro and macro-cycles, figs. 12 and 13). An added complication is that the cycles are nested. Also the micro-cycle proceeds through transient states on the demagnetisation step. Furthermore (fig. 15) on the demagnetisation step of the micro-cycle, the active element, the heat engine is a sub-microscopic magnetic dipole; just where are entropy and temperature defined? Considering only the bulk properties of the ferrofluid obscures the detail. Clearly the working substance needs to be broken into three sub-systems of the reservoir, magnetic and mechanical heat capacities. This was the rationale behind figures 57 and 58 which were extraneous or redundant information for the simple magneto-caloric heat engines discussed before in section 1.2.
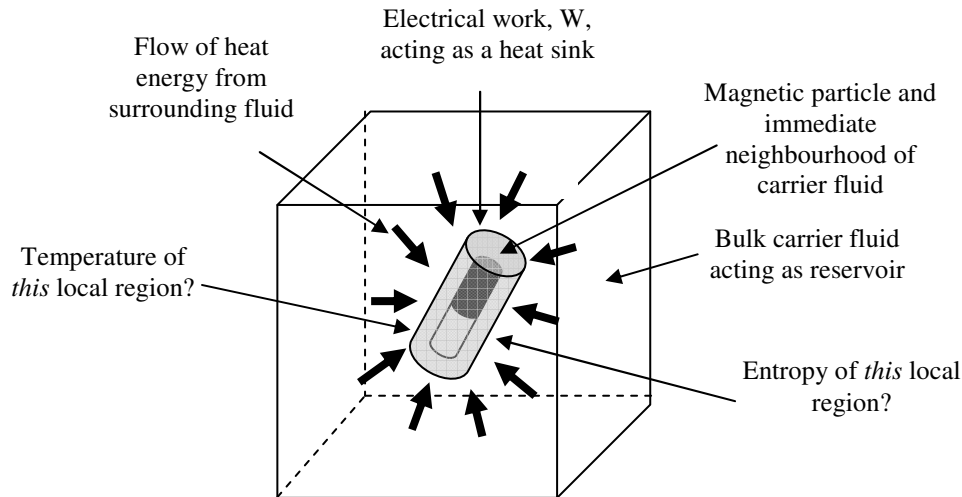
Figure 15 – The unit cell around a magnetic particle suspended in carrier fluid

The previous considerations let us define the foundations of our thermodynamic analysis:-

▪ A *Macro-cycle* where the working substance executes a loop between an heat exchanger that interfaces to the environment reservoir and the virtual cold sink of the power extraction area.

▪ A multitude of *Micro-cycles* in the power extraction area whose individual cycles consist of a magnetisation and demagnetisation step. The internal energy of the working substance decreases directly as it is converted into electrical energy by the dipole-work.

▪ A breakdown of the micro-cycle into three subsystems (appendix 6, fig. 60): A reservoir, magnetic and mechanical heat capacities. For the purposes of analysis an abstraction is made by separating the reservoir and magnetic systems by a diathermal wall. Only at points 2-3 and 4-1 (fig. 57) is the magnetic system brought into contact with the reservoir. Although this is artificial since, the magnetic system and reservoir are always in intimate contact and go through a series of transitory states, the same quantities are transferred and it makes no difference if they are done at set points or all at once, at certain times.

▪ On the short time scale of the micro-cycle, the carrier-fluid reservoir surrounding a magnetic particle looks like a *virtual reservoir*.

▪ This virtual reservoir will cool after many micro-cycles as the virtual heat sink of the dipole-work cools below the ambient of the carrier fluid.

▪ The dipole-work is best understood and fits nicely as an adjunct to the magneto-caloric effect on the demagnetise portion of the cycle (as discussed in the previous Kinetic Theory section).

2.2.2. Microcycle Analysis

As mentioned previously, analysis of the cycle benefits from considering the system composed of two magnetic subsystems: positional and velocity. The reader is directed to appendix 6 where the adiabatic magneto-caloric effect is analysed in this manner. The temperature is shown increasing with decrease in magnetic entropy there as a 2nd order phase transition is underway which depletes the number of magnetic particles in the magnetic thermal system, thus the average micro-kinetic energy (hence temperature) of the remaining thermal magnetic particles increase.

The reader will see a direct analogy between figures 16 and 61 following on the next page, then figures 17 and 62 and finally figures 19 and 63, the green lines indicates the original magneto-caloric effect whilst the other lines in figures 16, 17 and indicate additional processes.

It is now possible to construct a temperature entropy diagram for the micro-cycle and model the system energy balance based upon the analysis for the reversible magneto-caloric effect in appendix 6. As mentioned, we use the somewhat artificial construct of separating the magnetic and mechanical heat capacities by a diathermal wall and have the two systems come into thermal contact at set points in the cycle. The micro-cycle follows from this by the addition of three extra processes:

The various components are colour coded in figure 16 (once again only differential processes for simplicity):

- Green line is just the reversible magneto-caloric effect in contact with a reservoir.

- The solid red line is irreversible heat rejection (δQ_{irr}) on switching on the magnetising field faster than its relaxation rate (appendix 5).

- The dotted red line (process 3-4a-1) is the magnetisation energy becoming internal energy (fig. 18).

- The solid blue line is dipole-work.

- Processes 3-4'-4 (blue line) and 3-4a-1 (dotted red line) occur concurrently.

Figure 16 – Temperature-Positional (Magnetic) Entropy diagram

$$\Delta T = -\mu_0 \frac{T}{C_H}\left(\frac{\partial \mathcal{M}}{\partial T}\right)_H \Delta H$$

eqn. 48, Appendix 1

$$\Delta S = -\mu_0 \left(\frac{\partial \mathcal{M}}{\partial T}\right)_H \Delta H$$

eqn. 52, Appendix 1

$$\Delta T + \Delta T_{dw} = -\mu_0 \frac{T}{C_H}\left(\frac{\partial \mathcal{M}}{\partial T}\right)_H \left[\Delta H + K_e \Delta M_{rem}\right]$$

(eqn. 20)

Green circuit is the reversible MGC effect in contact with a reservoir (fig. 61, appendix. 6)

Extra cooling by dipole work

Figure 17 – Temperature-Velocity (Magnetic) Entropy diagram

We show processes 3-4'-1, 3-4a-1, concurrent and suggest this by mauve colour. The magnetisation energy becomes internal energy (fig. 18) and this is offset against the dipole-work cooling.

Dipole work makes line appear steeper than normal heat capacity as heat energy is taken from system.

1: $T_a S_{mag.vel.T_a}$

2a: $\left(T_a + dT + dT_{irr}\right)S_{mag.vel.\max}$

Figure 18 – The magnetisation energy becomes internal energy
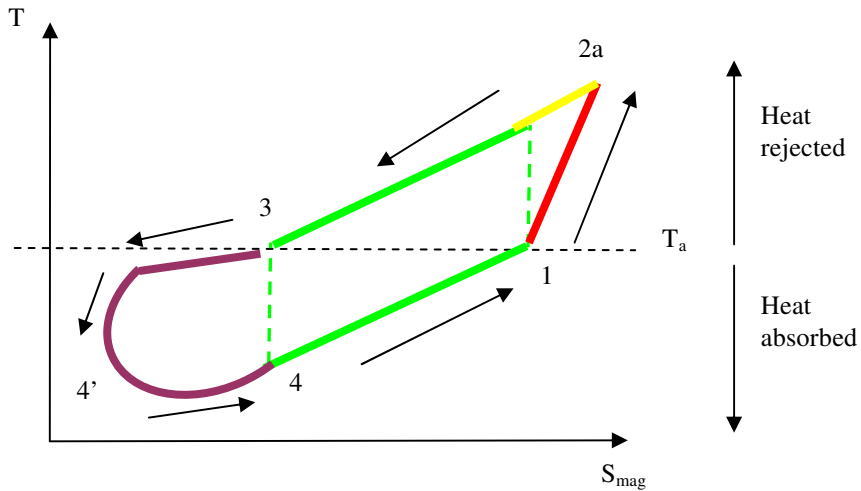
Figure 19 – Temperature-Entropy diagram for the Microcycle
Composed of the positional and velocity T-S diagrams sub-cycles

The diagram above is the summation of the various concurrent process components of the previous diagrams. It is similar to figure 63, appendix 6 and the reversible magneto-caloric cycle is shown superimposed as dotted green lines. Appendix 7 does a cycle analysis and relates the changes in entropy to the work. The final equation derived (eqn. 123) shows how the internal energy of the system directly decreases with the work.

2.2.3. The Work Available in the Micro-cycle

The proceeding thermodynamic analysis sets the upper limit of work convertible during the micro-cycle. A simple 1-D Fourier heat flow calculation (see figure 15) sets the maximum work available:

$$\frac{\partial q}{\partial t} = -k_{fluid}\frac{\partial T}{\partial x}$$
$$Q = \iint_{t,A} q \; ds \; dt$$

Where k_{fluid} is the thermal conductivity of the carrier fluid and ds is the infinitesimal surface area normal to the heat flux, q.

As we have seen, heat energy is converted into work over τ, the time scale of the magnetic relaxation. Let us write, (where A is the total surface area of the unit cells combined per volume):

$$\Delta w \text{ per volume} = \Delta Q = -\tau k_{fluid}\frac{A_{surf}}{\Delta x}\Delta T \qquad \text{eqn. 22}$$

Noting that on the magnetise step that the magneto-caloric effect is given by (Appendix 1):

$$\Delta T_{on} = -\mu_0 \frac{T}{C_H} \left(\frac{\partial \mathcal{M}}{\partial T} \right)_H \Delta H$$

And on the demagnetising step an enhanced magneto-caloric effect occurs by the dipole-work (eqn. 20, page 24 and then section 4.1 and appendix 4, this work comes from Faraday Induction):

$$\Delta T_{off} = -\mu_0 \frac{T}{C_H} \left(\frac{\partial \mathcal{M}}{\partial T} \right)_H \left(\Delta H + K_e \Delta M \right)$$

On this part of the cycle ΔH and $\Delta \mathcal{M}$ are negative and since $M \propto H$ we can write:

$$\Delta T_{off} = \mu_0 \frac{T}{C_{Virtual}} \left(\frac{\partial \mathcal{M}}{\partial T} \right)_H \cdot \Delta H \qquad \text{eqn. 23}$$

Noting that if $\left| \Delta T_{off} \right| > \Delta T_{on}$ it would appear that with this enhanced effect that $C_{virtual} < C_H$, the dipole-work and the fields from the external electrical circuit have lowered the heat capacity of the working substance, thus heat energy is repartitioned to the external electrical system.

We then substitute eqn. 23 into eqn. 22. The net work is the net difference in heat (work done by the system on the external world is negative) on the magnetisation and then the demagnetisation steps, thus:

$$\Delta w = \tau k_{fluid} \frac{A_{surf}}{\Delta x} \left(\Delta T_{on} - \Delta T_{off} \right)$$

And the work per volume,

$$\Rightarrow \Delta w / V = \frac{1}{V} \tau k_{fluid} \frac{A_{surf}}{\Delta x} T \cdot \mu_0 \Delta H \left(\frac{\partial \mathcal{M}}{\partial T} \right)_H \cdot \left(\frac{1}{C_H} - \frac{1}{C_{Virtual}} \right)$$

Into this we can substitute differential of the magnetisation with temperature (eqn. 21) which follows this approximate function very well:

$$\left(\frac{\partial \mathcal{M}}{\partial T} \right)_H = V \left(\frac{\partial M}{\partial T} \right)_H \approx -M_S(0) \frac{m_{nano} H}{3kT^2} V \qquad \text{eqn. 24}$$

Yielding the work per unit volume:

$$\Delta w \text{ p.v.} = \tau k_{fluid} \frac{A_{surf}}{\Delta x} M_S(0) \frac{m_{nano} H}{3kT} \left(\frac{1}{C_H} - \frac{1}{C_{virtual}} \right) \mu_0 \Delta H$$

$$= \tau k_{fluid} \frac{A_{surf}}{\Delta x} \frac{m_{nano} M_s(0) \cdot \mu_0 H^2}{3kT} \left(\frac{1}{C_H} - \frac{1}{C_{virtual}} \right) \quad \text{N.B. H is the same as } \Delta H \text{ if we start from 0}$$

Let us try some realistic values in this expression:

- The order of the number of particles per m^3 of ferrofluid suspension is N = 1 x 10^{23} (Rosensweig [2])
- Particles are about 5nm in radius giving a total surface area per litre of $4N\pi r^2 \approx$ 3 x 10^7 m^2
- The sheaf of carrier-fluid/surfactant around the core particle is of the order of Δx = 5x radius = 25nm

- M$_S$ for a typical ferrofluid is about 300gauss or about 25,000A/m
- The ferrofluid core particle magnetic moment, m$_{nano}$, is of the order of 1 x 10^{-25} J/A/m this is sufficient to saturate it at about 0.1T at 290K

- Let ΔH = 8000 A/m
- Assuming the carrier-fluid is water based, C$_H \approx$ 4.2MJ/K and quoted per m^3 as the calculation is per unit volume
- And k$_{fluid} \approx$ 0.6 W/m/K for water
- The relaxation rate of the ferrofluid we have in the laboratory commissioned for this project is 20ms

- Assume a 10% change in the heat capacity, that is $\dfrac{1}{C_H} - \dfrac{1}{C_{Virtual}} = \dfrac{1}{C_H} - \dfrac{1}{(1-0.1)C_H} = -\dfrac{1}{9C_H}$. This is

  not too wild as we shall see in the next chapter the work is a multiple of the magnetising/magneto-static energy. If the ferrofluid flux was 100gauss the magneto-static energy per litre at saturation is about 80J and if we are able to recoup this and an excess of say 400J (section 4.3), we would directly lower the internal energy of a water-based ferrofluid by about 10%.

At room temperature (about 290K), for the figures above, assuming a theoretical maximum of $\Delta W \approx$ 6.4MJ per m^3 or about 6.4kJ per litre is obtained. This corresponds to a temperature drop of about 1.5K for a water base ferrofluid. Obviously if the flow-rate of working substance from the heat exchanger is a litre per second, we'd achieve 6.4kW or for 1m^3/s, 6.4MW.

2.2.4. Macrocycle Analysis

If micro-cycles are run after one another (the end point is the start of the next cycle and so on) then a path can be traced through the start and end points on a T-S diagram for the working substance, as shown below (figure 20, thick black line through micro-cycles). It is of interest to note that this path is less steep than the heat capacity curve for the working substance when the micro-cycles aren't performed (second thick black line to the right of the first line).

$$\text{If for the normal state line: } S_0 = C_H \ln(T) + const$$

$$\text{Then: } C_H = T\frac{\partial S_0}{\partial T} = \frac{\delta Q}{dT} \approx T\frac{\Delta S}{\Delta T}$$

$$\text{And if: } C_{DW} = T\frac{\partial S_{DW}}{\partial T} = \frac{\delta Q_{DW}}{dT} \approx T\frac{\Delta S}{\Delta T_{DW}}$$

$$\text{Then: } S_{DW} = C_{DW} \ln(T) + const$$

$$\text{And if } \Delta T > \Delta T_{DW} \Rightarrow C_{DW} > C_H$$

It can be said that the material behaves as a different substance (from the point of view of plotting a T vs. S graph) with a higher heat capacity than the native material. Not surprising really since the material is "leaking" energy from its system to an external electrical system. A contradiction becomes apparent which needs explanation:

- In section 2.2.3 the virtual heat capacity was described as *lower* as the magnetising field "squeezed" out some degrees of freedom in the system, thus *lowering the magnetic heat capacity*. This was the mechanism by which energy was repartitioned from thermal system to the external electrical system on the magnetising step.

▪ Yet in figure 20 clearly the path that the system undergoing the temporary remanence cycle follows (the uppermost thick black line) indicates a *higher heat capacity*.

This conundrum is not paradoxical if one realises it is based upon whether we go down the micro-cycle line (rejecting heat to the external system) or up it, from the point of view of heating a substance whose T-S trajectory looks like the micro-cycle: we supply excess heat for both the material and to the external system.

Now the complete plant diagram (see figure 12 for the labels A, B, C and D) in relation to the macro-cycle and micro-cycles can be seen if we "zoom out" from figure 20. Once the cooling process is over it will intersect the trajectory of the normal working substance T-S curve. The area between the two is the heat energy converted to electrical energy.
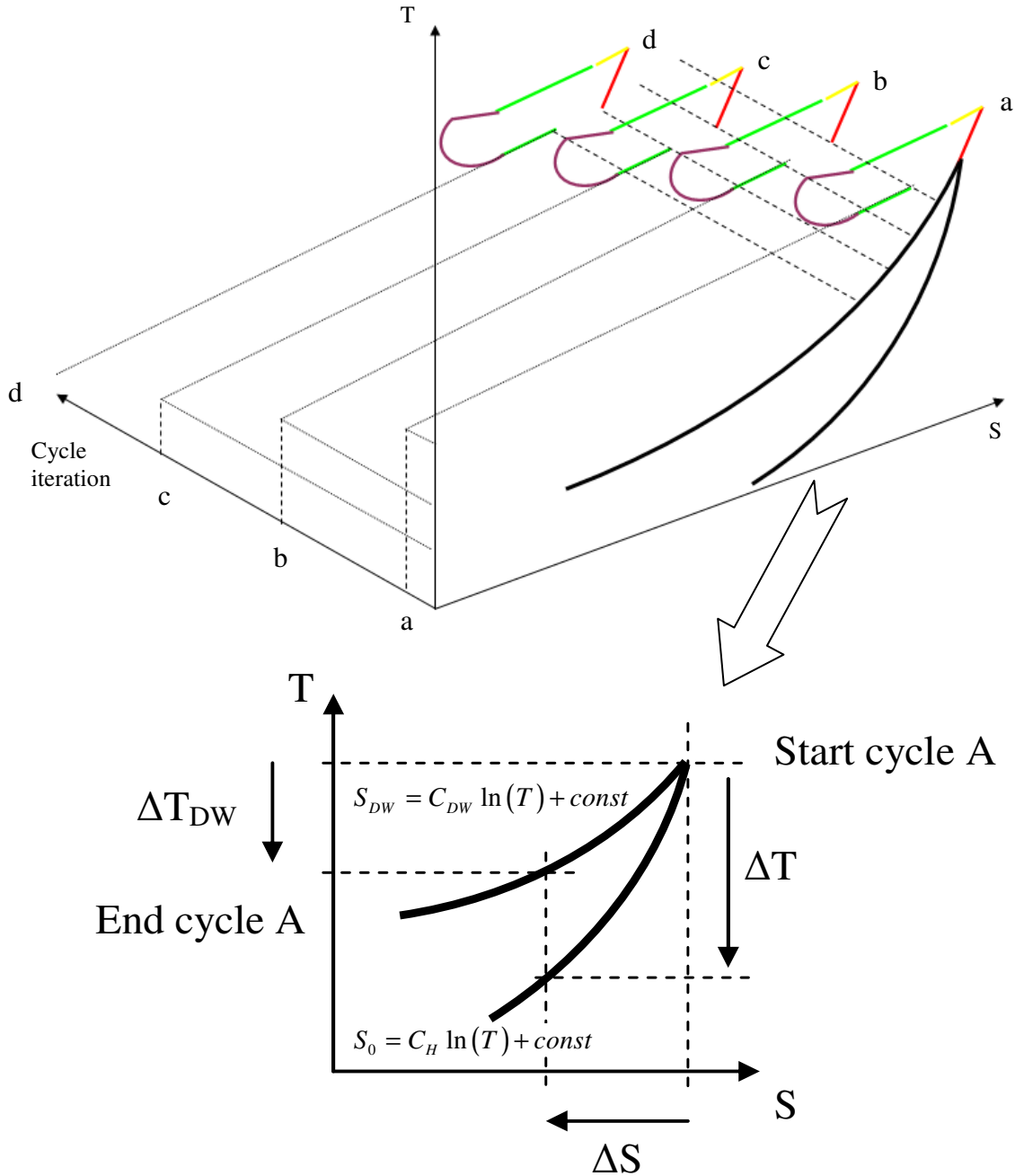
Figure 20 – How Micro-cycles relate to Macro-cycle on a T-S diagram
(subscript "DW" means relating to dipole-work)

In the figure below we have shown some variation in the cooling trajectory (S_{dw}) by the solid and dotted paths. The difference in these paths is dependent on the dipole-work and the electrical circuit (see section 4).
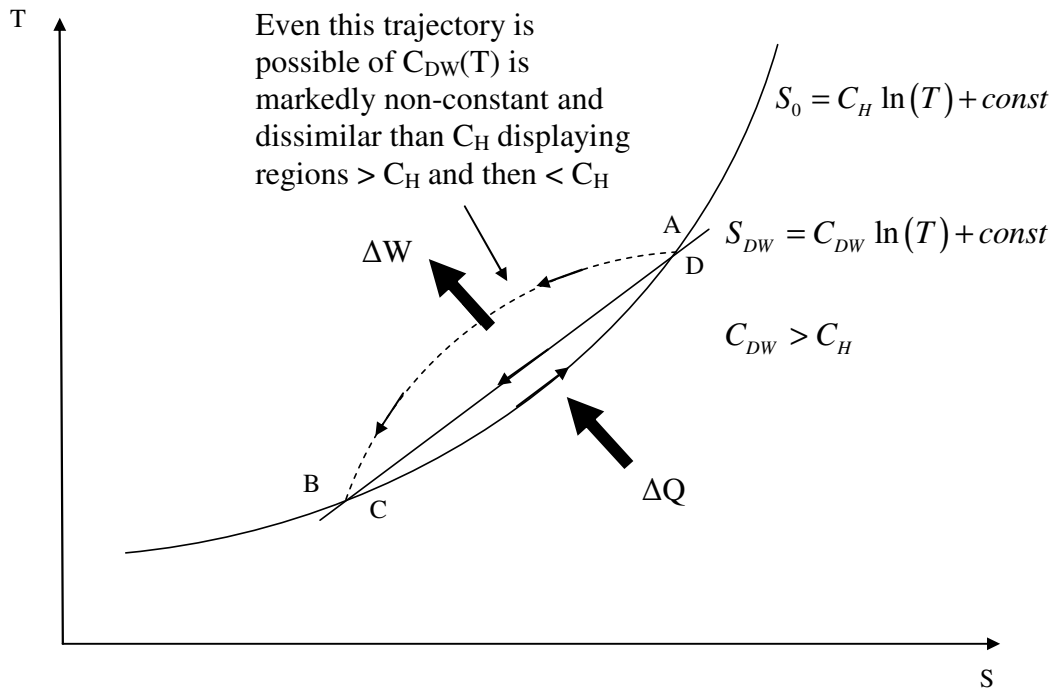
Figure 21 – Macro-cycle T-S diagram related to points on plant diagram

3. Experimental Apparatus

This experiment (fig. 22) is an unsophisticated means of rapidly producing a magnetic field in a small volume to test several early concepts in the project. It is a field cycler and uses a large battery bank and high current to create a field in a low inductance coil (fig. 23). The rig has been able to show proof of "independent flux" and temperature dependence of relaxation and the dipole-work exceeding the magnetisation energy.
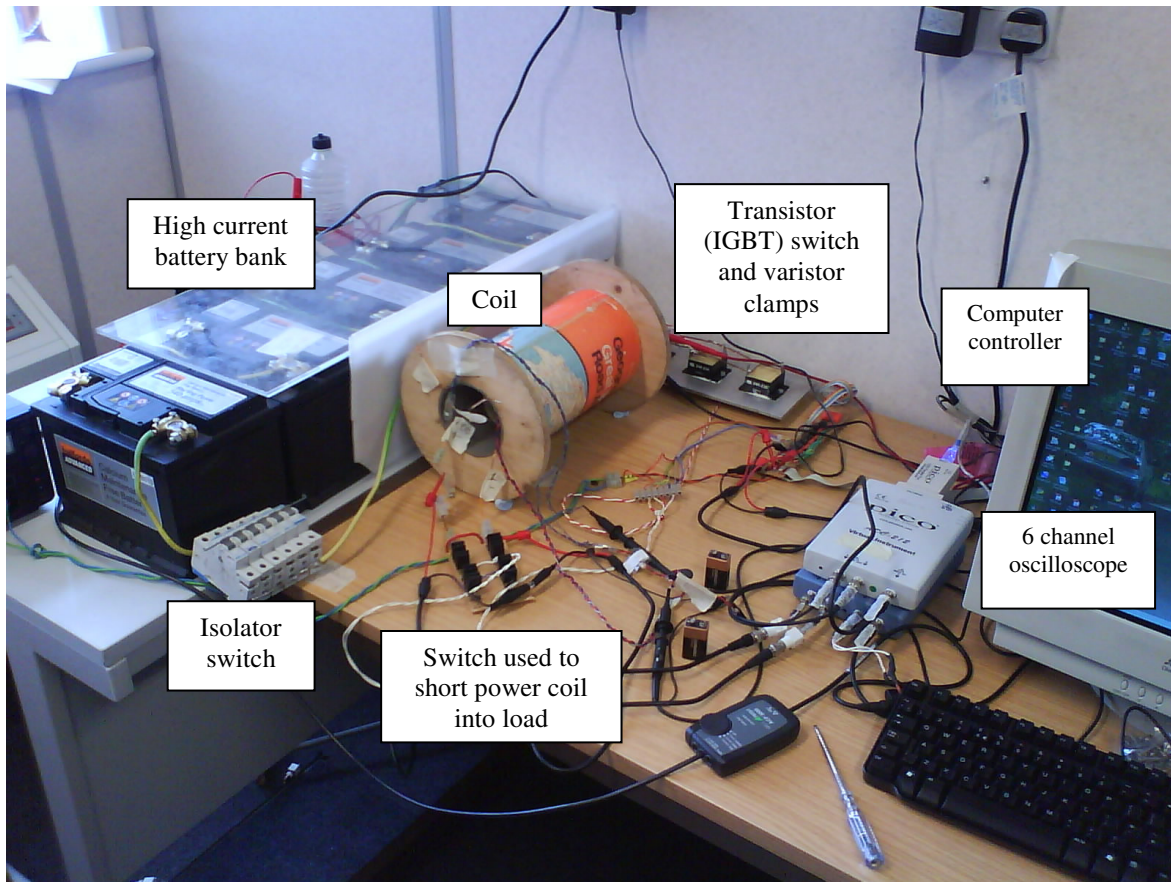
Figure 22 – Photograph of "Rig 1"

The circuit on the next page is the test rig used to perform the first phase of the project, the test of the independent flux criterion or put more simply, whether ferrofluids display temporary remanence. A current through the solenoid of about 1000A generated a field of 1850G in the centre and 810G at the extremities.

Figures 24 and 25 show the rig in operation doing an on-off cycle with no ferrofluid in the core (fig. 25 shows clearly the control of the switch by channel D and the causal variation in the other channels). On a four channel oscilloscope the measurements were:

- Channel A is the output from a hall-probe 2mv/G

- Channel B is the differential probe across the coil (figure A) Voltage/100V

- Channel C is the output from a more sensitive hall-probe 25mv/G

- Channel D is the control line voltage to the IGBT attenuated 20:1

Clearly the trace on figure 24 shows that the magnetising field is switched off very rapidly in the order of tenths of milli-seconds.
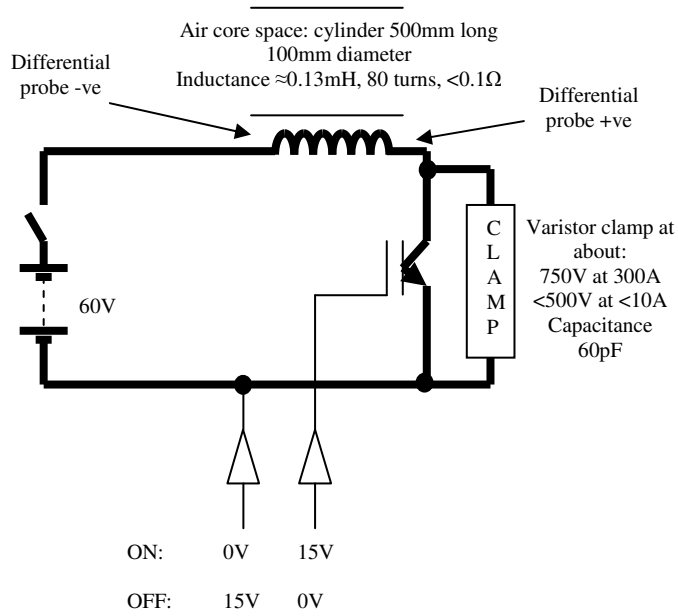
Figure 23 – Schematic of the rig circuit

3.1. Results from the 1st Rig
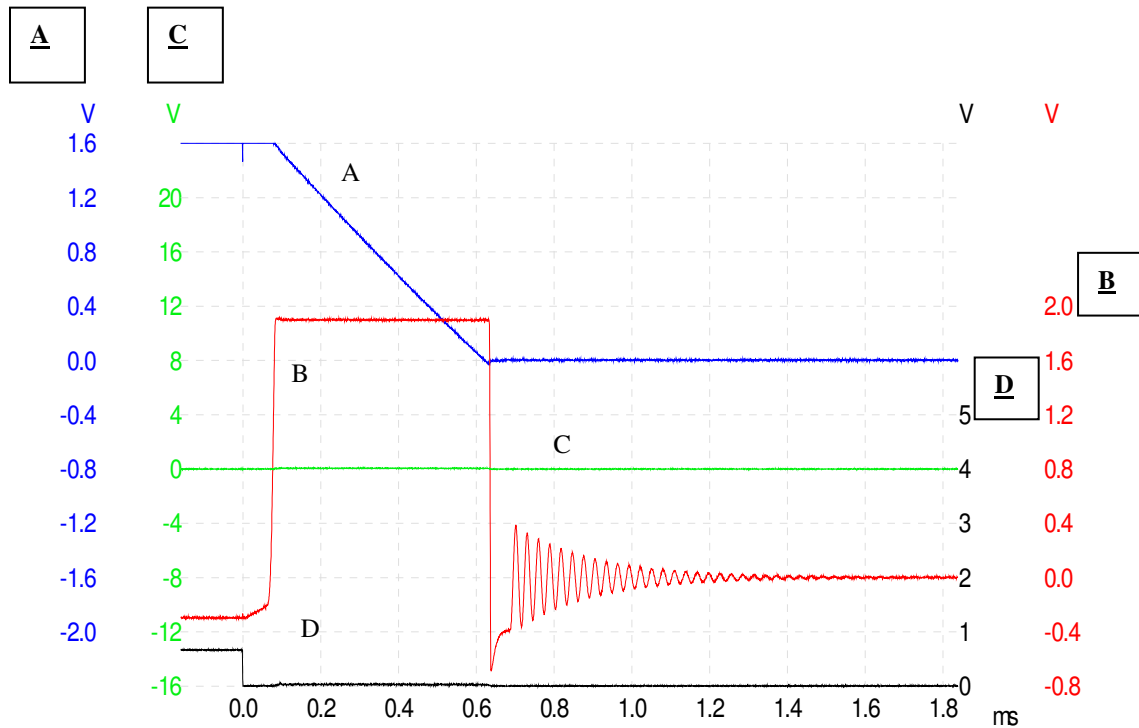
Figure 24 – Oscilloscope Traces from the Rig on a short time-base
(No ferrofluid in coil core and at point of switch-off of field)
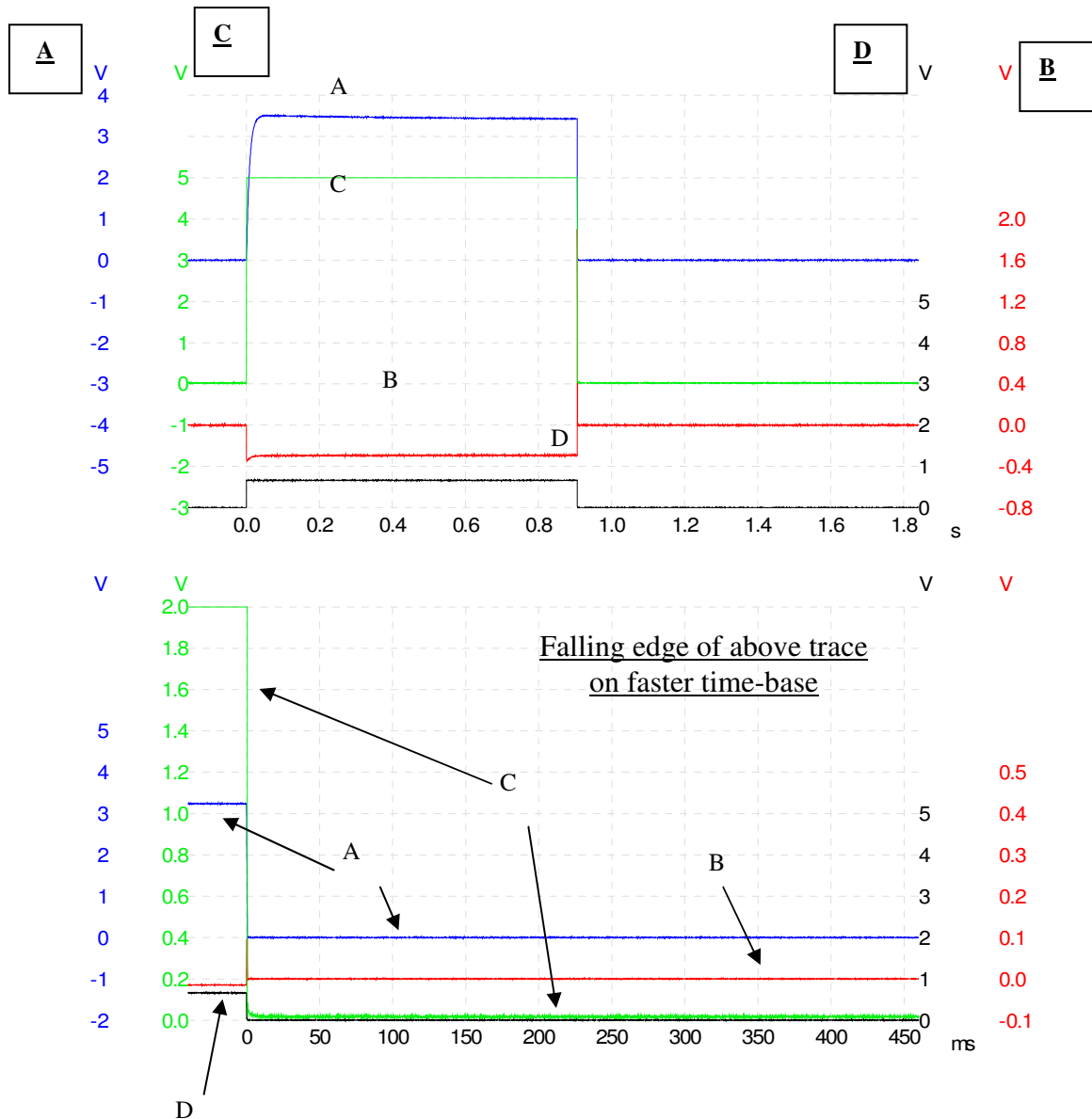
Figure 25 – Oscilloscope Traces from the Rig on a long time-base
(No ferrofluid in coil core)

Figure 24 is an implicit current measurement of current through the coil by measuring the voltage directly across it at switch off. The varistor clamps pin this voltage to about 200V (channel B) whilst the hall-probe (channel A) shows the field slewing in a linear manner, as it must do, by the relation $E = -Ldi/dt$ if the voltage is constant. The rate at which the field switches off is within 0.6ms. The ringing on the channel B waveform occurs when the electromagnet is open circuit. It is definite that this ringing current is exceedingly small as the sensitive hall probe on channel C did not pick up the small magnetic field from it. Clearly it must be less than 1G as 2V on the sensitive probe corresponds to 80G.

Consider now the following traces when ferrofluid (batch F1027A Liquids Research, UK, datasheet and reference on demand from author) is inserted in the coil at different temperatures.
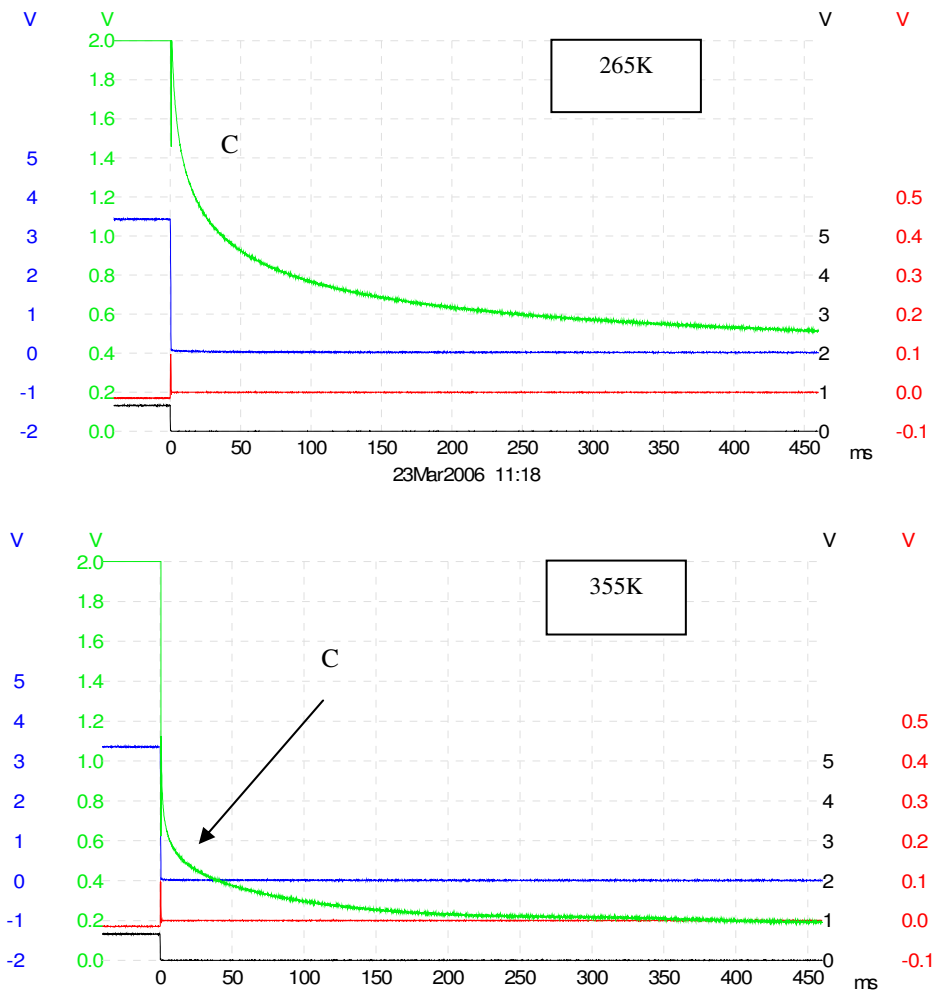
Figure 26 – Oscilloscope Traces from the Rig with Ferrofluid

The first point to notice is the difference in time scales than figure 25, when the field was switched off without ferrofluid.

A second point is to notice the small susceptibility, the magnetising field was about 1800G and the induced flux was about 80G so $\chi \approx 0.04$. The total field in the coil is given by:

$$B_{total} = B_{mag} + B_{ferro}$$

Where B_{mag} is the magnetising field and B_{ferro} is the induction of the ferrofluid.

The ferrofluid looks practically like an air core yet the time constant for B_{ferro} the remnant flux is 100s of milli-seconds. This cannot be explained by the core material of the solenoid somehow boosting the inductance of the coil – that would need a permeability of hundreds. It also would affect B_{mag} (the magnetising field) too and not just B_{ferro}.

Yet, a third point is that the ferrofluid is composed of domain sized ferromagnetic material far below the Curie point. An inductor whose core was made of solid ferrite material would not show temperature related permeability change. It can only be that the rate of relaxation change is related to Brownian or Néel relaxation mechanisms.

Clearly the flux is independent (appendix 8). Some peers struggled with this issue, not seeing how something that looks like an inductor could potentially generate excess power.

Next a power output coil around the ferrofluid sample was set inside the outer magnetising coil. A switch was synchronised to just after the point that the main IGBT power switch (figs. 22, 23) switched off the current to the magnetising coil (by figure 24 this was set about 0.8ms so the current had died down). The power coil switch activated and dumped energy from the remnant flux into a resistive load. Shown below is the plot of the square root of the electrical energy vs. the initial remnant magnetisation for 100 turns on the power coil, then 205 turns for a range of resistances (given in the right-hand panel).
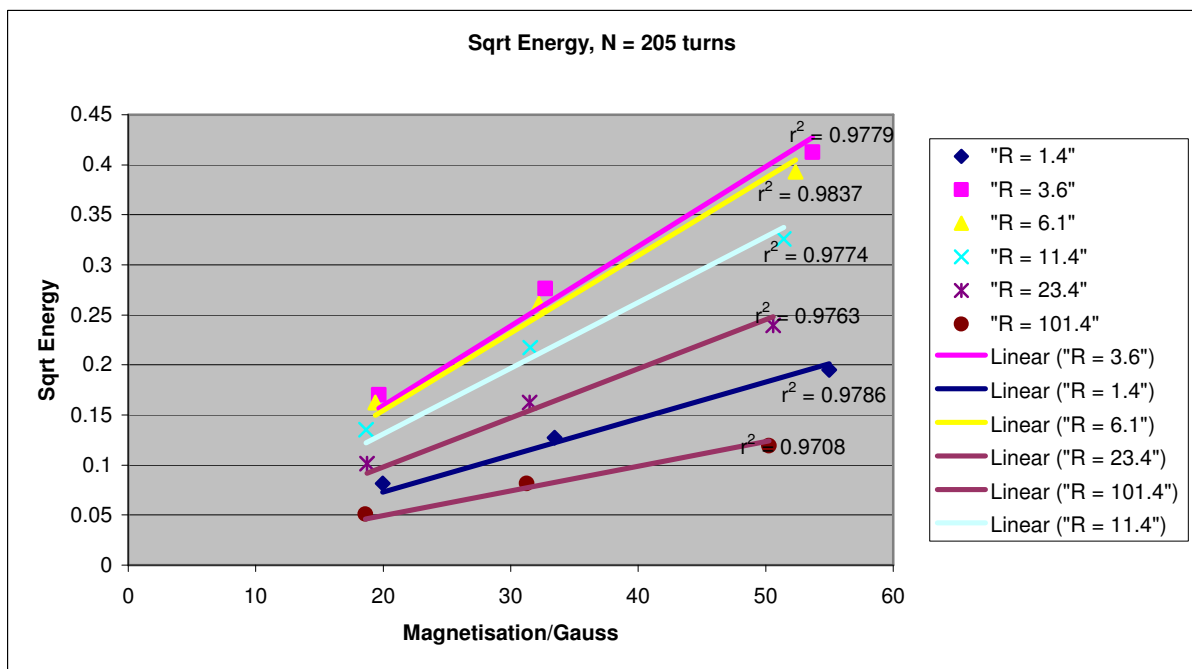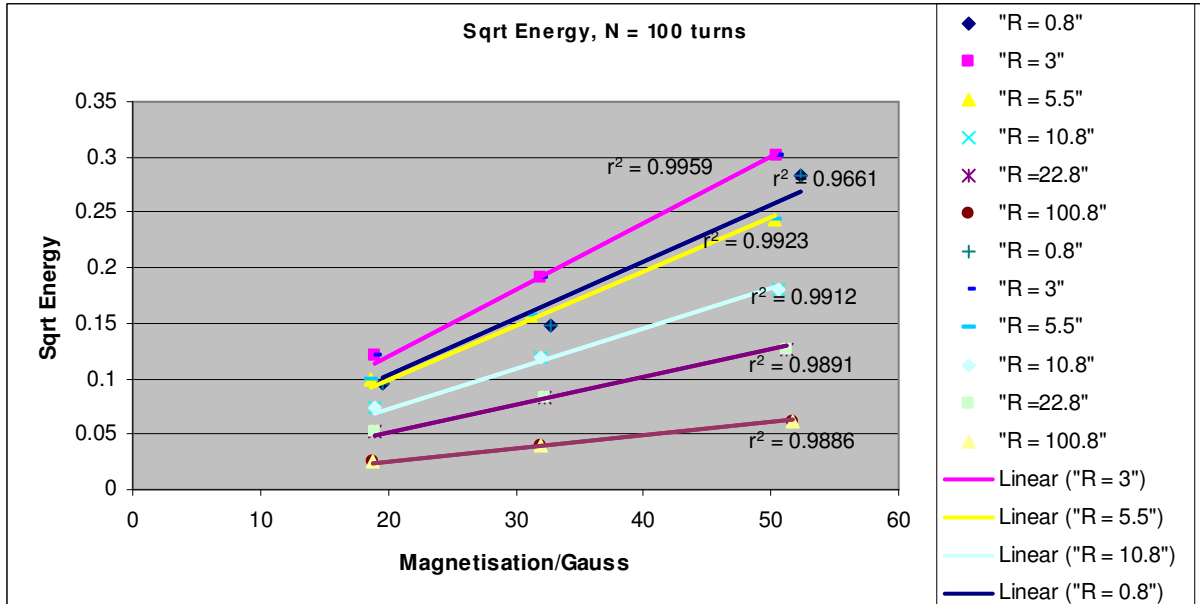
Figure 27 – Electrical energy dumped into load by remnant flux vs. M, N, R
(r^2 values indicate linear regression analysis correlation)

According to eqn. 90 in appendix 4, the electrical energy is proportional to M^2 and inversely proportional to R. The next step seemed straightforward, keep lowering the load resistance until excess power was achieved. A puzzling result was achieved (figure 28).
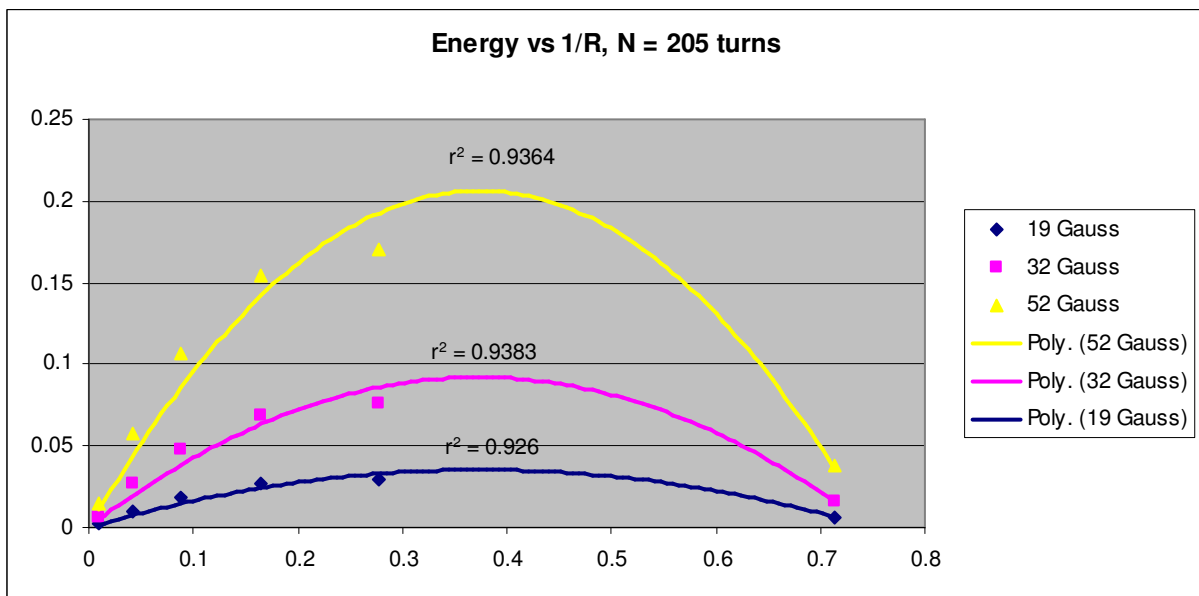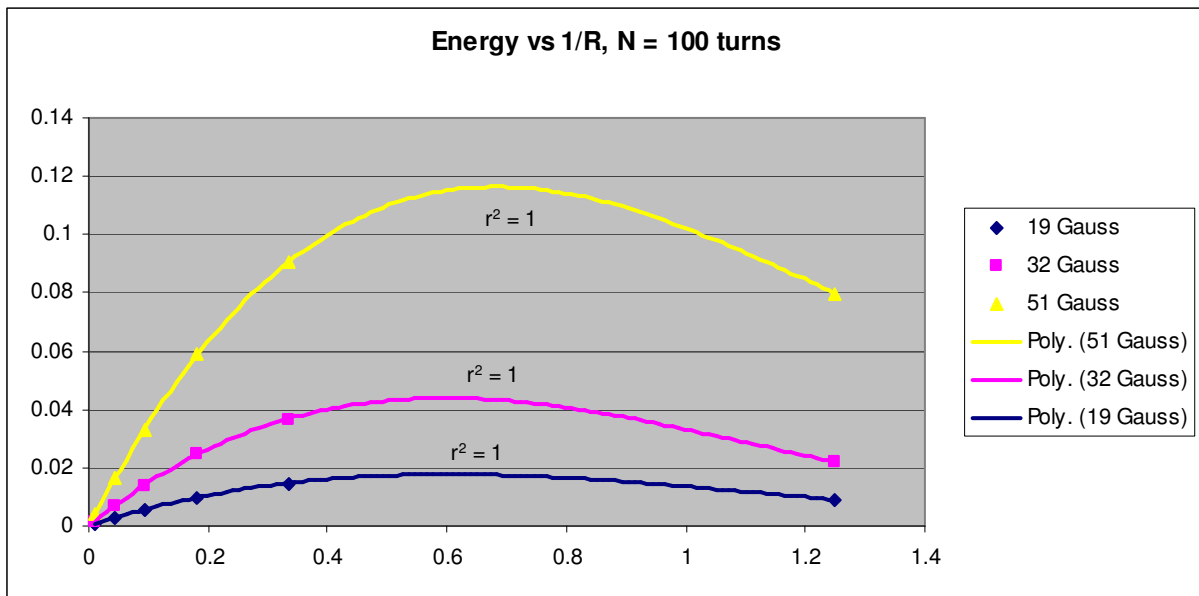
Figure 28 – Electrical energy dumped vs. 1/R by experiment
(r^2 values indicate linear regression analysis correlation)

Initially to the left-hand-side the graph was linear agreeing with eqn. 90, however it did not make sense that at low resistance (to the right-hand-side) that power should fall. It was realised that the reason for this was the power switch and coil in series with the load (figs. 23, 30) have finite resistance: it was a simple potential divider effect. A compensated graph was attempted (not presented) but it still had a maxima and this was due to the power switch (a field effect transistor) being non-linear. The form of the graph suggested was a plateau but this was still a puzzle.

Rig 1 is simple but it was able to show a phenomenon that the author hadn't initially accounted, power extraction wasn't a matter of simple induction.

On investigation with another oscilloscope connected directly across the load, the trace in figure 29 was obtained. There are two sets of traces of the induced voltage from the decaying flux in the power coil: the left-hand is from the load being 22.6 ohms, the right-hand 1.6ohms. (The electrical noise on the second trace isn't important). The right-hand trace is considerably slowed with lower resistance loading – this indicates that a fixed amount of energy is being returned and explains the plateau (once corrected) in the graphs of figure 28.
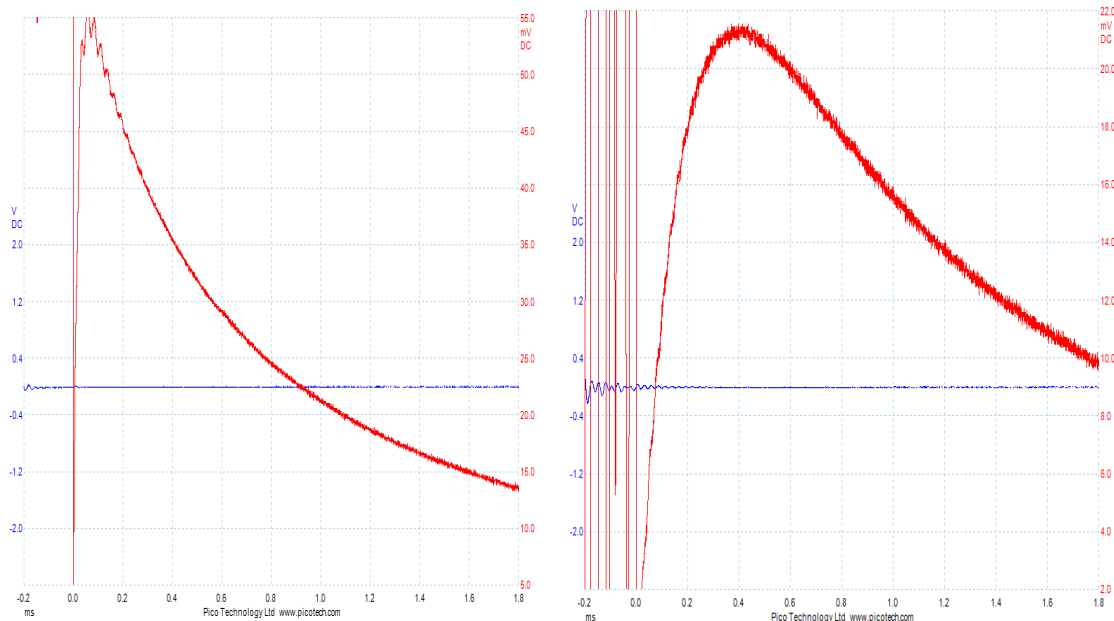
Figure 29 – Loading Effects

There appeared to be some "re-magnetising" effect from the induced current affecting the decay of the ferrofluid flux. This spurred on the development of the electrodynamic model which eventually resolved this puzzle by the model in section 4.

3.2. Design of the 2nd rig: An efficient means of cycling magnetising fields

The previous section suggested a means of applying the magnetising pulses to the ferrofluid however, on a practical level it is not easy to generate such pulses in a regenerative manner. Also their sudden switch off is desirable as it leaves the greatest remnant flux but the rapid switch on causes heating and hence dissipation by the high frequency components of the waveform (appendix 5). The field cycler method is wasteful as it does not recoup the magnetostatic energy of the "H-field". By analogy to a combustion engine, the flywheel is able to store power used in the compression process, recoup it for the next compression event. Here we shall find a relatively easy way to recoup the magnetising field energy between cycles. This leads to a more compact, elegant and efficient device.

Figure 30 shows a regenerative means to cycle the magnetising fields. A low resistance LCR circuit is commuted by a triac[18] (or better, an ohmic mosfet) at zero crossing. A power coil around the solenoid is then switched in after zero crossing in the first circuit, which collapsing the remnant flux into an electrical load. Some of the developed power can be used to re-charge the capacitor against the losses for the next cycle as well as, of course, deliver useable power conversion.

On the next page (fig. 31) is shown two simulation oscilloscope traces: the upper trace is the field H and the lower is the induced magnetisation M. It can be seen that the magnetisation typically follows the H field with a lag (more on this in a later section) and when the H field is zero, the magnetisation decays providing an independent flux. In the first trace, the H field cycles so slowly that there is hardly any lag and hence remnant flux. Figure 32 is the Multisym PSpice[19] front end of the simulation.
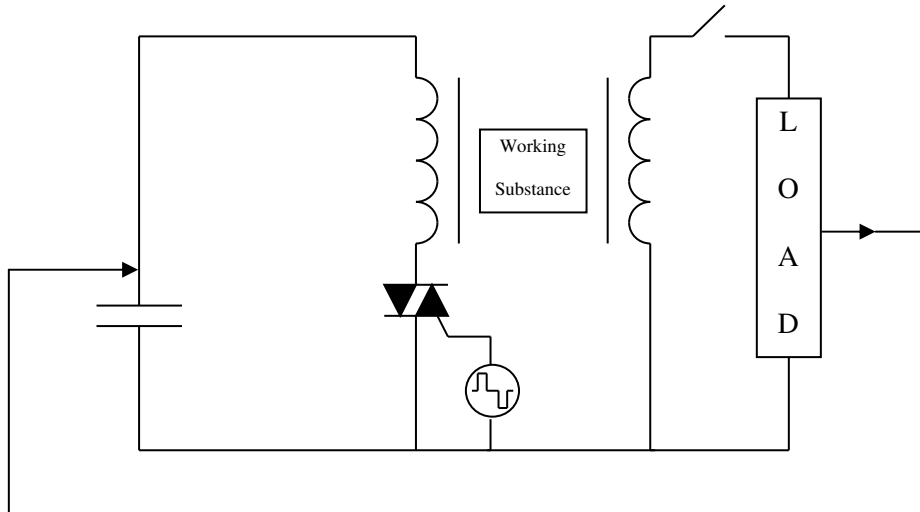
Figure 30 – A Regenerative means to Cycle the Magnetising Fields

Traics have a voltage drop but their natural commutating action can be used to switch FETs that behave quite ohmically when switched on "hard"; this would lead to a more efficient regenerator.

Other methods falling within the canon of electrical engineering include use of "Litz wire" to minimise the Skin Effect[6] (and hence the increase in circuit resistance with frequency) to lower resistive losses. The magnetising current can be greatly reduced by use of high permeability materials immersed into the ferrofluid such that the fringing fields penetrate the ferrofluid. In general, too, the whole plant would be under computer control to maintain a steady power output given the variation in temperature at the reservoir and the like.
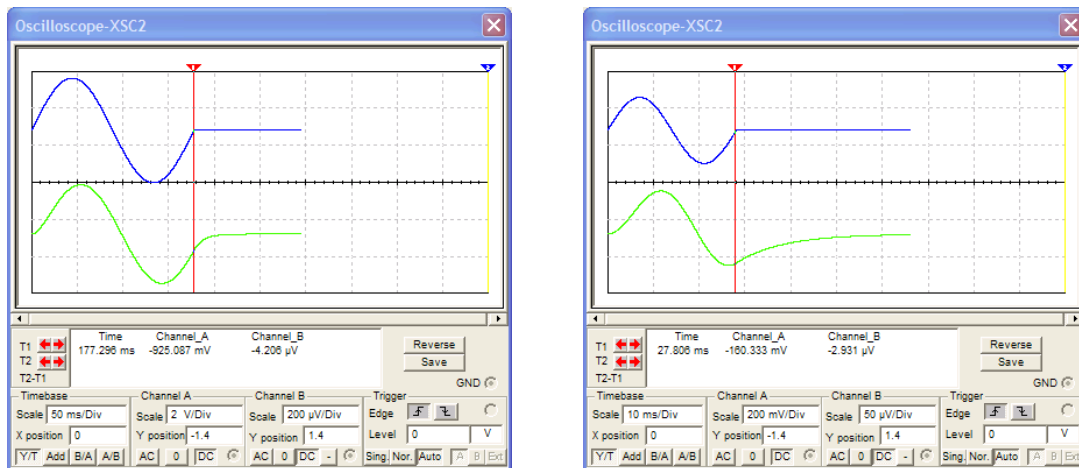
Figure 31 – Quick and Slow Ferrofluid response to Magnetising Field by simulation
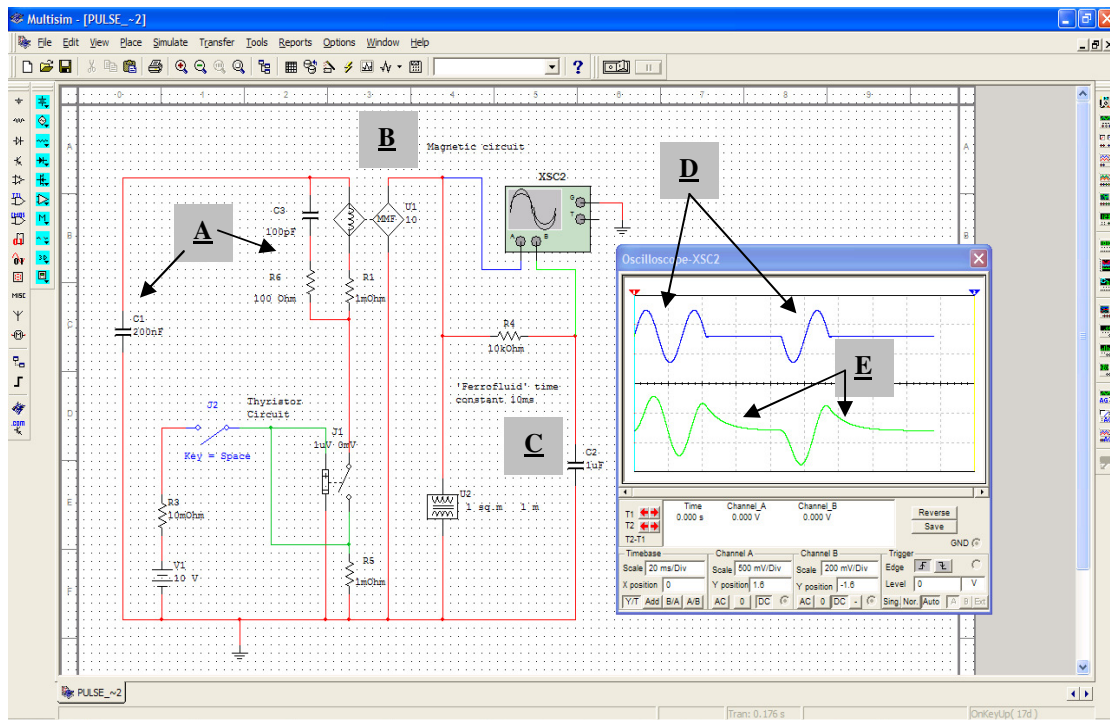
Figure 32 – Multisym PSpice front end showing parameters for simulation

3.3. Use of 2nd rig for excess power generation

The first rig was essentially one-shot in operation. The second rig was designed to allow the efficient, rapid and repetitive generation of pulses such that a temperature drop and power generation will be discernable, whilst on single shot operation this would be difficult. If the cycle frequency is F Hertz, we'd expect the main power input to be that required for magnetising, which would be a function of HdB[6, 9]:

$$P_{in} = \eta \frac{1}{2} \mu_0 \mu_r H^2 V \cdot F + \mu_0 \mu_r H M V \cdot F \qquad \text{eqn. 25}$$

The constant η in front of the magneto-static energy term is small and reflects the action of the field regenerative method of the second rig in recouping this energy. The constant is potentially less than 0.05 representing 95% efficiency in recouping ability and would compare favourably with switched mode power supplies[18]. The last term is the familiar magnetisation energy.

We shall see in section 4.3 that the power output doesn't go naively with a Faraday's Law/Ohm's Law result of being inversely proportional to the load resistance (eqn. 90, appendix 4) nor is it proportional to the inverse square of the ferrofluid relaxation rate; the best we can hope for is some factor K_{ou} (up to ten so far in simulation) greater than the magnetisation energy, thus:

$$P_{out} = K_{ou} \cdot \mu_0 \mu_r H M V \cdot F \qquad \text{eqn. 26}$$

The feature of the temporary remnant cycle is the dipole-work term that comes about from the abrupt removal of the magnetising field. Appendix 8 deals with the case when the magnetising field switch off is done at a finite speed; as the switch off time (slew-rate) dominates, the power output becomes less and less and this is reflected in a power de-rating factor eqn. 130 that multiplies eqn. 26. By these considerations we can gain an understanding as to the range of likely relaxation rate for the ferrofluid to be tailored to, given the limiting speed of the slew-rate on switch off. Power electronics semi-conductors are characterised by an obviously physically large size to allow heat dissipation through cooling surfaces. Their size means that their internal capacitances and inductances realistically limit switching speeds to the order of 1MHz and so we'd expect the fastest ferrofluid we could use to be of the order of 100KHz relaxation rate.

4. Electrodynamic Analysis and a complete Electro-thermodynamic Model

So far we have discussed the thermal system but equally important is the electrical system. In this section we explain a temporal phenomenon that seems to limit the dipole-work to being under the supplied magnetisation energy – if the load resistance is only linear (sec. 4.2). This limitation is caused by the re-magnetising field from the induced current and a method of circumventing this disturbance, without affecting the induced current, is then discussed (sec. 4.3). The last section lists all the equations for the complete electro-thermo model.

4.1. The Electrical State Equations

$$L = \mu_0\mu_r \frac{AN^2}{D}$$

$$\lambda = NA\mu_0\left(H + M\right)$$

FERRO FLUID

A cross-sectional area
D length
N turns

i

R
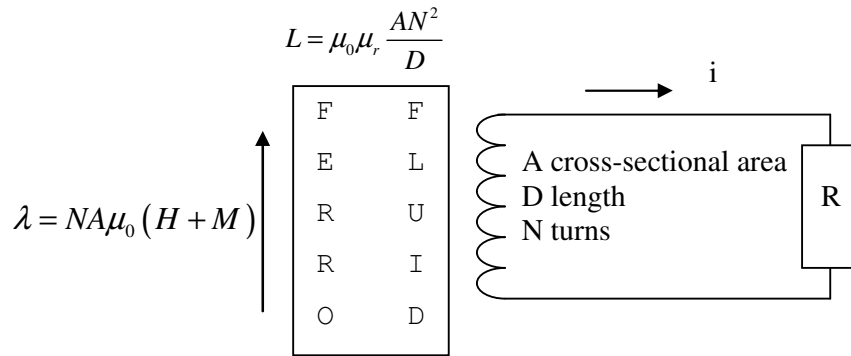
Figure 33 – The Electrical Schematic for the Electrical State Equations

A mathematical model can be constructed for the working substance and electrical output circuit. Let us first consider the ferrofluid flux decaying into a linear resistor, figure 33 shows the arrangement:

The flux linkage is given by (μ_r is the relative permeability):

$$\lambda = NAB \Rightarrow NA\mu_0\mu_r\left(H + M\right) \qquad \text{eqn. 27}$$

The magnetic field is given by:

$$H = \frac{N}{D}i \qquad \text{eqn. 28}$$

Where i is the current through the coil, N is the number of turns and D is the length. The ferrofluid or super-paramagnetic material in general obeys a 1st order equation (previous section) and implicit in this is the convolution of the H field with magnetisation M[‡]:

$$\frac{dM}{dt} = -\frac{1}{\tau}\left(M - \chi\mu_r H\right) \qquad \text{eqn. 29}$$

That is, the rate of change of the magnetisation is negatively proportional to the existing magnetisation minus the driving contribution of the magnetic field (boosted by the susceptibility χ and permeability μ_r), thus when H is substituted, the following is obtained:

$$\frac{dM}{dt} = -\frac{1}{\tau}\left(M - \chi\mu_r\frac{N}{D}i\right) \qquad \text{eqn. 30}$$

The LR circuit, on analysis considering the voltages yields the following, another state space equation:

[‡] A saturation factor $\frac{dM}{dt} = -\frac{1}{\tau}\left\{1 - \frac{M^2}{M_S^2(0)}\right\}\left(M - \chi\mu_r H\right)$ can be introduced from $M = M_S(0)\tanh\left(\chi H\right)$

$$-\frac{d\lambda}{dt} - iR = 0 \Rightarrow -\dot{\lambda}_M - \dot{\lambda}_H - iR = 0$$

$$\Rightarrow -\mu_0\mu_r AN\frac{dM}{dt} - \mu_0\mu_r\frac{AN^2}{D}\frac{di}{dt} - iR = 0$$

$$\therefore \frac{di}{dt} = -\frac{D}{\mu_0\mu_r AN^2}\left(\mu_0\mu_r AN\frac{dM}{dt} + iR\right) \qquad \text{eqn. 31}$$

Or substituting $\frac{dM}{dt}$ from eqn. 30,

$$\frac{di}{dt} = \frac{D}{N\tau}M - \left(\frac{\chi\mu_r}{\tau} + \frac{DR}{\mu_0\mu_r AN^2}\right)i \qquad \text{eqn. 32}$$

The two equations eqn. 30 and eqn. 32 are suitable for coding on a digital computer and figure 34 shows typical output from Matlab code (appendix 10)

4.2. A simple electrical load only returns part of the magnetisation energy

Simulation (figures 34 and 35) and indeed experiment have found that a simple resistive load always returns less energy than the magnetisation energy input. The work done magnetising is given by: $\int HdB \cdot dV$ of which the "H" field energy is discarded, as this can be returned with total efficiency if done by a mechanical magnetisation process or very nearly so with an electronic process (sec. 3.2), leaving:

$$\int_{M,V} \mu_0\mu_r HdM \cdot dV = \mu_0 HM'V$$

The integrand has been resolved with the relative permeability of the material in close proximity to the working substance (the "co-material") subsumed into M'. We can further write the integrand by $M' = \mu_r\chi H$ as (dropping the primes):

$$\boxed{E_{mag} = \frac{\mu_0}{\chi\mu_r}M^2V} \qquad \text{eqn. 33}$$
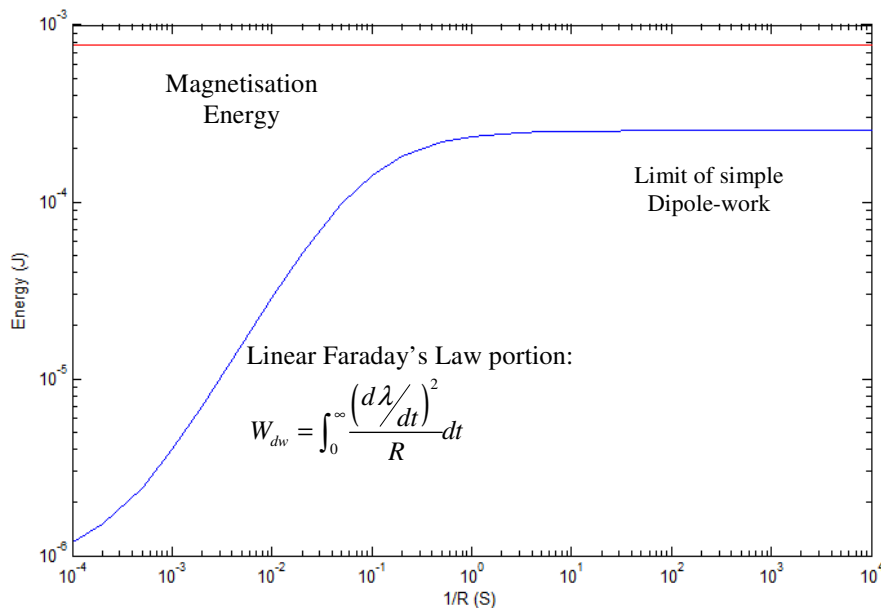
Figure 34 – Simulation Results: Energy vs. 1/R
(Parameters at start of simulation code, appendix 10)

We shall now show that the lower returned dipole-work is due to the phenomenon of the slowing of the current waveform (fig.35): Taking the Laplace Transform of eqn. 30 and eqn. 32 and the set solved for I(s) in the s-domain to yield $\left(\text{with } L = \dfrac{\mu_0 A N^2}{D} \right)$,

$$I(s) = \frac{\dfrac{DM_0}{N}}{s^2 \tau_{ferro} + s\left(\dfrac{R}{L}\tau_{ferro} + (1+\mu_r\chi) \right) + \dfrac{R}{L}}$$

eqn. 34

The dominant pole near the origin sets the dynamics, and a binomial series expansion of the roots of the denominator gives: $as^2 + bs + c = 0 \Rightarrow s \cong -\dfrac{b}{2a} \pm \dfrac{b}{2a}\left(1 + \dfrac{1}{2}\left(\dfrac{-4ac}{b^2} \right) + \dfrac{1}{2} \cdot - \dfrac{1}{2} \cdot \dfrac{1}{2!} \cdot \left(\dfrac{-4ac}{b^2} \right)^2 + O(n^3) \right)$
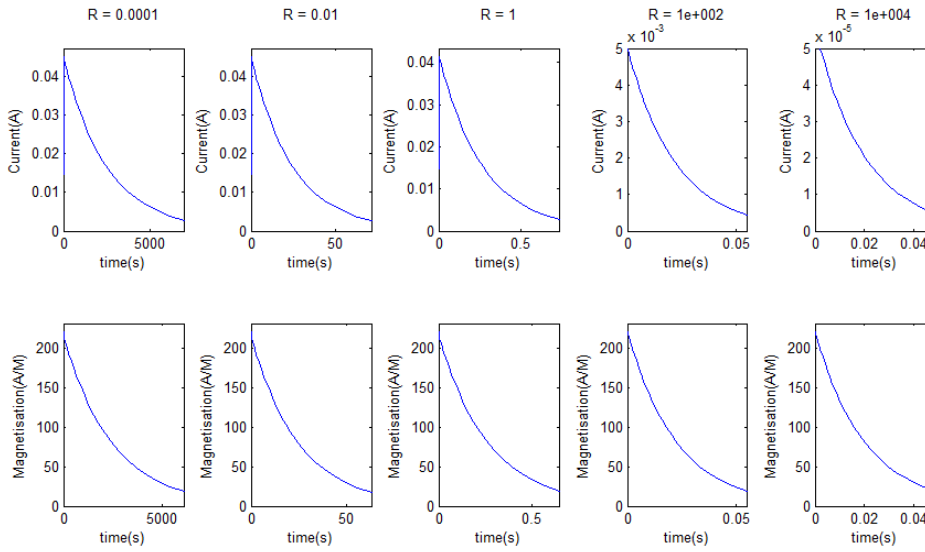
Figure 35 – Simulation Results: Current vs. Time
(Parameters at start of simulation code, appendix 10)

The dominant pole gives the response:

$$s \cong \frac{c}{b} \Rightarrow -\frac{1}{\tau'_{ferro}} = -\frac{1}{\tau_{ferro} + \dfrac{L(1+\mu_r\chi)}{R}}$$

eqn. 35

Thus $\tau'_{ferro} = \tau_{ferro} + \dfrac{L(1+\mu_r\chi)}{R} \ \Rightarrow \ \tau_{ferro}\big|_{R\to 0} \to \tau_{elec}$ the 2nd term is a purely electrical circuit effect (inductor-resistor circuit) which dominates at high loading (R→0). The current induced into the power coil is then:

$$i(t) = \frac{DM_0}{N} e^{-t/\tau'_{ferro}} = \frac{DM_0}{N} e^{-tR/L(1+\mu_r\chi)}$$

eqn. 36

The electrical work delivered to the load is: $\int_0^\infty i^2(t)\,R\,dt$ by which we can calculate the work as the time constant stretches to infinity (the plateau of the dipole-work on figure 34):

$$\boxed{W_{dw.L/R\to\infty} = \frac{1}{2}\frac{\mu_0}{(1+\chi\mu_r)}M^2 V}$$

eqn. 37

This expression for the ultimate simple dipole-work, eqn. 37 is seen to be less than the magnetisation energy eqn. 33.

4.3. The "H-Field Cancellation" Method

In the previous section it was shown that a resistive electrical load on its own only returned part of the input magnetisation work. What was manifest was a slowing in the time constant of the induced current waveform. Heuristically this effect arises due to the re-magnetisation term in eqn. 29, as without it the ferrofluid would relax at its native rate. This is shown circled below:

$$\frac{dM}{dt} = -\frac{1}{\tau}\left(M - \chi\mu_r H\right)$$

The technique is to provide a cancelling magnetic field that has no effect on the ferrofluid or the power extraction circuit and this is depicted in figure 36. Discussion proceeds to explain the most pertinent features of the circuit first.
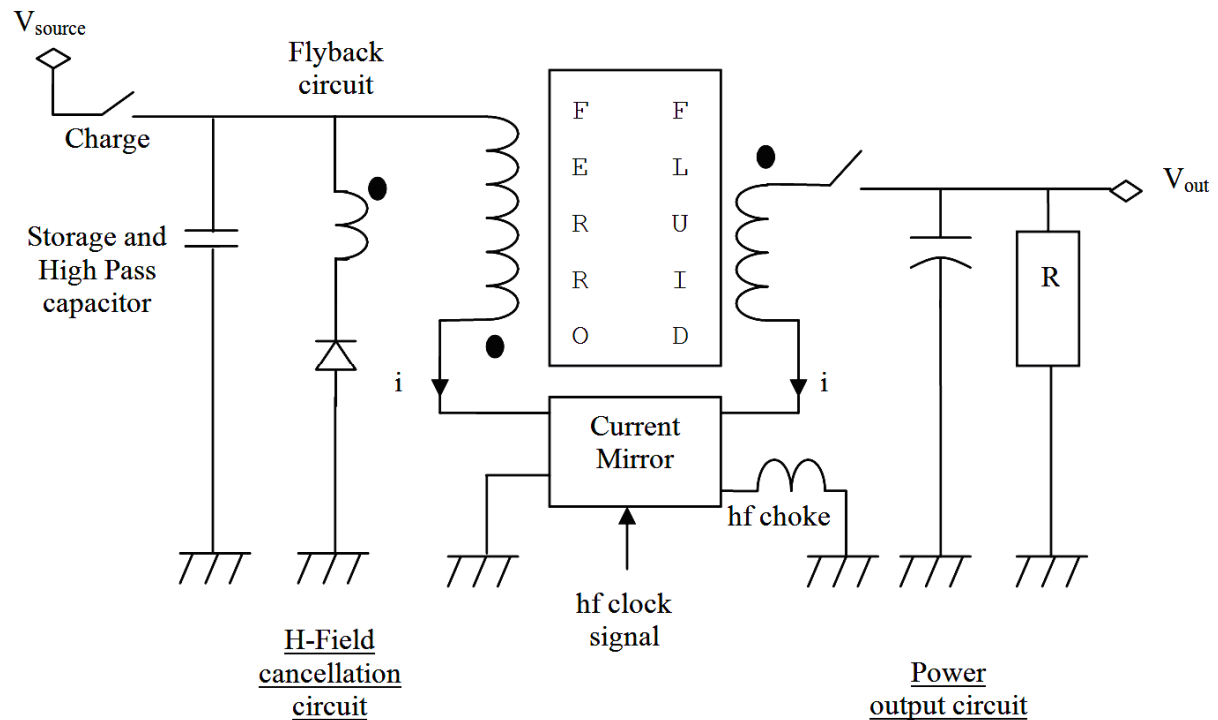
Figure 36 – The H-Field Cancellation Scheme (LHS circuit)

A current mirror[18] makes an inverted duplicate (or some proportion) of the induced current in the power output circuit (RHS) in the LHS circuit (hence it is proportional to H). This is "chopped" by the high frequency clock signal such that the current on the LHS has high frequency harmonics (fig. 37 and appendix 9).
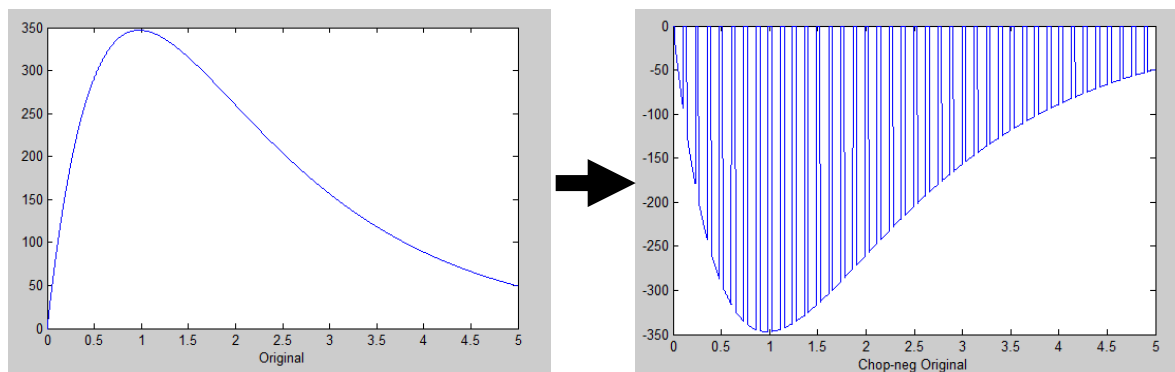
Figure 37 – Sampling, inverting and "chopping" the current/H-field

The magnetic field resulting from this current in the LHS coil (scaled by a different turns-ratio) superimposes on the H-field from the RHS coil to yield a resultant H field with high frequency harmonics (figure 38). The ferrofluid is impervious to high frequency signals (as figure 54, appendix 5 shows); if the frequency is very high, the induced moment will be so low that the dissipation in the ferrofluid will tend to zero. Comparing the right-hand graphic of figure 38 and comparing this with the left-hand graphic of figure 37, we can see that the H-field impinging on the ferrofluid and re-magnetising it has been reduced.
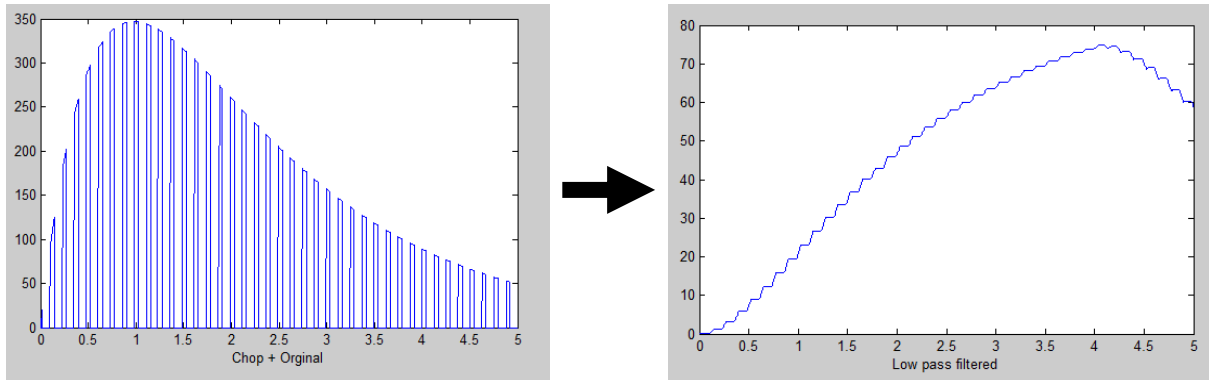
Figure 38 – The resultant high frequency H-field gets low-pass filtered

An even better scheme is depicted in figure 39 where a higher frequency is used with asymmetric summation, in this case -1.5 x the original current. The re-magnetising field is virtually eliminated. The ultimate electrical work that can be extracted by this scheme will be calculated in section 4.3.2 but first we shall explain the action of the other relevant circuit components in figure 36 with a view to the electrical work required to perform the cancellation method and whether it would exceed the work being generated by the right-hand-side circuit.
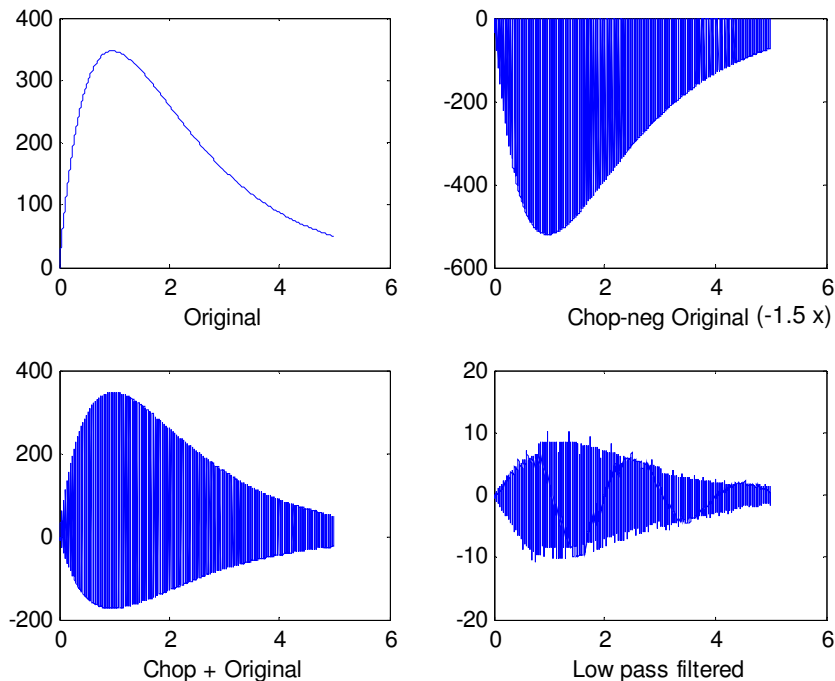
Figure 39 – Asymmetric sampling and summation

4.3.1. Electrical analysis of the work required by the H-field cancellation circuit

We proceed to analyse the energetics of the scheme by the equivalent circuit of a null transformer (fig. 40), that is, a transformer with two windings in intimate contact with equal and opposite currents flowing through the windings. The result is that there is obviously no effect in this case and by deviating from the arrangement, we show the validity of the circuit in figure 36.
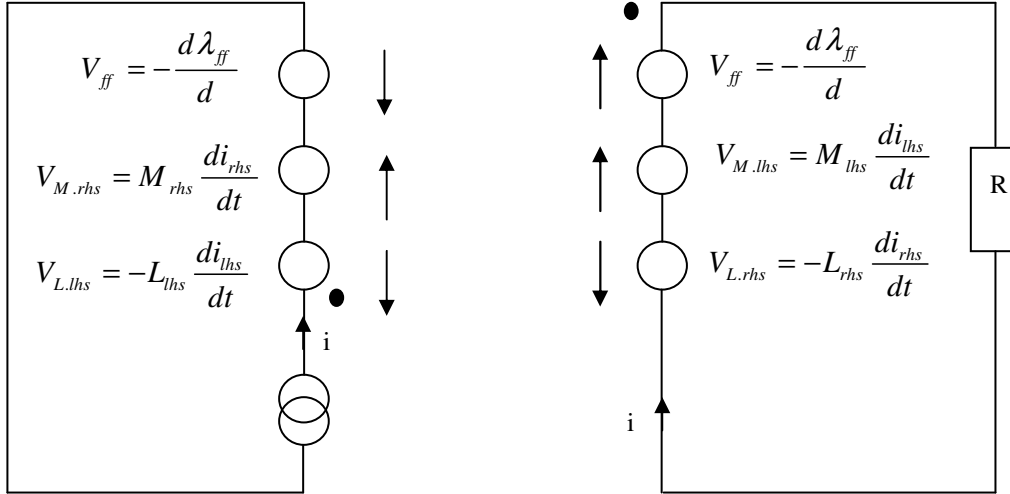
Figure 40 – Null transformer as starting point for analysis

The sense of the currents and voltages from the self and mutual inductances and the decaying ferrofluid flux, $V_{ff} = -\dfrac{d\lambda_{ff}}{d}$ is shown. It is quite clear that the LHS current mirror does work *against* the decaying ferrofluid flux and this is of course *at least* equal to the work that is supposed to be delivered onto the RHS into the load. It is obvious that no power is delivered to the load. Another way of putting this is, of course, that it is a null transformer with changes in magnetic field excluded from the coils' interior. Another way, still, is to note that the current in the LHS circuit is equal and opposite to the RHS and that this is induced into the RHS circuit nullifying all current.

Next we note the addition of the filtering circuit elements from figure 36, the high pass (and storage capacitor) on the LHS and the high frequency inductor (hf choke) on the RHS:
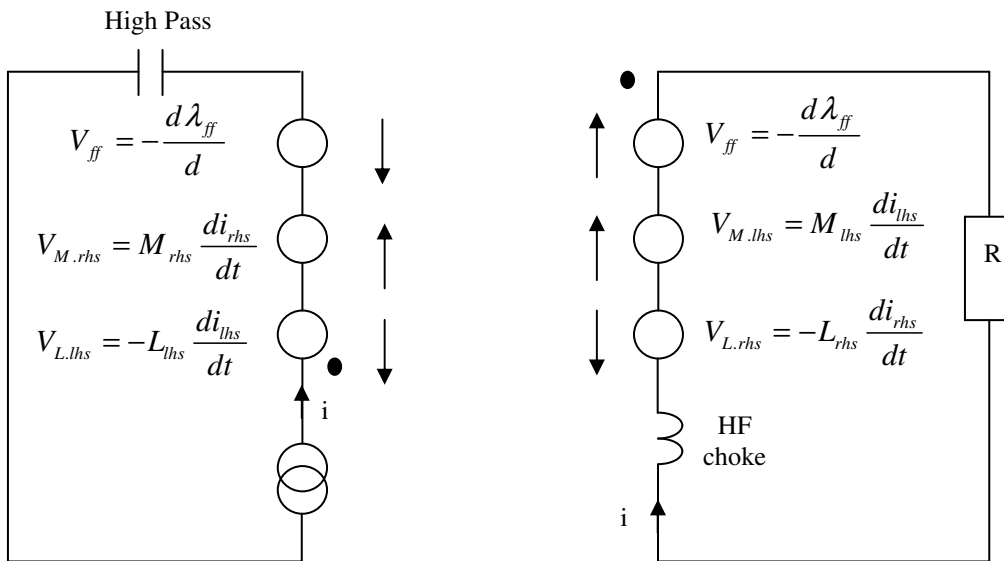
Figure 41 – Addition of filtering circuit elements

Now the situation is different: Firstly the high frequency series inductor (or "choke") blocks the high frequency chopped current from the LHS being induced into the RHS and the "high pass" capacitor blocks the low frequency current from the RHS being induced in LHS. This can be understood by a simple potential divider effect (fig. 42):

$$V_{ff} + V_{M.rhs} =$$
$$-\frac{d\lambda_{ff}}{dt} + M_{rhs}\frac{di_{rhs}}{dt}$$

C_{HP}

R_{CS}

$$V_{chop} = -\frac{d\lambda_{chop}}{dt}$$

L_{choke}

R

LHS circuit potential
divider

RHS circuit potential
divider
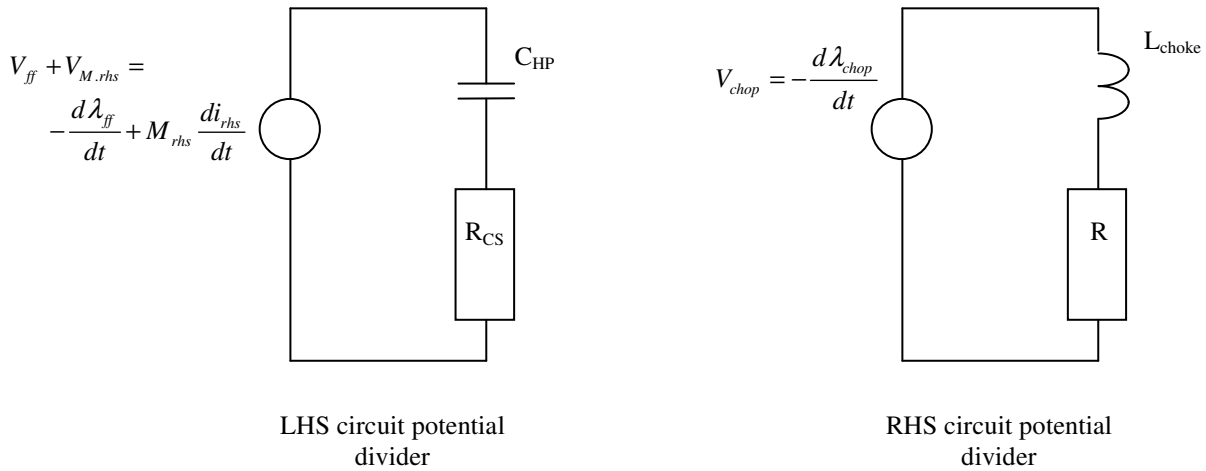
Figure 42 – Potential divider to analyse electrical work

In the left-hand figure, the dynamic impedance of the current source is represented by R_{CS}. It is a simple matter to find the voltage across the current source induced by the changing ferrofluid flux and deduce that with a relatively low rate of change of ferrofluid flux, with a small capacitance, very little voltage and hence work is done against the current source.

$$V_{R_{CS}} = V_{ff}\left(\frac{R_{CS}}{\dfrac{1}{j\omega C_{HP}} + R_{CS}}\right)$$

The current in the LHS circuit is set-up by the current mirror and this can be a fraction of the current on the RHS, all that matters is that the turns-ratio of the coil is sufficient to cancel the H-field from the RHS circuit. In the limit of small current, it is obvious that the electrical work performed by the changing ferrofluid flux is less than that performed on the RHS circuit.

Further to the argument, the current source mainly performs electrical work establishing the cancellation magnetic field on the LHS. This can be recouped with high efficiency by a "flyback" circuit (fig. 36). The current source performs net work against the electrical resistance of the left-hand circuit and this can be made arbitrarily small, in fact to labour the point, a fractional current mirror (fig. 43) can be used (since all that matters is the current multiplied by the left-hand turns to establish the cancelling field) and this makes it even more obvious.

$I_{LHS} = 1/3 \; I_{RHS}$

I_{RHS}

Or in general 1/N, where, N is the number of matched transistors on the RHS. In other words, it is the ratio of the areas of the emitter-base/gate-source regions.
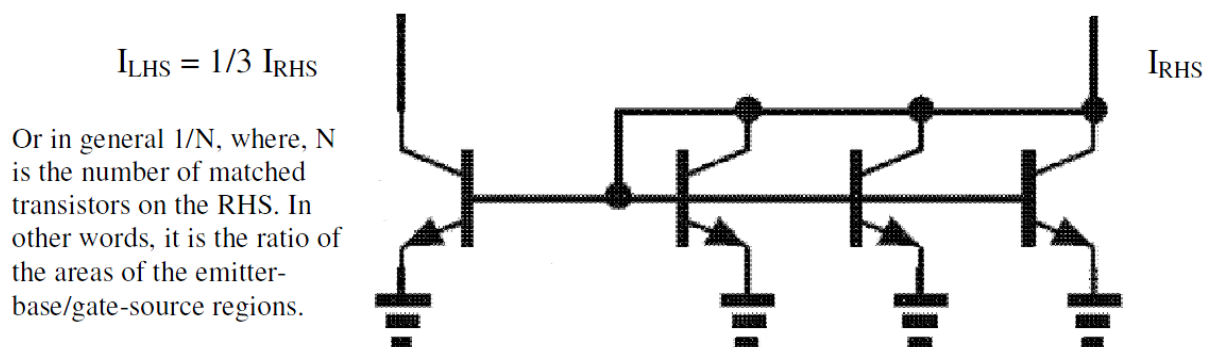
Figure 43 – Current mirror delivering a fraction of the copied current

Considering now the work of the chopping circuit on the right-hand circuit, on figure 42 we can see a similar potential divider effect:

$$V_R = V_{chop} \left(\frac{R}{j\omega L_{choke} + R} \right)$$

This time we note that, the high frequency chopping field results in an high impedance from the choke; very little electrical work is thus expended by the chopping circuit on the power output circuit.

All that remains that needs to be said of the method is that, the capacitor on the left-hand circuit (fig. 36) is charged to a high voltage such that the chopping field changes can be rapidly achieved. Obviously the recuperative effect the flyback circuit won't be perfect and so this capacitor is periodically recharged by the high voltage source, $V_{source.}$

4.3.2. Dynamic analysis of the H-field cancellation method and the ultimate electrical work

We now follow the same procedure with the state equations of 29/30 and 29/30 in section 4.2 but with the re-magnetising H-field removed from equation 29, to yield the transform of the induced current:

$$I(s) = \frac{\dfrac{DM_0}{N}}{s^2 \tau_{ferro} + s\dfrac{R}{L}\tau_{ferro} + \dfrac{R}{L}} \qquad \text{eqn. 38}$$

Whereupon the current in the time domain by the dominant pole is:

$$i(t) = \frac{DM_0}{N} e^{-t/\tau_{ferro}} = \frac{DM_0}{N} e^{-tR/L} \qquad \text{eqn. 39}$$

The dipole-work by the cancellation method in the limit is obtained, once again, by $\int_0^\infty i^2(t)R\,dt$:

$$\boxed{W_{dw.cancel.L/R\to\infty} = \frac{1}{2}\mu_0 M^2 V} \qquad \text{eqn.40}$$

This is seen to be the magnetic field energy of the ferrofluid flux.

The cancellation method has been proven in experiment and simulation (appendix 10) in the first instance by the simple expedient of zeroing the re-magnetisation term:

```
%#################################################
dMdt = (1./tor) .* fac .* ( M - 0.*H.*Xchi.*CONST_perm );
```

The results are displayed in figures 44 and 45. Straightaway, logically, one can see the effect of the ferrofluid relaxing at its native rate in figure 45, lower trace, compared to figure 35.

A more physical simulation, other than the "trick" of zeroing the H-field is implemented at the end of appendix 10 by a high frequency cancellation H-field:

```
%#################################################
dMdt = -(1./tor) .* fac .* ( M - H.*(1-Cancel(t)) ...
    .*Xchi.*CONST_perm);

...
    function field = Cancel(t)
        % Generate square waveform 0-1.5 at frequency "freq"
        freq = 20000; % freq = 100/tor;

        field = 1.5.*(0.5+0.5.*sign(0.5+freq.*t-round(freq.*t+0.5)));
    end
```

Though this code is much slower to run due to the fine time-scale needed to simulate the cancellation field and the potentially long time scale of the electrical circuit.

Comparison is now made to the limit ratios (fig. 44) of equations eqn. 33, eqn. 37 and eqn.40, that is:

$\dfrac{1}{\chi\mu_r} : \dfrac{1}{2(1+\chi\mu_r)} : \dfrac{1}{2}$ with variation of the parameter $\chi\mu_r$ which is the effective susceptibility of the ferrofluid

with the high permeability co-material present and this is plotted in figures 46 and 47. For all variation of parameters, the magnetisation energy is always greater than the dipole-work without the cancellation method. However if $\chi\mu_r > 2$ the dipole-work, with the cancellation method, will exceed the magnetisation energy input.

The power produced by the device is then:

$$P = \left(W_{dw.cancel} - E_{mag} - W_{losses} \right) F_{cycle}$$
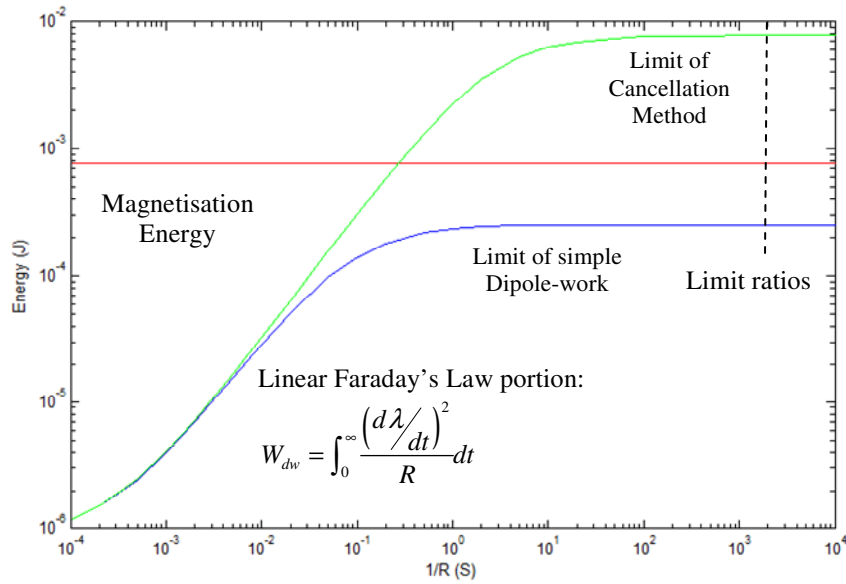
Figure 44 – Dipole-work exceeding magnetisation energy
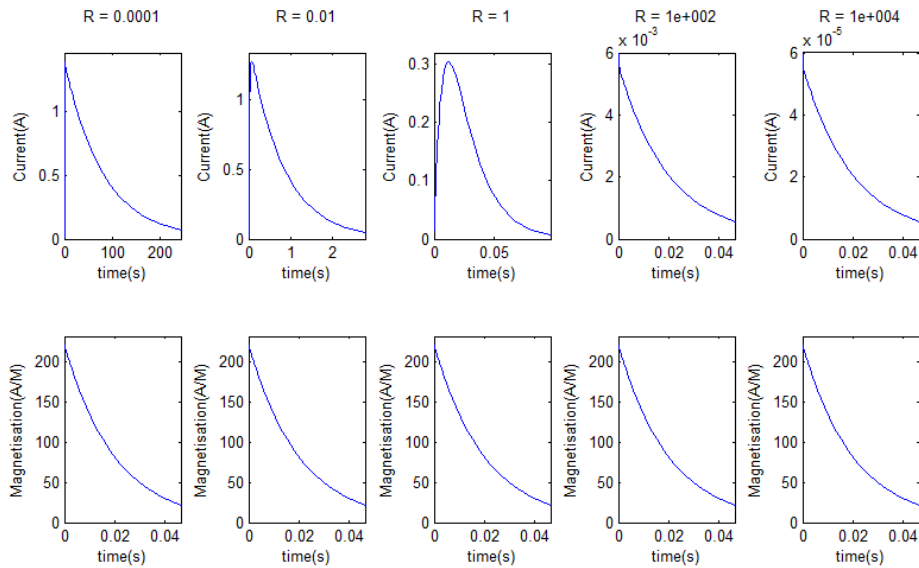
Figure 45 – Results Cancellation Method: Current vs. Time
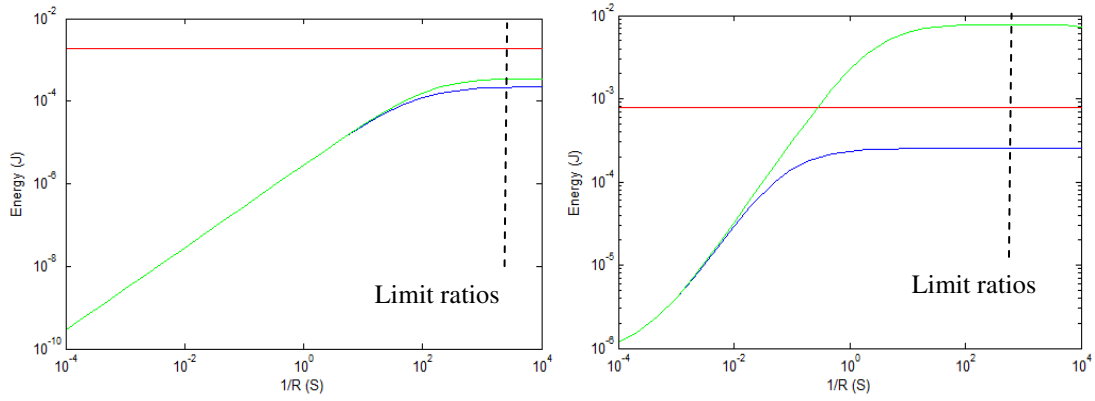
Figure 46a, b – Variation of parameter $\chi\mu_r \approx 0.6, \approx 30$ and $\chi = 0.6$

Red, E_{mag} : $\qquad \dfrac{1}{\chi\mu_r}$

Blue, $W_{dw.L/R\rightarrow\infty}$: $\qquad \dfrac{1}{2(1+\chi\mu_r)}$

Green, $W_{dw.cancel.L/R\rightarrow\infty}$: $\qquad \dfrac{1}{2}$
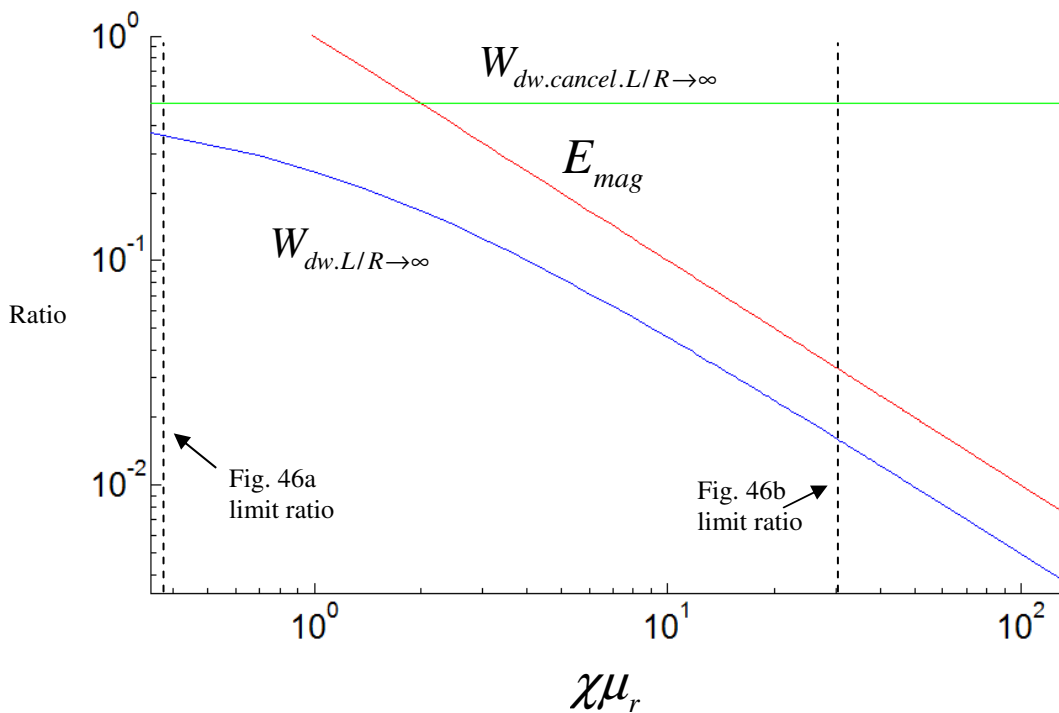
Figure 47 – Variation of parameter $\chi\mu_r$

4.4. The Complete Electro-thermodynamic Model

This section represents the bringing together of all the proceeding sections to build an electro-thermodynamic model of a complete micro-cycle with the working substance held static in the power extraction area. Notes on the model follow the tables.

Physical Properties

Magnetisation: $M = 0.9 M_S(0) \tanh\left(\dfrac{m_{nano} H}{3kT}\right)$ eqn. 67

Brownian: $\tau_B = \dfrac{3V\eta_0}{kT}$ eqn. 66

Néel: $\tau_N = \dfrac{1}{f_0} e^{\frac{KV}{kT}}$ eqn. 65

Susceptibility: $\chi = \dfrac{\partial M}{\partial H}$

State Eqns.

Magnetisation: $\dfrac{dM}{dt} = -\dfrac{1}{\tau}\left(M - \chi\mu_r \dfrac{N}{D} i\right)$ eqn. 30

Current: $\dfrac{di}{dt} = \dfrac{D}{N\tau} M - \left(\dfrac{\chi\mu_r}{\tau} + \dfrac{DR}{\mu_0 \mu_r A N^2}\right) i$ eqn. 32

Temperature: $\dfrac{dT}{dt} = \dfrac{1}{C_H}\left(\dfrac{dQ_{net}}{dt} - \dfrac{dW_{net}}{dt}\right)$ eqn. 123

Entropy: $\dfrac{dS}{dt} = \dfrac{C_H}{T}\dfrac{dT}{dt} - \mu_0 K \dfrac{dH}{dt}$ Note 1

Work

Work balance: $\dfrac{dW_{net}}{dt} = \dfrac{dW}{dt} - \dfrac{dW_{mag}}{dt} - \dfrac{dW_{other}}{dt}$

Net magnetic work: $\dfrac{dW_{mag}}{dt} = f(\omega)\mu_0 H \dfrac{dM}{dt}.V + \mu_0 \dfrac{1}{\tau}\dfrac{L}{R} M \dfrac{dM}{dt}.V$ eqn. 18

(Note 2)   eqn. 97

Other electrical work: $\dfrac{dW_{other}}{dt}$ (e.g. electrical input for regenerative cycling)

Final work: $\dfrac{dW}{dt} = i^2 R$ (this is our final output)

Heat and dissipative elements

Balance Heat:
$$\frac{dQ_{net}}{dt} = T\frac{dS}{dt} - \frac{dQ_{irr}}{dt} - \frac{dQ_{other}}{dt}$$

Dissipation in ferrofluid:
$$\frac{dQ_{irr}}{dt} = f_{irr}(\omega)\mu_0 H\frac{d\mathcal{M}}{dt}\cdot V + f(\omega)\mu_0 H\frac{dM}{dt}.V \qquad \underline{\text{Note 3}} \qquad \text{eqn. 17}$$

Other dissipation:
$$\frac{dQ_{other}}{dt}$$ (eg. can include electrical loss from regenerative cycling)

Figure 48 – The Complete Electro-Thermodynamic Model

Notes:

1. See Rosensweig[2] for the change in entropy $-\mu_0 K\frac{dH}{dt}$ of a (super) paramagnetic material with field. K is called the pyromagnetic coefficient.

2. $f(\omega)\mu_0 H\frac{dM}{dt}.V$ applies on the magnetisation step (V is volume), the function $f(\omega)$ is discussed in section 2.2. On the demagnetisation step the dipole-work $\mu_0\frac{1}{\tau}\frac{L}{R}M\frac{dM}{dt}.V$ applies.

3. On the magnetisation step the dissipation in the ferrofluid is $f_{irr}(\omega)\mu_0 H\frac{d\mathcal{M}}{dt}\cdot V$ (sec. 2.2) and during the second part of the cycle, the demagnetising step, the magnetisation energy $f(\omega)\mu_0 H\frac{dM}{dt}.V$ becomes internal energy (section 2.2.2, figure 16).

4. The model has infinite slew rate when switching off the magnetic field so the considerations of appendix 8 have not been added.

5. Conclusion

A new type of magnetic heat engine has been presented here that can both directly generate electricity and cool. It is based on the recognition of a 3rd new term in the thermodynamic identity called, dipole-work. This dipole-work is able to utilise the collapse by Brownian motion of the remnant flux in the latter half of its cycling regime. This thesis is built on the foundations of Kinetic Theory, Thermodynamics, Electrodynamics and experiment.

Kinetic Theory shows that the relaxing magnetic field acts as a velocity damping term to each magnetic dipole undergoing Brownian motion. The torque each dipole experiences is const x MdM, that is proportional to the dipole self-work. The electromagnetic field couples to the thermal system, the electromagnetic system then couples to the external electrical system to which power is transferred.

Thermodynamics shows:

- A "delta T", a change in temperature of the working substance from the magnetic work related to the magnetic properties of the material.

- On considering the magnetic enthalpy[11], a new term "MdM" called the dipole-work is added onto the thermodynamic identity and is only relevant when heat transfer occurs. This happens on the second half of the Temporary Remanence cycle. This ties in with the Kinetic Theory where MdM is the velocity damping term.

- T-S diagrams show how the entropies of the magnetic system form a heat engine. Tying in with Kinetic Theory, once again, the variation in entropy associated with the velocity distribution of the magnetic particles is the source of the heat transference.

- An energy balance equation that shows how the internal energy of the working substance falls with electrical work it performs.

Electrodynamics shows:

- The dynamics of the electrical generation process.

- The work delivered to an electrical load by Faraday/Lenz/Maxwell induction law and that this is of the form MdM, once again.

- The work delivered to an electrical load with the field cancellation technique and that this exceeds the input magnetisation energy substantially. The difference comes from the conversion of heat energy to electrical energy.

The heat engine has a greater range of temperature operation than would be expected from the magneto-caloric effect, as it is based upon magnetic ordering in super-paramagnetic materials. Theory has given a full electro-thermodynamic model which can account for irreversibilities, relate the entropy changes in the working substance to the work and give an estimate of power density of over 6kW per litre; this is substantial and comparable to existing heat engines. Experiment has proven crucial premises that the property of interest, the relaxation rate, is a strong function of temperature and that the temporary remnant flux can provide excess electrical power.

Appendix 1. Magneto-caloric effect Thermodynamic Analysis

Starting with the thermodynamic identity[2, 9, 20, 21] (the magnetic moment is related to the volume magnetisation/dipole moment thus $\mathscr{M} = MV$)

$$dU = TdS + \mu_0 H d\mathscr{M} \qquad \text{eqn. 41}$$

Where H is the magnetic field and M is the magnetisation. Comparing this with the first variation in U with S and H as independent variables (since we control H directly by applying a magnetising field),

$$dU = \left(\frac{\partial U}{\partial S}\right)_H dS + \left(\frac{\partial U}{\partial H}\right)_S dH \qquad \text{eqn. 42}$$

By double differentiation we can see immediately that if $\left(\frac{\partial U}{\partial S}\right)_H = T$ then,

$$\frac{\partial^2 U}{\partial H \partial S} = \left(\frac{\partial T}{\partial H}\right)_S \qquad \text{eqn. 43}$$

Also from eqns. 41 and 42, if $\left(\frac{\partial U}{\partial H}\right)_S = \frac{\mu_0 H \partial \mathscr{M}}{\partial H}$ then on substitution for H by $H \partial \mathscr{M} = -\mathscr{M} \partial H$ double

differentiation gives:

$$\left(\frac{\partial}{\partial S}\right)_H \left(\frac{\partial U}{\partial H}\right)_S = -\left(\frac{\partial}{\partial S}\right)_H \frac{\mu_0 \mathscr{M} \partial H}{\partial H}$$

$$\Rightarrow \frac{\partial^2 U}{\partial H \partial S} = -\mu_0 \left(\frac{\partial \mathscr{M}}{\partial S}\right)_H \qquad \text{eqn. 44}$$

By the chain rule,

$$\left(\frac{\partial \mathscr{M}}{\partial S}\right)_H = \left(\frac{\partial \mathscr{M}}{\partial T}\right)_H \left(\frac{\partial T}{\partial S}\right)_H \qquad \text{eqn. 45}$$

The double differentials are equivalent so,

$$\left(\frac{\partial T}{\partial H}\right)_S = -\mu_0 \left(\frac{\partial T}{\partial S}\right)_H \left(\frac{\partial \mathscr{M}}{\partial T}\right)_H \qquad \text{eqn. 46}$$

By definition, the heat capacity at constant field strength is:

$$C_H = \left(\frac{\delta Q}{\delta T}\right)_H = T\left(\frac{\partial S}{\partial T}\right)_H \qquad \text{eqn. 47}$$

Combining this with the previous equation, we obtain:

$$C_H = -\mu_0 T \left(\frac{\partial H}{\partial T}\right)_S \left(\frac{\partial \mathscr{M}}{\partial T}\right)_H \qquad \Rightarrow \qquad (\Delta T)_S = -\frac{\mu_0 T}{C_H}\left(\frac{\partial \mathscr{M}}{\partial T}\right)_H \Delta H \qquad \text{eqn. 48}$$

The magneto-caloric effect is obviously symmetric in ΔH and that a positive excursion of this variable leads to a positive rise in temperature since $\left(\frac{\partial \mathscr{M}}{\partial T}\right)_H < 0$

The Curie Point Defined

Bozorth[9] replaces $\left(\dfrac{\partial \mathcal{m}}{\partial T}\right)_H$ in eqn. 48 by a change of variables by $\left(\dfrac{\partial H}{\partial T}\right)_{\mathcal{m}}$ to give:

$$\left(\Delta T\right)_S = \frac{\mu_0 T}{C_H}\left(\frac{\partial H}{\partial T}\right)_{\mathcal{m}}\Delta \mathcal{m} \qquad \text{eqn. 49}$$

He is then able to evaluate $\left(\dfrac{\partial H}{\partial T}\right)_{\mathcal{m}}$ by use of the Langevin function (eqn. 64, Appendix 2) which describes the alignment of the spins by the external magnetising field and the self-field of the spin ensemble. Thus he writes:

$$\frac{\mathcal{m}}{\mathcal{m}_0} = L\left[\frac{\mu\left(H + NM\right)}{kT}\right] \qquad \text{eqn. 50}$$

Where N is the "Molecular" or "Weiss mean field constant" related to the exchange force (Appendix 2) And calculates $\left(\dfrac{\partial H}{\partial T}\right)_{\mathcal{m}}$ by differentiating eqn. 50 with respect to H and T whilst holding $\mathcal{m}$ constant, thus:

$$0 = \frac{\mu k T \partial H - \mu k\left(H + NM\right)\partial T}{k^2 T^2}\cdot L'$$

Therefore $\left(\dfrac{\partial H}{\partial T}\right)_{\mathcal{m}} = \dfrac{H + NM}{T}$ and substitution into eqn. 49 yields and noting that $MdM = \dfrac{1}{2}d\left(M^2\right)$,

$$\left(\Delta T\right)_S = \frac{\mu_0\left(H + NM\right)}{C_H}\Delta \mathcal{m} \Rightarrow \frac{\mu_0\left(N + H/M\right)}{2C_H}\Delta \mathcal{m}^2 \qquad \text{eqn. 51}$$

By the graphs below, the Curie point can be seen to be where the change of magnetisation vs. temperature is at its greatest and we note that temperature change is squared in the magnetisation.
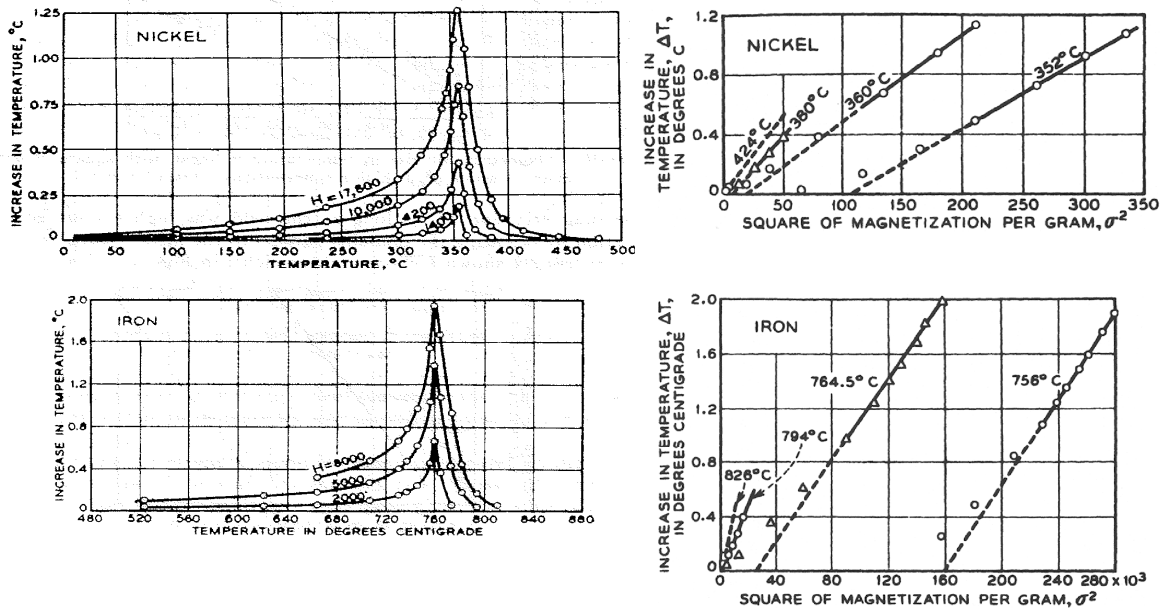
Figure 49 – Magneto-caloric for Nickel and Iron
ΔT vs. T (the magnetic field shown (H) is measured in Oersteds)
and temperature rise is linear with the square of magnetisation.
Figures taken from Bozorth[9]

Temperature Entropy diagram for the Magneto-caloric Effect
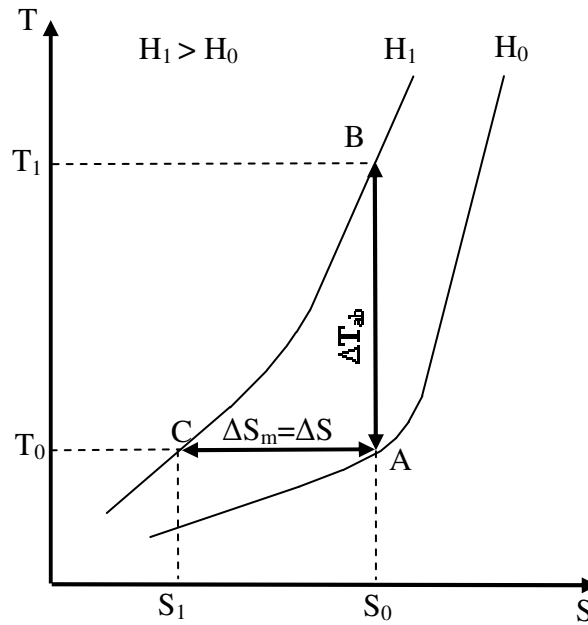
Figure 50 – Dependence of entropy and temperature on the applied field
for a paramagnetic, super-paramagnetic, ferrimagnetic or ferromagnetic material

There are two aspects to the magneto-caloric effect which we can define as occurring adiabatically (ΔT_{ab}) and isothermally (ΔS_m) when the field is changed from H_1 to H_2. In the latter case we note,

$$\left(\frac{\partial T}{\partial H}\right)_S = -\mu_0 \left(\frac{\partial m}{\partial S}\right)_H$$

Whereupon,

$$\Delta S = -\mu_0 \left(\frac{\partial m}{\partial T}\right)_H \Delta H \qquad \text{eqn. 52}$$

The entropy of the material is made up of two quantities, the entropy of the magnetic dipoles and the entropy of the mechanical aspects of the system which itself includes the entropy of the lattice vibrations and the free electron gas.

Appendix 2. The relation between Paramagnetism, Super-paramagnetism and Ferromagnetism

Paramagnetism, super-paramagnetism, ferromagnetism and ferrimagnetism have a unifying micro-magnetic basis starting from the basic unit of magnetism, the Bohr Magneton[4, 6, 9, 20, 21] and/or orbital spin. This unit of spin is the building block where the act alone in a paramagnetic gas, to acting in concert in a super-paramagnetic "gas" or are acting in concert again but constrained by anisotropy forces to yield ferromagnetism or ferrimagnetism.

Key to both cycles and materials is the Brillouin function[2, 6, 10, 14, 18] which describes the statistical mechanics for an ensemble of spin elements:

$$B(x) = \frac{2S+1}{S}\coth\left(\frac{2S+1}{S}x\right) - \frac{1}{2S}\coth\left(\frac{x}{2S}\right)$$

eqn. 53

Where,

$$x = \frac{\mathbf{m}_{nano} \cdot \mathbf{H}}{kT}$$

eqn. 54

Which is the ratio of the energy of a fundamental dipole in a field (eqn. 11 appropriately scaled since H rather than B is used here) to thermal energy. This can be written another way to show the quantised nature of the magnetic moment:

$$x = \frac{g\mu_B \mathbf{S} \cdot \mathbf{H}}{kT}$$

eqn. 55

Where g, the Landé spectrographic splitting constant and μ_B, the Bohr Magneton are beyond the relevance of the discussion[2, 6, 10, 17, 20] and refer to the relation between fundamental quantum spins (angular momentum) and the magnetic moment – they are just a proportionality constant. However the spin S, is relevant to what we consider our "fundamental" magnetic particle in our following discussion – be that single electrons or clusters of atoms.

The Brillouin function is derived using classical statistical mechanics as the probability of finding the system in the state of our concern. The partition/occupancy function[10, 17] is defined as:

$$Z = \sum_s e^{-\frac{E_s}{kT}}$$

eqn. 56

Where s, represents a numbered state and E_s, the energy of that state.

The probability of finding the system in a certain state (degeneracy is not discussed here) is:

$$P_s = \frac{1}{Z}e^{-\frac{E_s}{kT}}$$

eqn. 57

The expected value of a property is given by:

$$\langle A \rangle = \sum_s A_s P_s$$
$$= \frac{1}{Z}\sum_s A_s e^{-\frac{E_s}{kT}}$$

eqn. 58

Of interest to the current discussion is the average magnetisation in the z direction:

$$\langle m_z \rangle = \frac{\sum_{n=-S}^{n=+S} m(n)e^{-\frac{\mathbf{m}(n) \cdot \mathbf{H}}{kT}}}{\sum_{n=-S}^{n=+S} e^{-\frac{\mathbf{m}(n) \cdot \mathbf{H}}{kT}}}$$

eqn. 59

Where the energy of the state, E_s, has been shown as $\mathbf{m}(n)\cdot\mathbf{H}$ where the moment, m, itself is a function of the amount of spin the particle has. Eventually this expression yields the Brillouin function.

The point of this discussion hasn't been to merely retread the argument but to show the underlying relationship between three types of magnetism: Paramagnetism, Super-paramagnetism and Ferromagnetism – the energy and the spin.

Paramagnetism

In the first instance for spin ½ and energy $\mathbf{m}\cdot\mathbf{H}$ the Brillouin function reduces to paramagnetic "spin gas" which many slightly magnetic materials (including solids) obey:

$$M(T) = M_S(0)\,tanh\left(\frac{m_{nano}H}{kT}\right)$$

eqn. 60

Where $M_S(0)$ is the saturation magnetisation at absolute zero and is related to the spin or magnetic moment density. For higher spins it is possible to truncate the Brillouin function[20]:

$$B(x) = \frac{(2S+1)^2 - 1}{12S^2}x + O(x^3) = \frac{S+1}{3S}x + O(x^3)$$

eqn. 61

It is very hard to saturate such materials and the relation can be linearised if H (see eqn. 54) is not too high giving the Curie Law[2, 6, 10, 17, 20]:

$$M(T) = NS(S+1)(g\mu_B)^2\frac{H}{3kT} = M_S(0)\frac{H}{T}$$

eqn. 62

The Heisenberg Exchange Interaction and ther energy terms

Let us now change the energy function in eqn. 56 to include additional terms:

$$E_s = -\sum_i g\mu_B\mathbf{S}_i\cdot\mathbf{H} - \sum_{ij}{}'J_{ij}\mathbf{S}_i\cdot\mathbf{S}_j - \sum_i KV\sin^2\theta_i$$

eqn. 63

The first term we have covered is of the form $\mathbf{m}\cdot\mathbf{H}$ and is the energy of a dipole in the field. The second term is the so-called "Heisenberg Exchange Interaction"[2, 6, 10, 17, 20] which is a very strong quantum mechanical interaction of spins from the Pauli Exclusion Principle (via an intermediary electron – the wavelength of participant electrons must overlap so this applies to solids) that tends to keep the spins in alignment. The references analyse this further using the so-called "Weiss" or "Mean field approximation" and what this amounts to is to a permanent field H' tending to align the field even without the external field H. It is then possible to have a material with the spins near saturation even at normal temperatures.

Super-paramagnetism

Returning to the Brillouin function and letting S→∞ we arrive at the Langevin function:

$$L(x) = \coth x - \frac{1}{x}$$

eqn. 64

The third term in eqn. 63 is an anisotropy term which reflects an intrinsic tendency of the moments to align along the crystalline axis, or even the shape anisotropy where the magnetic fields of an elongated particle self-reinforce along the long axis of the particle. K is the anisotropy constant and V is the volume of the particle. In such a particle the magnetic moment swishes back and forth due to the influence of the thermal energy with a relaxation rate:

$$\text{N\'eel:}\quad \tau_N = \frac{1}{f_0}e^{\frac{KV}{kT}}$$

eqn. 65

Where f_0 is called the Néel frequency and is the order of 10GHz. The particles of magnetic material then potentially have a moment with temporal variation and depending on the time scale of interest, they are called <u>super-paramagnetic</u>. The particle size is the so-called "sub-domain" size.

Another relaxation rate can be identified with ferrofluids from hydrodynamic effects. This is called the Brownian relaxation rate:

$$\text{Brownian:} \quad \tau_B = \frac{3V\eta_0}{kT} \qquad \text{eqn. 66}$$

When both types of time constant are present the principle of least time[5] determines the mode of relaxation.

In ferrofluid, the core of some 10s of nanometres radius behaves as a particle of massive spin (over $10{,}000\mu_B$) and the Langevin equation (eqn. 64) applies to the variation of magnetisation with temperature. Let us then write, for brevity and simplicity, both the magnetisation vs. temperature and the impulse time response for a super-paramagnetic material such as ferrofluid (both Brownian and Néel),

$$M = 0.9 M_S\left(0\right) tanh\left(\frac{m_{nano}H}{3kT}\right)e^{-\frac{1}{\tau(T)}} \qquad \text{eqn. 67}$$

The impulse response is just "bolted onto the magnetisation" as we know to a very good approximation (appendix 5) that ferrofluids have a 1st order pole time response.

Super-paramagnetism by Brownian motion

Section 2 mentioned that if the Néel rate becomes so slow relative to the Brownian disruption in the fluid, then the time constant for relaxation would be set by the latter. The ferrofluid behaves as a magnetic liquid composed of tiny permanent magnets subject to Brownian motion.

Ferromagnetism, Anti-ferromagnetism and Ferrimagnetism

When the particle size becomes large two more energy term enter eqn. 63 to do with the total magneto-static energy and the minimisation of this by domain wall formation. On larger scales, energy minimisation of the magnetic field will progressively overcome the exchange interaction breaking the material up into domains separated by a domain wall where the moments gradually reverse from one orientation in one domain to the opposite at the adjoining domain. It is these domain walls that give rise to the characteristic hysteresis in the B-H curve of ferromagnetic materials.

Anti-ferromagnetism is very similar to ferromagnetism but the material is made from two sets of fundamental spins that cancel each other. The material has a magnetic heat capacity but no bulk field. Ferrimagnetism is once again similar to ferromagnetism and anti-ferromagnetism, however the cancellation in the two sets of fundamental dipoles is not total leaving a residual field. Ferrites are ferrimagnetic materials with saturation magnetisations less than elemental iron.

We have hence shown the inter-relatedness between paramagnetism, super-paramagnetism and ferromagnetism as one of quantity of spin and the energy interaction term. Now the precise relation to the working substances of the two cycles can be discussed and expressions for their entropy developed.

Appendix 3. Field Energy and Work regarding Magnetic Materials

The magnetisation of substances from the fundamental spin currents can wholly be represented as an equivalent solenoidal current acting on the surface of the material[6, 9, 21]. This follows from one of Maxwell's electrodynamic equations/Ampère's Law:

$$c^2 curl\mathbf{B} = \frac{\mathbf{j}}{\varepsilon_0} + \frac{\partial \mathbf{E}}{\partial t} \qquad\text{eqn. 68}$$

In the magneto-static scenario this just limits to:

$$c^2 curl\mathbf{B} = \frac{\mathbf{j}}{\varepsilon_0} \qquad\text{eqn. 69}$$

Although **B** *is* the fundamental magnetic field density whose field energy[6, 9, 21] is given by (the permittivity of free space and the speed of light are considered the more fundamental units than μ_0, the latter is more associated with electrical engineering and general magnetic texts):

$$\varepsilon_0 c^2 \int_V B^2 dV \equiv \frac{1}{\mu_0} \int_V B^2 dV \qquad\text{eqn. 70}$$

The magnetic field is considered in engineering and materials texts as composed of a magnetising "H" field which we can directly control and results from electrical currents and a field called "M" which is a function of the magnetising field, thus:

$$\mathbf{B} \triangleq \mu_0 \left(\mathbf{H} + \mathbf{M} \right) \qquad\text{eqn. 71}$$

Another Maxwell equation gives the relation between H and M:

$$div\mathbf{B} = 0 \qquad\text{eqn. 72}$$

That is, the magnetic field has no sources but we can write for a magnetised material from eqn. 71 that:

$$div\mathbf{H} = -div\mathbf{M} \qquad\text{eqn. 73}$$

The magnetic field "H" is just the same if it arises from macroscopic flowing electrical currents eqns. 69 and 71 if M is zero or from the field of a permanent magnet composed of microscopic spin currents, eqn. 73. We note too that the field "H" behaves in a similar manner to the electrical field "E" in having polar sources. Thus Magneto-statics and its solutions is just the same form as electrostatics.

The diagram below shows the partitioning of a system, composed of a material being magnetised, into regions of energetic interest:

- The Thermodynamics of the Magnetic material encompassing the internal energy and the changes in magnetisation spin currents of the sample.

- The energetics solely of the field and the coils, that is, the energetics of the dipole.

- The energetics of the external electrical circuit.

As discussed at the start, microscopic spin currents are exactly equivalent to macroscopic circulating solenoidal currents. Thus the magnetisation is shown by "Coil 1" as a superconducting loop, magnetising losses can be modelled with a resistance whose heat output goes to the internal energy of the system but it is not relevant to the present discussion.
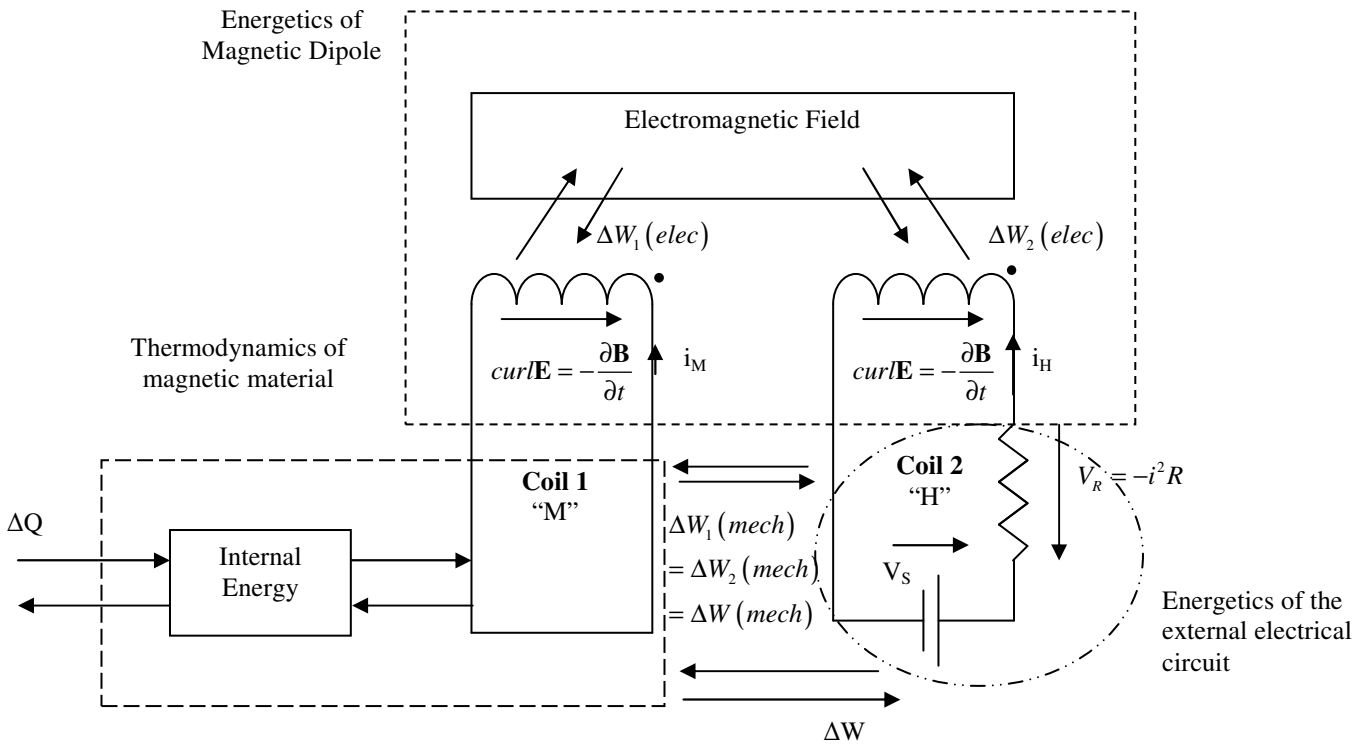
Figure 51 –The relation between the Internal Energy, Field and External Circuit Subsystems

Overall the external electrical system couples to the thermodynamic system performing work, whilst the latter performs heat transfer with the environment. We can limit the argument to purely the electrical work by looking at the Helmholtz Free Energy:

$$F = U - TS \qquad \text{eqn. 74}$$

Hence,

$$dF = dU - SdT \qquad \text{eqn. 75}$$

The changes in work at constant temperature is the same as the work term in the internal energy thermodynamic relation which deals with changes in heat and work.

The next figure is the dipole system in closer detail. Looking first at the coil 2 subsystem the power balance is:

$$\int V_s i_H \cdot dt - \int i_H^2 R \cdot dt - \int i_H \frac{d\lambda}{dt} \cdot dt = 0 \qquad \text{eqn. 76}$$

That is, the electrical source does work on the circuit dissipating some as internal energy of the resistor and the rest as work on the electromagnetic field by the integral of the change in flux linkage λ multiplied by the current i_H.

Ampère's Law, the spatial integral of eqn. 69 gives the result for a long solenoid that,

$$H = \frac{N_2 i_H}{l} \qquad \text{eqn. 77}$$

The number of turns in the solenoid is N_2, its length is "l" and area "A". The "H" field is nothing more than the "B" just scaled in Amp/m.
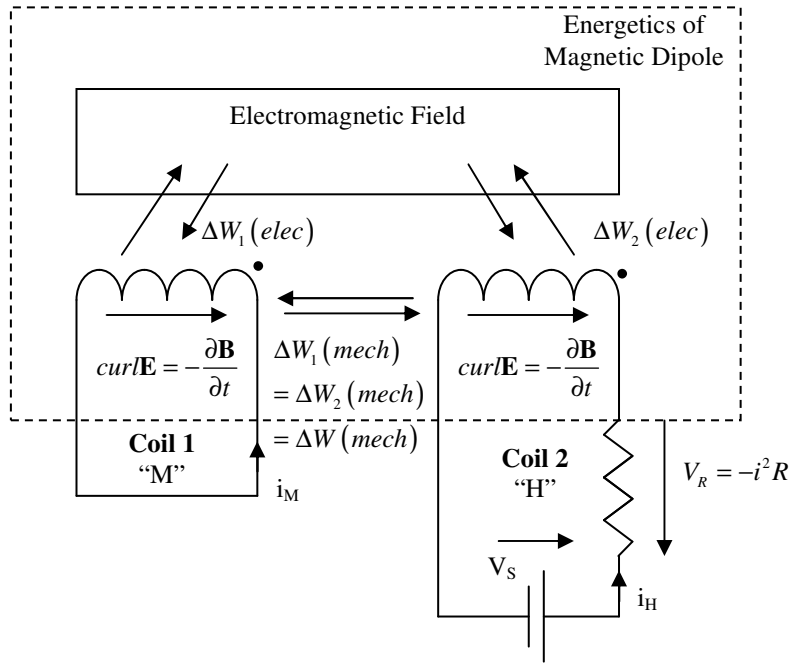
Figure 52 – The Energetics of the Magentic Dipole

.

The work done on the field interests us and we derive,

$$\Delta F_2\left(elec\right) = \int i_H \frac{d\lambda}{dt} \cdot dt = H\frac{l}{N_2} \cdot N_2 A \frac{dB}{dt}$$

$$\Rightarrow \Delta F_2\left(elec\right) = HdB \cdot dV = -\Delta\left(\text{Source Work}\right) \qquad \text{eqn. 78}$$

The general condition of a differential volume element is quoted and similarly for the second coil, the change in work done on the circuit is:

$$\Delta F_1\left(elec\right) = MdB \cdot dV = -\Delta\left(\text{Work Spin Currents}\right) \qquad \text{eqn. 79}$$

It is interesting to note that the sum of these free energies (it is an extensive property after all) is:

$$\Delta F_1\left(elec\right) + \Delta F_2\left(elec\right) = \frac{1}{\mu_0} BdB \cdot dV = \frac{1}{2} d\left(\frac{B^2 dV}{\mu_0}\right) \qquad \text{eqn. 80}$$

That is, the change in electrical free energies corresponds to the change in the magnetic field density energy, as it should; the field just acts as a store of work. Referring to the first diagram we can see that a component of the spin currents relates to the magnetostatic field proportional to MdM from the "M" field, if we subtract this, we arrive at the component of work related to magnetising the working substance:

$$\Delta\left(W_{mag}\right) = -\mu_0 MdH \cdot dV \qquad \text{eqn. 81}$$

Around a cycle the quantity d(MH) is exact and is zero, so re-writing,

$$\oint \Delta\left(W_{mag}\right)_{nett} = \oint\left(d(\mu_0 MH) \cdot dV - \mu_0 MdH\right) = \oint \mu_0 HdM \cdot dV \qquad \text{eqn. 82}$$

This Helmholtz free energy term is of course just the relevant work term in the thermodynamic identity of the thermodynamic system.

Another term can be added to the free energy of the dipole system by considering the mechanical work separating the coils at constant magnetisation current. If we know $\Delta F_1(elec)$ then separating coil 1 to infinity must mean that the free energy of the coil 1 subsystem has gone to zero, thus,

$$\Delta F_1\left(elec\right) + \Delta F\left(mech\right) + \Delta F_2\left(elec\right) = -\Delta F\left(mech\right) \qquad \text{eqn. 83}$$

By symmetry, coil 2 moving off to infinity achieves the same result and so we'd know that (differential quantities in dB and dV have been integrated),

$$\Delta F_2\left(mech\right) = \int_0^\infty \mathbf{F}\cdot d\mathbf{r} = -\boldsymbol{\mathcal{M}}\cdot\mathbf{B} = \Delta F_1\left(mech\right) \qquad \text{eqn. 84}$$

The total free energy of the dipole system is then,

$$\Delta F_1\left(elec\right) + \Delta F\left(mech\right) + \Delta F_2\left(elec\right) = -\Delta F\left(mech\right)$$

$$\Rightarrow \Delta F_{dipole} = \boldsymbol{\mathcal{M}}\cdot\mathbf{B} \qquad \text{eqn. 85}$$

If we consider the whole dipole system as part of the thermodynamic system, the "magnetic enthalpy" can be derived to consider only the changes in heat when the intensive variable, B, is held constant:

$$\mathcal{H} = U - \mathcal{M}B \qquad \text{eqn. 86}$$

Giving,

$$d\mathcal{H} = TdS + \mu_0 Hd\mathcal{M} - \mathcal{M}dB - \mu_0 Hd\mathcal{M} - \mu_0 Md\mathcal{M}$$
$$= TdS - \mathcal{M}dB - \mu_0 Md\mathcal{M} \qquad \text{eqn. 87}$$

$$d\mathcal{H}\big|_{\text{B const}} = TdS - \mu_0 Md\mathcal{M} \qquad \text{eqn. 88}$$

By analogy to work performed at constant pressure to changes in volume, we might concede that changes in heat are accompanied by the quantity $\mu_0 Md\mathcal{M}$ or the "dipole-work": Enthalpy is a property of the system and around a cycle, clearly the heat transferred is equivalent to the dipole-work.

Appendix 4. Additional "Dipole-work" resulting from a temporary remnant flux
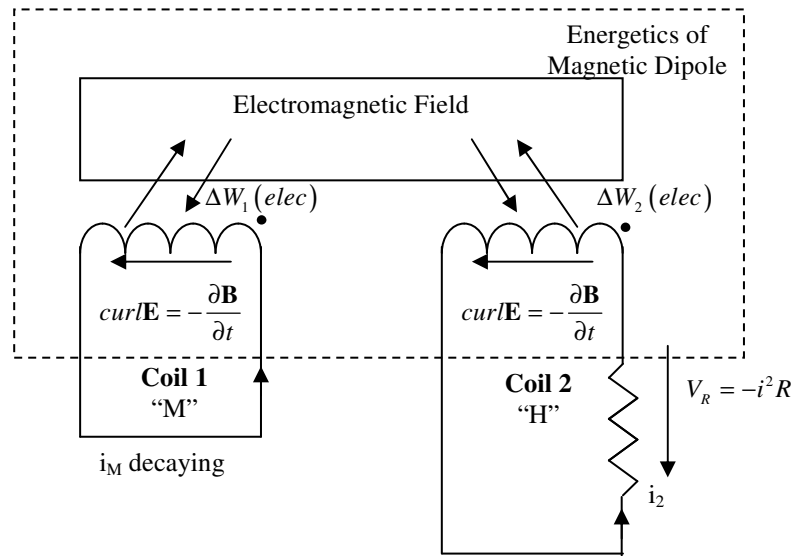
Figure 53 –The Dipole-work of an Independent Flux

The previous appendix showed how the quantity $\mu_0 M d\mathcal{M}$ the dipole-work can lead to changes in heat of the system; it is just a different way of viewing magnetisation work. We seek to show in this appendix that an additional work term, in the same form as the dipole-work, arises from the collapse of remnant magnetic flux.

Once again we compute the Helmholtz free energy. We note that the "H" field of coil 2 has already been switched off (and the work recouped or deposited in the external resistance, $\oint H dH = 0$) and both coils experience the same flux change. The decaying current flowing in coil 1 is the Ampèrian surface current equivalent of the spin currents of the magnetisation. By transformer action, if the turns ratio is 1:1 between the two coils, the same current will flow in coil 2. Nether-the-less, if the turns ratio is different, the change in free energy will be experienced by both coils be zero as the product of the current and the EMF will be the same: coil 1's free energy will fall as it is considered the source of the work and coil 2's will rise for it to be ultimately dissipated in the resistance:

$$\Delta F_1\left(elec\right)+\Delta F_2\left(elec\right)=0 \qquad \text{eqn. 89}$$

$$\Delta F_2\left(elec\right)=\int i_2 \frac{d\lambda}{dt}\cdot dt$$

$$\text{By Ohm's law } i_2 = \frac{1}{R}\frac{d\lambda}{dt}$$

Noting that $\lambda = BAN$ and using a high permeability μ_r material in conjunction with the working substance,

$$\Rightarrow \Delta F_2\left(elec\right)=\int_0^\infty \frac{N^2}{R}A^2\mu_0^2\mu_r^2\left(\frac{dM}{dt}\right)^2 dt \qquad \text{eqn. 90}$$

We can rearrange this expression using the volume magnetisation and length of the coil to include the inductance of a long coil $L = \frac{\lambda}{i}$,

$$L = \frac{\mu_0 A N^2}{l} \qquad \text{eqn. 91}$$

Also we can subsume the high permeability material into the magnetisation as an effective susceptibility ($M' = \mu_r \chi H$ instead of $M = \chi H$),

$$\Delta F_2(elec) = \int_0^\infty \frac{1}{V} \mu_0 \frac{L}{R} \left(\frac{d\mathcal{M}}{dt} \right)^2 dt \qquad \text{eqn. 92}$$

Upon substitution of magnetisation of the ferrofluid decaying temporary remnant flux[2]:

$$\mathcal{M}(t) = \mathcal{M}_0 e^{-\frac{t}{\tau_{ferro}}} \qquad \text{eqn. 93}$$

We arrive at this expression,

$$\Delta F_2(elec) = \int_0^\infty \frac{1}{V} \mu_0 \frac{L}{R} \frac{1}{\tau_{ferro}^2} \mathcal{M}_0^2 e^{-\frac{t}{\tau_{ferro}}} dt$$

$$\Rightarrow$$

$$\Delta F_2(elec) = \int_0^\infty \mu_0 \frac{\tau_{elec}}{\tau_{ferro}} \frac{1}{\tau_{ferro}} M_0 \cdot \mathcal{M}(t) dt \qquad \left(\text{getting rid of the volume magnetisation} \right)$$

And the infinitesimal change in the free energy on substitution of $\dfrac{d\mathcal{M}(t)}{dt} = -\dfrac{1}{\tau_{ferro}} \mathcal{M}(t)$ is,

$$dF_2(elec) = \mu_0 \frac{\tau_{elec}}{\tau_{ferro}} M_0 \cdot d\int_0^\infty \frac{1}{\tau_{ferro}} \mathcal{M}(t) dt$$

$$\Rightarrow$$

$$dF_2(elec) = \mu_0 \frac{\tau_{elec}}{\tau_{ferro}} M_0 \cdot d\int_\infty^0 \frac{d\mathcal{M}(t)}{dt} dt$$

Finally we just drop the sub-script on M and write the infinitesimal change as,

$$dF_2(elec) = \mu_0 \frac{\tau_{elec}}{\tau_{ferro}} M d\mathcal{M} \qquad \text{eqn. 94}$$

As was noted in the previous appendix by eqn. 79,

$$\Delta F_1(elec) = -\Delta(\text{Work Spin Currents})$$

Again, the work of the spin currents covers the magneto-static field and the magnetisation and it is this term minus the magneto-static field that enters into the thermodynamic identity for the thermodynamic system. We can say however,

$$\Delta(\text{Work Spin Currents}) = \mu_0 \frac{\tau_{elec}}{\tau_{ferro}} M d\mathcal{M} \qquad \text{eqn. 95}$$

Thus, for the device to generate excess electrical work and turn heat energy into electricity,

$$\frac{\tau_{elec}}{\tau_{ferro}} M d\mathcal{M} > H d\mathcal{M} \qquad \text{eqn. 96}$$

We write the grand thermodynamic identity of the magnetic material with this extra work term and K_e for generality now,

$$dU = TdS + \mu_0 H d\mathcal{M} + \mu_0 K_e M d\mathcal{M} \qquad \text{eqn. 97}$$

The last term only applies on the demagnetisation part of the cycle.

Appendix 5. Irreversible Losses and Ferrofluid as a circuit element

We shall now model irreversible processes in the ferrofluid. Figure 54 shows measured loss angle for a real ferrofluid supplied by Sustech Gmbh, the actual specifics of the ferrofluid are not important but the graphs show how well the first order pole approximation applies to real data[2, 18-21]. The susceptibility χ is the measure of the response of a magnetic material to an external field (eqn. 54). On the graph X'(f) is the real or component in-phase with the magnetisation H of the susceptibility and X''(f) is the imaginary part.
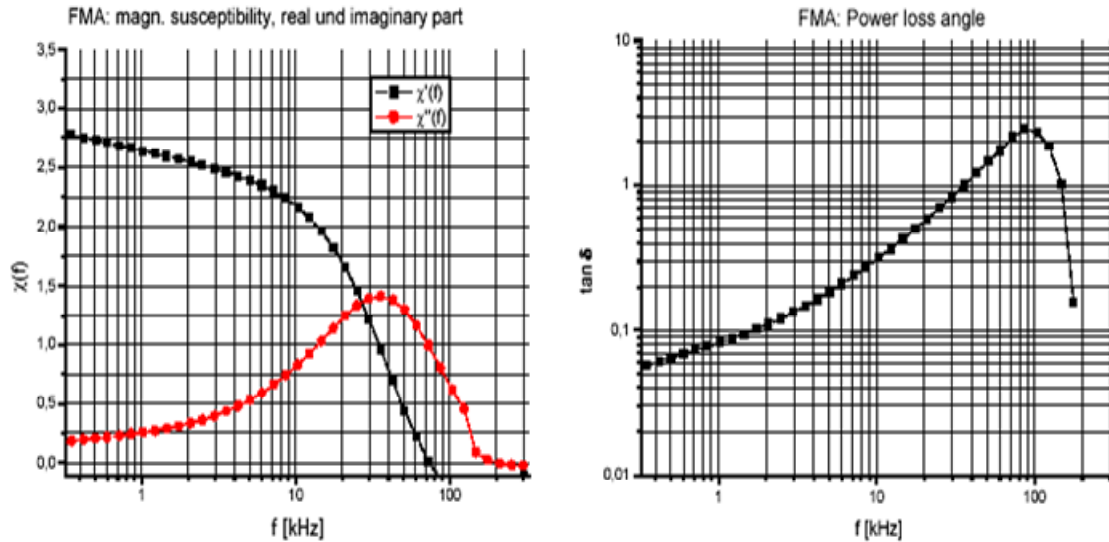
Figure 54 – Power Loss in Ferrofluids, Bode plots
From a Sustech Gmbh technical report[22]

$$\chi = \frac{\chi_0}{1 + j\omega\tau(T)}$$

eqn. 98

Where:

χ_0 is the DC susceptibility, $M = \chi_0 H$
$\tau(T)$ is the ferrofluid relaxation rate
ω the frequency in radians per second

When magnetising the ferrofluid, it behaves essentially as a lossy inductor. Inductance is defined[6] as the magnetic flux per unit current:

$$L = \frac{\lambda}{i} = \frac{\mu_0 M A}{i}$$

eqn. 99

The flux is related to the magnetisation and cross-sectional area A of the coil, hence the inductance is directly proportional to the susceptibility.

Let a current flow through the inductor be represented by the phasor method[6] as:

$$\hat{I} = I_0 e^{jwt}$$

eqn. 100

The relationship between the complex voltage, current and impedance is:

$$\hat{V} = \hat{I}\hat{Z}$$

eqn. 101

Hence:

$$\hat{Z}_{ind} = -j\omega L(\omega)$$

eqn. 102

Since $V = -L\,di/dt$. Using the expression for the frequency response of the ferrofluid, given by eqn. 98, we proceed to find the real and imaginary parts of χ:

$$\mathrm{Re}(\chi) = \frac{\chi_0}{1 + \omega^2 \tau^2 (T)} \quad \mathrm{Im}(\chi) = \frac{-\chi_0 \omega \tau (T)}{1 + \omega^2 \tau^2 (T)} \quad Tan\delta = -\omega \tau (T) \qquad \text{eqn. 103a,b,c}$$

Thus the imaginary part of the susceptibility is the resistive loss and the real part gives inductive behaviour. The ratio of real to imaginary parts gives the power factor and this is linear in frequency. Figure 54 shows a good approximation to this.

Clearly at low frequency the magnetisation-demagnetisation of the ferrofluid tends to a thermodynamically reversible process. The magnitude of the magnetisation is:

$$M(\omega) = \mathrm{Re}(\chi) H(\omega) \qquad \text{eqn. 104}$$

And that the magnetisation energy is:

$$W_{mag}(\omega) = \mathrm{Re}\left[\mu_0 H(\omega) \mathcal{M}(\omega) \right]$$

or

$$W_{mag}(t) = \mathcal{F}^{-1}\left\{ \mathrm{Re}\left[\mathcal{F}\{ \mu_0 H(t) \otimes \mathcal{M}(t) \} \right] \right\} \qquad \text{eqn. 105}$$

The irreversible generation of heat is then related to the Fourier Transform of the imaginary parts $M = \mathrm{Im}(\chi) H$ of the magnetising energy,

$$Q_{irr}(\omega) = \mathrm{Im}\left[\mu_0 H(\omega) \mathcal{M}(\omega) \right]$$

or

$$Q_{irr}(t) = \mathcal{F}^{-1}\left\{ \mathrm{Im}\left[\mathcal{F}\{ \mu_0 H(t) \otimes \mathcal{M}(t) \} \right] \right\} \qquad \text{eqn. 106}$$

The incremental forms of the magnetisation and irreversible heat in the frequency domain are:

$$\delta E_{mag}(\omega) = \mathrm{Re}\left[\mu_0 H(\omega) d\mathcal{M}(\omega) \right] \qquad \text{eqn. 107}$$

$$\delta Q_{irr}(\omega) = \mathrm{Im}\left[\mu_0 H(\omega) d\mathcal{M}(\omega) \right] \qquad \text{eqn. 108}$$

And in the time domain, by Parseval's Theorem[23], the incremental forms of the magnetisation energy and irreversible heat generation is just:

$$\delta W_{mag} = \sum_{\omega} \left(\frac{\mathrm{Re}^2\left[\chi H(\omega) \right]}{\mathrm{Re}^2\left[\chi H(\omega) \right] + \mathrm{Im}^2\left[\chi H(\omega) \right]} \right) \cdot \mu_0 H d\mathcal{M} = f(\omega) \mu_0 H d\mathcal{M} \qquad \text{eqn. 109}$$

$$\delta Q_{irr} = \sum_{\omega} \left(\frac{\mathrm{Im}^2\left[\chi H(\omega) \right]}{\mathrm{Re}^2\left[\chi H(\omega) \right] + \mathrm{Im}^2\left[\chi H(\omega) \right]} \right) \cdot \mu_0 H d\mathcal{M} = f_{irr}(\omega) \mu_0 H d\mathcal{M} \qquad \text{eqn. 110}$$

Equations 109 and 110 are directly implementable on computer. The functions $f(\omega)$ and $f_{irr}(\omega)$ are really just constants as we'd know the Fourier components of our regular magnetising signal H(t). Figure 55 shows the relation between the magnetisation energy and the loss graphically.

$$Q_{irr} = \mathrm{Im}\left[\int_{\mathcal{M},\omega} \mu_0 H(\omega)\, d\mathcal{M}(\omega) \right]$$

M

Re(M) + Im(M)

$$E_{mag} = \mathrm{Re}\left[\int_{\mathcal{M},\omega} \mu_0 H(\omega)\, d\mathcal{M}(\omega) \right]$$

Re(M)

H
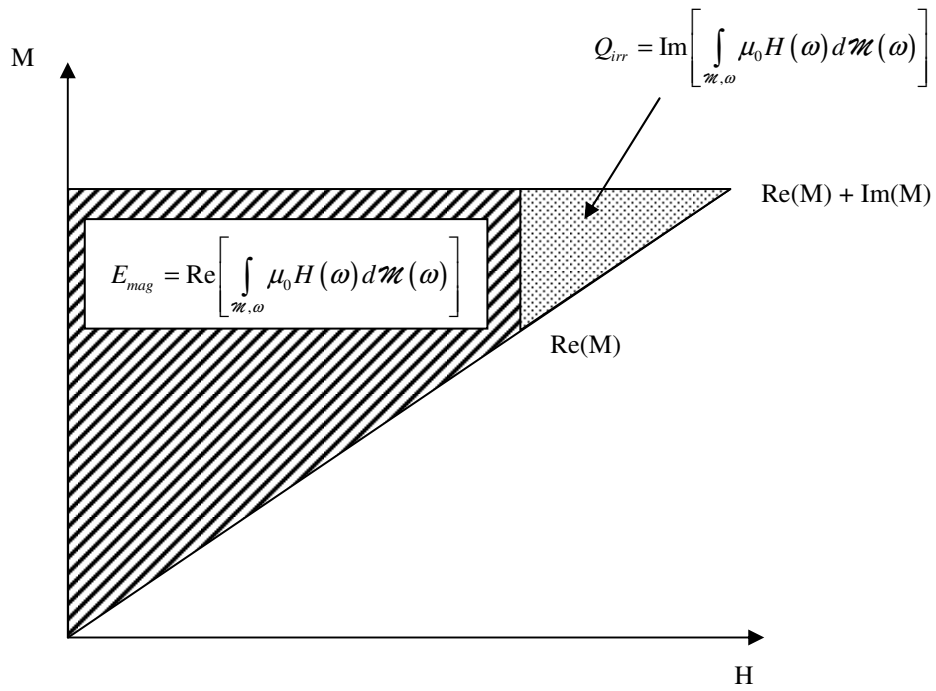
Figure 55 – Magnetising energy and Irreversible loss on a H-M (B-H minus field energy) graph

Appendix 6. Sub-system T-S diagrams for the Magneto-caloric Effect

Magnetic materials display gradual ordering of their atomic dipoles as a function of temperature, so-called order-disorder or 2nd order phase transitions[17, 20]. Appendix 1 models the thermodynamics of this and defines the Curie point and appendix 2 covers the similarities between paramagnetism, super-paramagnetism, ferrimagnetism, anti-ferromagnetism and ferromagnetism by a statistical mechanics treatment.

As seen from these appendices there is most change in the magnetic heat capacity around the Curie point and it is informative to look at an isentropic magneto-caloric cycle on a T-S diagram. We partition the system into entropies that are solely magnetic and mechanical which correspond to entropy associated with position and velocity distributions respectively. It is noted that:

$$\Delta S_{total} = \Delta S_{mag.pos} + \Delta S_{mag.vel}$$

eqn. 111

There is heat flow between the two sub-systems:
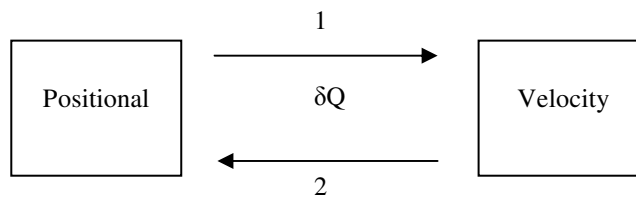
Figure 56 – Heat flow between the two subsystems
As the H-field is switch on, 1 then off, 2

Thus the reversible magneto-caloric effect is shown as:
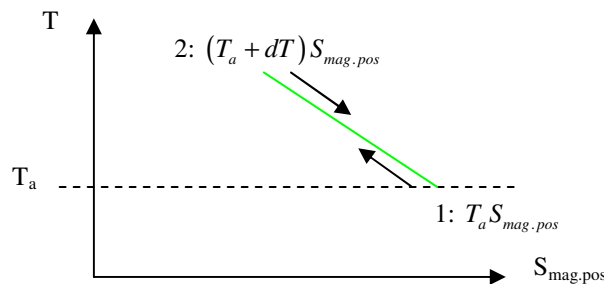
Figure 57 – Positional Entropy
(N.B. This is a 2nd order phase transition with the number of particles decreasing with magnetic order)
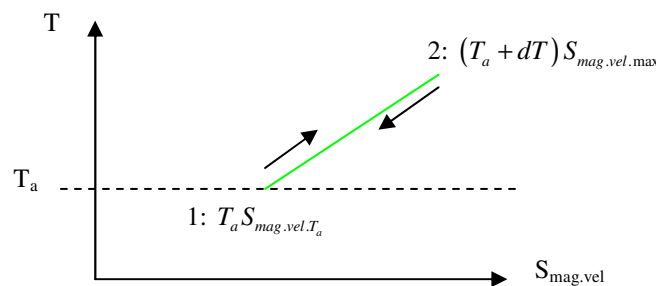
Figure 58 – Velocity Entropy

Only infinitesimal changes are shown in the figures as it needlessly complicates the argument to show higher order contributions to the paths on the diagram.
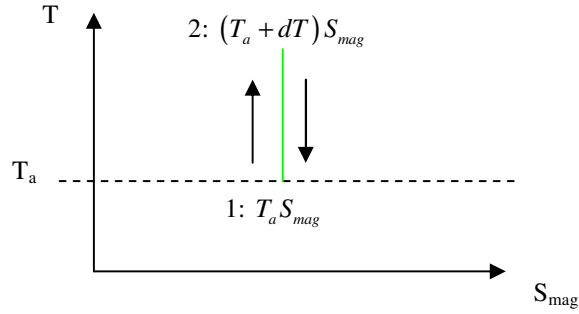
Figure 59 – Entropy of the combined positional and velocity systems. Isentropic process.

Figures 57 and 58 give a level of detail not normally entertained and figure 59 gives the total entropy and is usually most useful. Nethertheless, we shall see that the earlier two figures are useful in analysing the new temporary remanence cycle presented in this document. Moving around the cycle we shall calculate the changes in entropy and work for the two systems, $\Delta U = \Delta U_{mag.pos} + \Delta U_{mag.vel}$ and sum all at the end for the reversible magneto-caloric effect (fig. 59). Thus:-

$$\sum \Delta U = \sum \Delta Q - \sum \Delta W \quad \text{and} \quad \Delta Q = \int_{S_{start}}^{S_{finish}} T(S) dS$$

For the incremental and linear relations depicted in figure 57, the change in heat is:

$$\Delta Q \approx T_{finish} S_{finish} - T_{start} S_{start} \qquad \text{eqn. 112}$$

Temperature changes above ambient (T_a) lead to heat being rejected from the system and below ambient, the opposite. Analysing figure 57, the heat flows are computed:

Step 1-2: $\quad \Delta U_{mag \cdot pos} = \left[(T_a + dT) S_{mag.pos.\min} - T_a S_{mag.pos.\max} \right] + \left[\mu_0 H d\mathcal{M} \right] \quad$ Heat rejection

Step 1-2: $\quad \Delta U_{mag.vel} = \left[(T_a + dT) S_{mag.vel.\max} - T_a S_{mag.vel.T_a} \right] + 0 \quad$ Heat input

Step 2-1: $\quad \Delta U_{mag \cdot pos} = \left[T_a S_{mag.pos.\max} - (T_a + dT) S_{mag.pos.\min} \right] - \left[\mu_0 H d\mathcal{M} \right] \quad$ Heat input

Step 2-1: $\quad \Delta U_{mag.vel} = \left[T_a S_{mag.vel.T_a} - (T_a + dT) S_{mag.vel.\max} \right] + 0 \quad$ Heat rejection

Summing all the steps, we find for this reversible process that $\sum \Delta U = 0 \quad \sum \Delta Q = 0$ and $\sum \Delta W = 0$

We note that what has occurred is a <u>modulation in the heat capacity</u> of the magnetic positional system by "freezing out" some degrees of freedom of the system by the magnetic field. Energy simply re-partitions to the other modes such that the average energy of these modes increases – more simply, the temperature increases.

Magneto-calorific Effect (MCE) in contact with reservoir

Now the effect of an external reservoir in contact with the thermo-magnetic system <u>at set points in the cycle</u> is shown. The cycle is conveniently broken up into 4 steps:
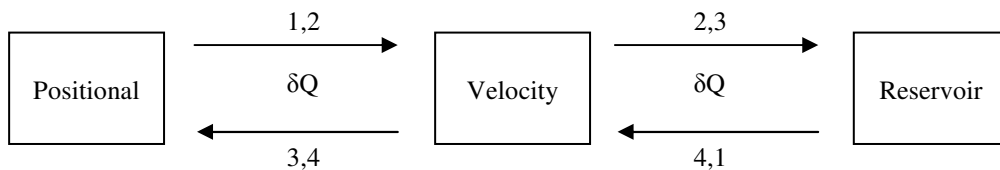
Figure 60 – Heat flow between the three subsystems

2nd order phase transition means magnetic particle "population" becomes smaller so there is <u>effective heat input</u> from the magnetic modes "frozen out".

Heat is then rejected to liquid reservoir step 2-3 (see diagram below).

When field is switched off, heat is repartitioned to greater population so temperature falls.

Heat returned to magnetic system from mechanical system on step 4-1.

Figure 61 – Positional Entropy T-S diagram
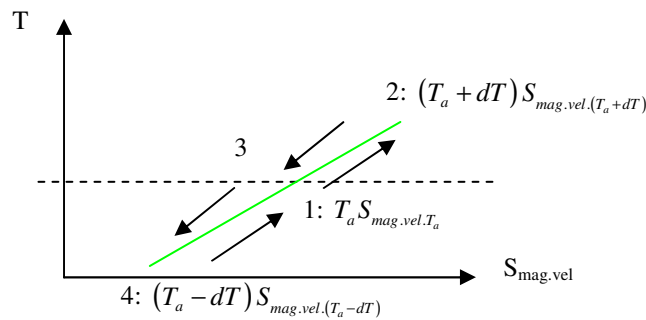
Figure 62 – Velocity Entropy T-S diagram
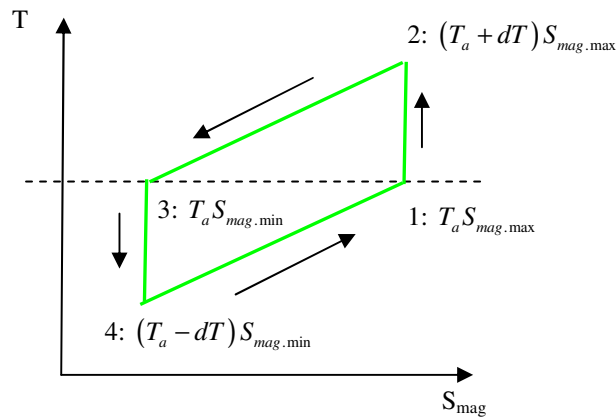
Figure 63 – Entropy of the combined positional and velocity systems

Analysis of the total magnetic system proceeds as follows:

Step 1-2:
$$\Delta U_{mag} = \begin{bmatrix} (T_a + dT) S_{mag.pos.\min} - T_a S_{mag.pos.\max} \\ (T_a + dT) S_{mag.vel.\max} - T_a S_{mag.vel.T_a} \end{bmatrix} + [\mu_0 H d\mathcal{M}]$$
Adiabatic
temperature rise

Step 2-3:
$$\Delta U_{mag} = \begin{bmatrix} T_a S_{mag.pos.\min} - (T_a + dT) S_{mag.pos.\min} \\ T_a S_{mag.vel.T_a} - (T_a + dT) S_{mag.vel.\max} \end{bmatrix} + 0$$
Heat rejection
to reservoir

$$\left\{ so\ \Delta U_{liq.2 \to 3} = -\Delta U_{mag.2 \to 3} \right\}$$

Step 3-4:
$$\Delta U_{mag} = \begin{bmatrix} (T_a - dT) S_{mag.pos.\max} - T_a S_{mag.pos.\min} \\ (T_a - dT) S_{mag.vel.\min} - T_a S_{mag.vel.T_a} \end{bmatrix} - [\mu_0 H d\mathcal{M}]$$
Adiabatic
temperature fall

Step 4-1:
$$\Delta U_{mag} = \begin{bmatrix} T_a S_{mag.pos.\max} - (T_a - dT) S_{mag.pos.\max} \\ T_a S_{mag.vel.T_a} - (T_a - dT) S_{mag.vel.\min} \end{bmatrix} + 0$$
Heat input
from reservoir

$$\left\{ so\ \Delta U_{mag.4 \to 1} = -\Delta U_{liq.4 \to 1} \right\}$$

The Temporary Remanence Cycle

It is but a short step from the magneto-calorific cycle in contact with an external reservoir to the temporary remanence cycle as the figure shows below.
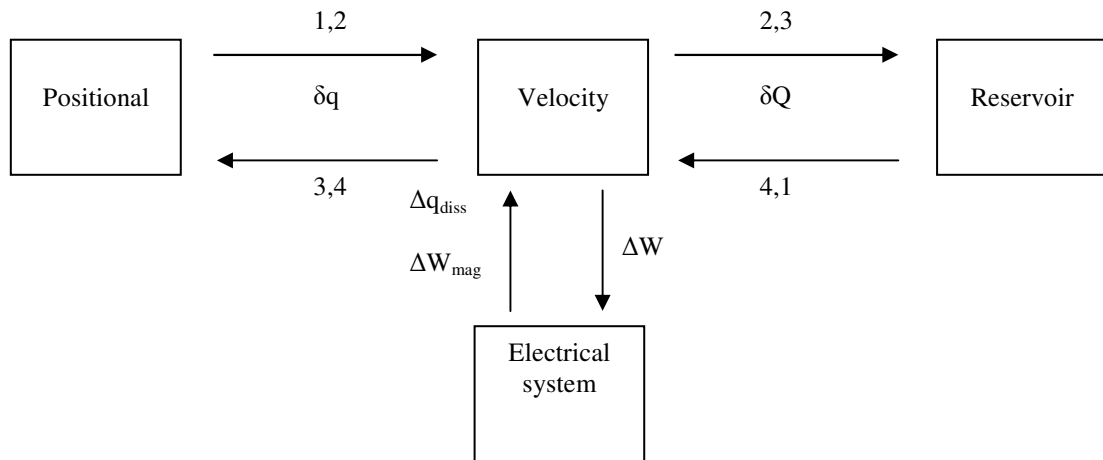
Figure 64 – Heat and work flow between the four subsystems

Appendix 7. The Energy Balance Equation for the Micro-cycle

Figure 16 is very similar to figure 57 with the addition of the dissipative and generative processes discussed before. Note that no heat input other than δQ_{irr} is shown. The analysis proceeds in a similar manner to appendix 6 with the reversible magneto-caloric effect at its core. The heat flows are approximately $T_{finish}S_{finish} - T_{start}S_{start}$ by eqn. 112, appendix 6.

Notes on the magnetic angular velocity entropy:

$S_{vel.T_a}$ occurs at temperature T_a

$S_{vel.\max}$ occurs at temperature $T_a + dT + dT_{irr}$

$S_{vel.dw}$ occurs at temperature $T_a - dT - dT_{dw}$

Step 1-2a:
$$\Delta U = \begin{Bmatrix} +(T_a + dT + dT_{irr})S_{\min} - T_a S_{\max} \\ +(T_a + dT + dT_{irr})S_{vel.\max} - T_a S_{vel.T_a} \end{Bmatrix} + \{\mu_0 Hd\mathcal{M} + \delta W_{irr}\} \text{ MC effect and Irreversibility}$$

Step 2a-3:
$$\Delta U = \begin{Bmatrix} T_a S_{\min} - (T_a + dT + dT_{irr})S_{\min} \\ T_a S_{vel.T_a} - (T_a + dT + dT_{irr})S_{vel.\max} \end{Bmatrix} \qquad \text{Heat rejection to reservoir}$$

Step 3-4' (4a-1):
$$\Delta U = \begin{Bmatrix} (T_a - dT - dT_{dw})S_{\max} - T_a S_{\min} \\ (T_a - dT - dT_{dw})S_{vel.dw} - T_a S_{vel.T_a} \end{Bmatrix} - \{\mu_0 Hd\mathcal{M} - \delta W\} \quad \begin{array}{l} \text{Reverse MC effect, work} \\ \text{and then magnetisation energy} \\ \text{becomes internal energy} \end{array}$$

Step 4'-1:
$$\Delta U = \begin{Bmatrix} +\delta Q_{mech} \\ +T_a S_{\max} - (T_a - dT - dT_{dw})S_{\max} \\ +T_a S_{vel.T_a} - (T_a - dT - dT_{dw})S_{vel.dw} \end{Bmatrix} \qquad \text{Heat addition from reservoir}$$

We return to the initial co-ordinates around a cycle, thus $\sum \Delta U = \sum \Delta Q - \sum \Delta W = 0$

Let us first consider simplification of the steps with the substitutions for the irreversible heat, magneto-caloric effect and work:

The magnetising work is:
$$\Delta W_{mag} = \mu_0 Hd\mathcal{M} \qquad\qquad \text{eqn. 113}$$

The irreversible loss on magnetisation is (see appendix 5 for ferrofluid losses),
$$\Delta Q_{irr} = dT_{irr}\left(S_{\min} + S_{vel.\max}\right) = \Delta Q_{irr}\left(\Delta W_{mag}, \frac{d\mathcal{M}}{dt}\right) \quad = \quad -\Delta W_{irr} \qquad \text{eqn. 114}$$

The forward magneto-caloric heat is defined as:
$$\Delta Q_{MC}^+ = \begin{Bmatrix} (T_a + dT)S_{\min} - T_a S_{\max} \\ +(T_a + dT)S_{vel.\max} - T_a S_{vel.T_a} \end{Bmatrix} \qquad \text{eqn. 115}$$

So we write:
$$\Delta U_{1-2a} \quad = \quad \{\Delta Q_{irr} + \Delta Q_{MC}^+\} + \{\Delta W_{mag} + \Delta W_{irr}\} \quad = \quad \{\Delta Q_{MC}^+ + \Delta W_{mag}\} \qquad \text{eqn. 116}$$

$$\Delta U_{2a-3} = \{-\Delta Q_{irr} - \Delta Q_{MC}^+\} \qquad\qquad \text{eqn. 117}$$

Similarly the reverse magneto-caloric effect is defined as:

$$\Delta Q_{MC}^- = \begin{Bmatrix} (T_a - dT)S_{min} - T_a S_{max} \\ +(T_a - dT)S_{vel.max} - T_a S_{vel.T_a} \end{Bmatrix} \qquad \text{eqn. 118}$$

The heat associated with the cooling of the dipole-work is:

$$\Delta Q_{dw} = \begin{Bmatrix} -dT_{dw}S_{max} \\ -dT_{dw}S_{vel.dw} \end{Bmatrix} \qquad \text{eqn. 119}$$

The final steps are:

$$\Delta U_{3-4'(4a-1)} = \{\Delta Q_{MC}^- + \Delta Q_{dw} - \Delta W\} \qquad \text{eqn. 120}$$

$$\Delta U_{4'-1} = \{\Delta Q_{mech} - \Delta Q_{MC}^- - \Delta Q_{dw}\} \qquad \text{eqn. 121}$$

Taking the sum of the cycle:

$$\Delta U = \Delta U_{1-2a} + \Delta U_{2a-3} + \Delta U_{3-4'(4a-1)} + \Delta U_{4'-1} = 0$$

$$\Rightarrow \{\Delta Q_{MC}^+ + \Delta W_{mag}\} + \{-\Delta Q_{irr} - \Delta Q_{MC}^+\} + \{\Delta Q_{MC}^- + \Delta Q_{dw} - \Delta W\} + \{\Delta Q_{mech} - \Delta Q_{MC}^- - \Delta Q_{dw}\} = 0$$

The magneto-caloric portions cancel as the reversible cycle in section 1.1.

$$\{\Delta Q_{MC}^+ - \Delta Q_{MC}^+\} + \{\Delta Q_{MC}^- - \Delta Q_{MC}^-\} = 0$$

The input of heat energy from the mechanical system is equal to the quantity of heat associated with the dipole-work:

$$\{\Delta Q_{mech} - \Delta Q_{dw}\} = 0$$

Thus

$$\Rightarrow \Delta U = \{+\Delta Q_{dw} - \Delta Q_{irr}\} - \{\Delta W - \Delta W_{mag}\} = 0$$

The lower temperature swing comes from the magneto-caloric effect supplemented with dipole-work:

$$\Delta T = -\mu_0 \frac{T}{C_H} \left(\frac{\partial \mathcal{M}}{\partial T}\right)_H (\Delta H + K_e \Delta M) \qquad \text{(eqn. 20)}$$

If we neglect the term $\mu_0 \Delta H$ and ignore the magneto-caloric effect we arrive at the additional change in entropy solely from the dipole-work:

$$\Delta T_{dw} dS = \frac{T}{C_H} \left(\frac{\partial \mathcal{M}}{\partial T}\right)_H K_e \Delta M \cdot dS \qquad \text{eqn. 122}$$

Thus a quantity of heat ΔQ (positive) has flowed from the surrounds to the heat engine and write,

$$\Delta Q_{dw} = \Delta T_{dw} dS$$

$$\Rightarrow \Delta Q_{dw} = \frac{T}{C_H} \left(\frac{\partial \mathcal{M}}{\partial T}\right)_H \frac{1}{V} K_e \Delta \mathcal{M} \frac{dQ_{dw}}{dT}$$

$$\Rightarrow \Delta Q_{dw} \simeq \frac{1}{V} K_e \Delta \mathcal{M}(T) T \left(\frac{\mathcal{M}(T) - \mathcal{M}(0)}{T} \right)_H \quad \Rightarrow \quad \frac{1}{V} K_e \mathcal{M}(T) \Delta \mathcal{M}(T)$$

Or in differential quantities:

$$\Rightarrow \delta Q_{dw} = K_e M d\mathcal{M}$$

That is, a quantity of heat ΔQ_{dw} has entered the system from the mechanical reservoir (the fluid surrounding the magnetic cores) and been converted to useful work ΔW (the dipole-work) which leaves the system.

$$\Delta U_{magnetic} = \left(\Delta Q - \Delta Q_{dissipative} \right) - \left(\Delta W - \Delta W_{irreversible} \right) \quad = 0$$

$$\Rightarrow \Delta U_{magnetic} = \Delta Q_{net} - \left(\Delta W - \Delta W_{irreversible} \right) \quad = 0$$

If this heat isn't replenished then the reservoir around the magnetic cores will cool and hence the internal energy directly lowers since,

$$\Delta Q_{net} = -\Delta Q_{mechanical}$$

Then,

$$\text{if } \Delta U_{mechanical} = \left(\Delta Q_{external} - \Delta Q_{net} \right) - \Delta W_{mechanical} = C_H \Delta T_{mechanical} \quad = \quad 0$$

$$\text{and } \Delta W_{mechanical} = 0$$

$$\Rightarrow C_H \Delta T_{mechanical} = \Delta Q_{external} - \Delta W + \Delta W_{irrversible} \quad = \quad 0$$

Or in differential form with respect to time,

$$-C_H \frac{d}{dt} \left(T_{mechanical} \right) = \frac{d}{dt} \left(Q_{external} \right) - \frac{d}{dt} \left(W \right) + \frac{d}{dt} \left(W_{irreversible} \right) \quad = \quad 0 \qquad \text{eqn. 123}$$

Appendix 8. The Independent Flux Criterion and Slew-rate

In this appendix a de-rating function shall be derived that shows how, if the rate of turn-off of the magnetising field (the "slew-rate") is slow, in the limit the flux becomes dependent and there is no excess power production (fig. 65).
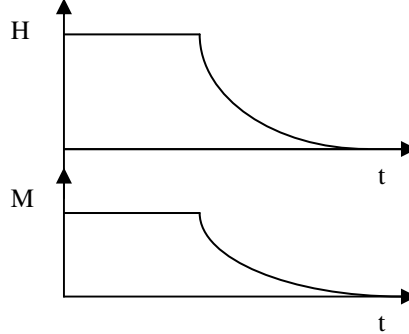
Figure 65 – Long slew-rate and the effect on ferrofluid decay
H is the magnetising field and M is the ferrofluid response

In the limit, the flux must just become dependent on the current and we'd have nothing more than an inductor; if the flux was "independent" we could generate excess power by shaft-work. Let us explore this by means of a contrary proof. Consider an inductor as some circuit element:

The net energy for a cycle is given by (where λ is the flux linkage):

$$\oint vi \, dt = -\oint \frac{d\lambda}{dt} i \, dt$$

eqn. 124

Integrating the RHS by parts:

$$\oint i(t) \frac{d\lambda(t)}{dt} dt = \left[i(t)\lambda(t) - \int \lambda(t) \frac{di(t)}{dt} dt \right]_{0^+}^{0^-}$$

eqn. 125

$$= i(0^-)\lambda(0^-) - i(0^+)\lambda(0^+) - F\left(\lambda(0^-), i(0^-)\right) + F\left(\lambda(0^+), i(0^+)\right)$$

Where F(..) is the integrand of the parts term. Now, since $i(0^+) = i(0^-)$ and $\lambda(0^+) = \lambda(0^-)$ the first two terms cancel.

Let a _dependent flux_ be represented by (where g is an arbitrary function):

$$i(t) \ = \ g\left(\lambda(t)\right)$$

eqn. 126

The second integral of eqn. 125 can be integrated by parts a second time by applying the chain rule:

$$\int \lambda(t) \frac{di(t)}{dt} dt = \int \lambda(t) \frac{dg\left(\lambda(t)\right)}{d\lambda(t)} \frac{d\lambda(t)}{dt} dt$$

eqn. 127

Thus:

$$\oint \lambda(t) \frac{dg\left(\lambda(t)\right)}{d\lambda(t)} d\lambda(t) = \left[\lambda(t) g\left(\lambda(t)\right) - \int g\left(\lambda(t)\right) \cdot 1 \cdot d\lambda(t) \right]_{0^+}^{0^-}$$

$$\Rightarrow G\left(\lambda(0^+)\right) - G\left(\lambda(0^-)\right) = 0$$

eqn. 128

The first term on the RHS cancels due to the flux being the same at the start and end of the cycle. The integrand on the RHS cancels for the same reason. The above result shows that a dependent flux (eqn. 126) cannot lead to net power. The proof sheds more light on the necessary condition for an independent flu*x: the flux is constant for any current including zero current* – it bares no relation to the modulations of the current. The proof also dispels any form of dependent relation, non-linear or even a delayed effect.

If equation 126 was $i(t) = g(\varphi(t-n))$ this could be expanded as a Taylor series about $g(\phi(t))$ but there would still be a relation, the flux would still be dependent. Thus it is a statement of the obvious (the First Law of Thermodynamics) that excess power production in an electrical circuit cannot happen by electrical means alone; flux changes must happen by some <u>outside agency</u> such as electro-mechanical shaft-work to cause energy transduction.

The basic operation in deriving a figure of merit for this process is to convolve the two responses of the field slewing and the impulse response of the ferrofluid. Shown below are the functions and their Laplace Transforms. We used for the exciter pulse a unit step (to set the initial conditions) followed after a time delay by a negative unit step and a decaying exponential.

$$M(t) = H(t) \otimes F_{impulse}(t)$$

U$_{-1}$ unit step
$$H(t) = u_{-1} - u_{-1}(t-t_D) + u_{-1}(t-t_D)e^{-\frac{t+t_D}{\tau_E}}$$

Laplace Transform
$$L\{H(t)\} = \frac{1}{s} + e^{-t_D s}\left(-\frac{1}{s} + \frac{1}{s + \frac{1}{\tau_E}}\right)$$

Impulse Response
Ferrofluid
$$F_{impulse}(t) = \frac{e^{-\frac{t}{\tau_F}}}{\tau_F}$$

Laplace Transform
$$L\{F_{impulse}(t)\} = \frac{1}{\tau_F\left(s + \frac{1}{\tau_F}\right)}$$

The solution contains terms for the switch on transient that we discard. The solution is below:

$$r(t) = \frac{\tau_F}{\tau_F - \tau_E}e^{-\frac{t}{\tau_F}} - \frac{\tau_E}{\tau_F - \tau_E}e^{-\frac{t}{\tau_E}}$$

$$\tau_F \gg \tau_E \Rightarrow r(t) \to e^{-\frac{t}{\tau_F}}$$

$$\tau_F \ll \tau_E \Rightarrow r(t) \to e^{-\frac{t}{\tau_E}}$$

eqn. 129

In the limit of infinite exciter slew rate ($\tau_F \gg \tau_E$) that the response is dominated by the ferrofluid $e^{-\frac{t}{\tau_F}}$ and the flux is <u>independent</u>. At the other limit of extremely slow exciter slew rate the flux is <u>dependent</u> $e^{-\frac{t}{\tau_E}}$ and there is no net power generation. Let us derive a power de-rating factor by taking the ratio of the energy from the decay of r(t) and hence M(t), against the ideal, independent flux case:

$$Power \propto \left(\frac{dr}{dt}\right)^2 \Rightarrow Energy \propto \int_0^\infty \dot{r}^2 dt$$

$$\Rightarrow Power \text{ De-rating Factor} = \frac{\int_0^\infty \dot{r}^2 dt}{\int_0^\infty \dot{r}_{IF}^2 dt}$$

Where r$_{if}$ is the maximum energy obtained when the flux is independent ($\tau_F \gg \tau_E$). Therefore,

$$Power \text{ De-rating Factor} = \frac{\tau_F}{\tau_F + \tau_E}$$

eqn. 130

Appendix 9. The Cancellation Method in the Frequency Domain

The process of making the chopped equivalent of the re-magnetising field by the current mirror is nothing more than modulation (akin to amplitude modulation) so using the trigonometric identity:

$$\sin A \cdot \sin B = \frac{1}{2}\cos(A-B) - \frac{1}{2}\cos(A+B)$$

The Fourier components of the chopping signal repeat at harmonic intervals of the basic chopping frequency and these multiply with the baseband signal to yield "sum and difference sidebands" around the harmonic intervals.
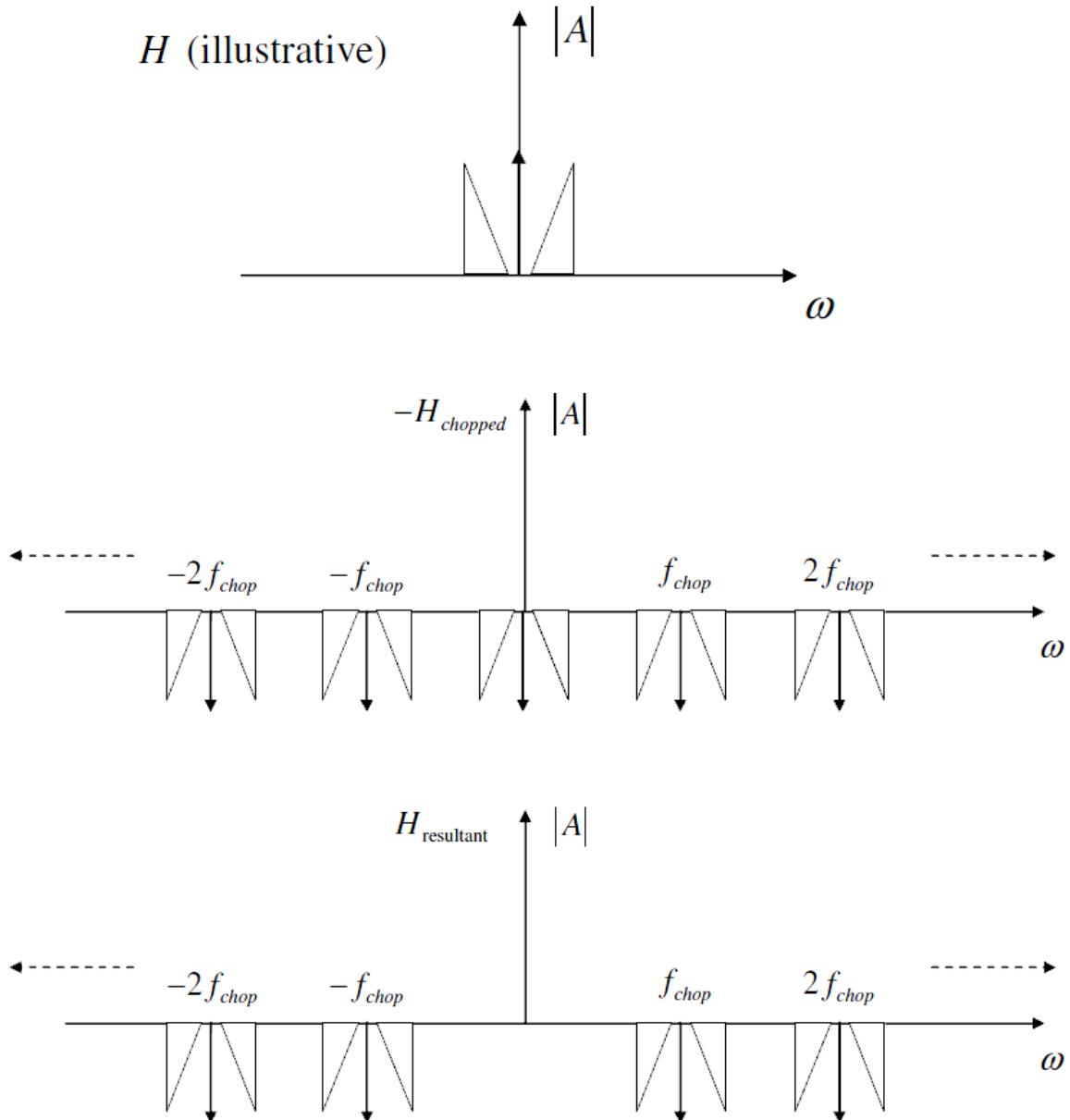
Figure 66 – Fourier Transforms for the H-field cancellation technique

© Remi Cornwall 2013

We can now see the effect of the high-pass capacitor on the LHS and the high-frequency "choke" on the RHS.
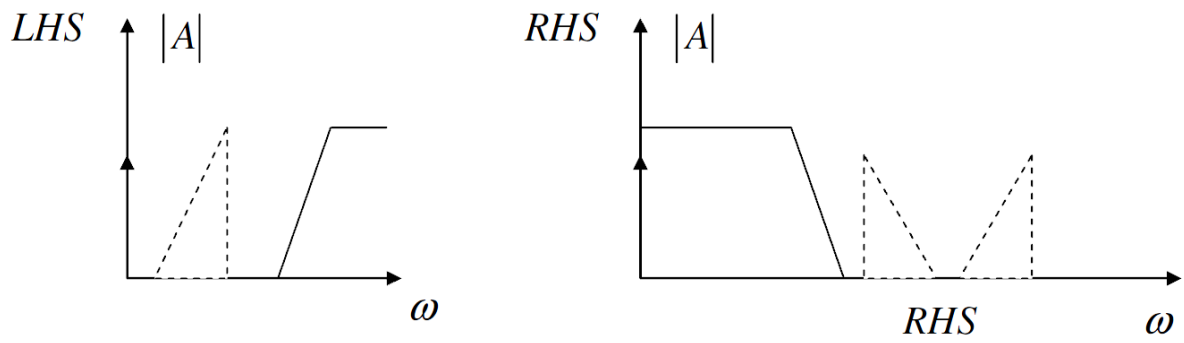
Figure 67 – The filtering effect of the capacitor on the LHS and the inductor on the RHS

Appendix 10. Simulation code

```matlab
function electro_thermo_Cancel()
% Simulates complete electo-thermo model for field on, field off, then
% temporary remenance and dipole-work with remagnetisation field
% cancellation method
% Written on MatLab v.7.10.0.499 (R2010a)
%
    global CONST_MU_0     % Permeability free space
    global CONST_Area
    global CONST_Length
    global CONST_Nturns
    global CONST_kBoltz   % Boltzman's constant
    global CONST_Ms       % Saturation magnetisation at 0K
    global CONST_mom      % magnetic moment of particle
    global CONST_Tneel    % Neel frequency constant
    global CONST_Kcryst   % Crystaline anisotropy constant
    global CONST_Vff      % Single domain particle size
    global CONST_perm     % Permeability

    % Global simulation parameters
    CONST_MU_0 = 4.*pi.*1e-7;
    CONST_Area = 0.01;
    CONST_Length = 0.5;
    CONST_Nturns = 80;
    CONST_kBoltz = 1.38e-23;
    CONST_Ms = 24000; % A/M or about 300 gauss
    CONST_mom = 1e-25; % J per A/M so sat. at about 0.1T at 290K tanh(uH/kT)
    CONST_Tneel = 1e-9; % 10^-9 s
    CONST_Kcryst = 60e3; % 60kJ/m^3 is typical for Co ferrite
    CONST_Vff = 1.1213e-024; % setup to give tor about 20ms radius about 10nm
    CONST_perm = 50;

    Ti = 290; % Initial temperature 290K

    [h1 h2 h3 h4] = setup_windows();

    % Returns total energy from source and resistive energy loss,
    % called with initial temperature and handle to output window
    % Plots graphs into figure h3
    [IM MM TM Emag Etot ERloss tsim] = H_field_on(Ti, h3);

    % Keeps running total of energy loss whilst switching off
    % magnetising field, this energy finally dumped into the resistor is
    % ERloss
    [IF MF Tf Emagrem] = H_field_off(IM, MM, TM, tsim, Emag, h3);

    Do_sims(IF, MF, Tf, Emag, h1, h2);

    % Numerical value in middle of call is the over-unity figure we wish to
    % achieve
    Do_sim_cancel(IF, MF, Tf, h1, h4);
    free_windows([h1 h2 h3 h4]);
end

function [h1 h2 h3 h4] = setup_windows()
    % Setup some graph output windows
    h1 = findobj('Name', 'Energy vs 1/R');
    if isempty(h1)
        h1 = figure();
        set(h1, 'Name', 'Energy vs 1/R');
        xlabel('Resistance');
        ylabel('Energy');
    end
    h2 = findobj('Name', 'Current and Magnetisation vs time');
    if isempty(h2)
        h2 = figure();
        set(h2, 'Name', 'Current and Magnetisation vs time');
    end

    h3 = findobj('Name', 'Switch on Current/Mag vs time');
    if isempty(h3)
        h3 = figure();
        set(h3, 'Name', 'Switch on Current/Mag vs time');
    end
```

```matlab
    h4 = findobj('Name', 'Cancellation method Current and Magnetisation vs time');
    if isempty(h4)
        h4 = figure();
        set(h4, 'Name', 'Cancellation method Current and Magnetisation vs time');
    end

end

function free_windows(han)

    for i = 1:numel(han)
        figure(han(i));
        hold off;
    end
end

function [If Mf Tf Emag Etot ERloss tsim] = H_field_on(Ti, h3)
    % Inputs:-
    % Initial temperature, graphics handle
    % Outputs:-
    % If final current, Mf final magnetisation, Tf final temp
    % Magnetisation Work
    % Total energy taken from power source
    % Energy in resistive losses
    % Simulation time
    global CONST_Area
    global CONST_Length
    global CONST_perm
    %####################################################################
    % Magnetising code
    %
    % H FIELD ON
    %####################################################################


    % Simulate input: time, I0, M0, T0, Rsupply, Vsupply,
    % Time: 0.02s
    % Ii: 0, initial current
    % Mi: 0, initial magnetisation
    % Ti: initial temperature
    % Rsupply: 0.1 Ohms
    % Vsupply: 60V

    sfilename = sprintf(...
        'SIM_DATA/electro_thermo_linear_data_field_ON_MU%0.3g.mat', ...
                CONST_perm);
    try
        % if we've done the simulation before, the data might exist
        % in the current directory
        load(sfilename);

    catch ME % if no data, run the simulation
        [t y] = Simulate_Linear(0:5e-4:0.02, 0, 0, Ti, 1e-1, 0.60, ...
            'electro-thermo.m busy, magnetisation step, H-field on step');

        % Now save the data if no data has been saved before
        warning('off', 'MATLAB:MKDIR:DirectoryExists');
        mkdir('SIM_DATA');
        warning('on', 'MATLAB:MKDIR:DirectoryExists');
        try
            save(sfilename, 't', 'y');
        catch ME
            disp('Cannot save');
            disp(sfilename);
        end
    end
    % Simulate output:-
    % y(1) = current
    % y(2) = flux from M
    % y(3) = specf. magnetising work = mu0*mu*HdM (total specf. work = HdB)
    % y(4) = total work by power source
    % y(5) = work lost in resistance
    % y(6) = temperature

    % Int HdM.V
```

```matlab
    Emag = y(end,3).*CONST_Area.*CONST_Length;

    % y(4) = total work by power source
    Etot = y(end,4);

    % y(5) = ohmic losses in resistance (battery, switches and wires)
    ERloss = y(end, 5);

    % Carry forward previous simulation results to the next sim
    % Let the H-field decay, ie switch off magnetising current
    If = y(end, 1);
    Mf = y(end, 2);
    Tf = y(end, 6);
    tsim = t(end);

    figure(h3);
    clf;
    title('Switch on Current and Magnetisation vs. time');
    subplot(2, 1, 1);
    plot(t, y(:,1) ); % Current
    xlabel('time(s)');
    ylabel('Current(A)');

    figure(h3);
    subplot(2, 1, 2);
    plot(t, y(:,2) ); % Magnetisation
    xlabel('time(s)');
    ylabel('Mag (A/M)');

    s = sprintf(...
        '\n\nSwitch on magnetising field\n~~~~~~~~~~~~~~~~~~~~~~~~~~~~~\n');
    disp(s)
    %s = sprintf('Initial temperature %0.5g K\n', Ti);
    %disp(s)
    %s = sprintf('Final temperature %0.5g K\n', Tf);
    %disp(s)
    s = sprintf('Total energy %0.5g J\n', Etot);
    disp(s)
    s = sprintf('Magnetisation work Int(mu0.mu.HdM.V) %0.5g J\n', Emag);
    disp(s)
    s = sprintf('I^2R loss %0.5g J\n', ERloss);
    disp(s)
    %Effloss = Etot - ERloss - Emag;
    %s = sprintf('Ferrofluid loss %0.5g J\n', Effloss);
    %disp(s)
    s = sprintf('Current %0.5g A\n', If);
    disp(s)
    s = sprintf('Magnetisation %0.5g A/M\n\n', Mf);
    disp(s)

end

function [If Mf Tf Emagrem] = H_field_off(Ii, Mi, Ti, tend, Emag, h3)
    global CONST_Area
    global CONST_Length
    global CONST_perm
    %#################################################################
    % De-magnetising code
    %
    % H FIELD OFF
    %#################################################################
    % Carry forward previous simulation results to this sim
    % Let the H-field decay, ie switch off magnetising current
    % Inputs:-
    % Ii, Mi, Ti
    % time end of last sim, tend
    % Outputs:-
    % Current, magnetisation, temperature,
    %  Energy dumped in load resistance, magnetic work

    % Model switch off of H-field leaving magnetisation in ferrofluid
    % Ii initial current
    % Mi initial magnetisation
    % Ti: initial temperature
    % time = 0.3ms, Ii, Mi, Ti, Rdump = 500, Vsupply = 0,
    % y(1) = current
    % y(2) = flux from M
```

```matlab
    % y(3) = specf. magnetising work = mu0*mu*HdM (total specf. work = HdB)
    % y(4) = total work by power source
    % y(5) = work lost in resistance
    % y(6) = temperature

    sfilename = sprintf(...
        'SIM_DATA/electro_thermo_linear_data_field_OFF_MU%0.3g.mat', ...
            CONST_perm);
    try
        % if we've done the simulation before, the data might exist
        % in the current directory
        load(sfilename);

    catch ME % if no data, run the simulation
        [t y] = Simulate_Linear(tend + (0:3e-6:0.3e-4), Ii, Mi, Ti, ...
                500, 0, 'electro-thermo.m busy, H-field off step');

        % Now save the data if no data has been saved before
        warning('off', 'MATLAB:MKDIR:DirectoryExists');
        mkdir('SIM_DATA');
        warning('on', 'MATLAB:MKDIR:DirectoryExists');
        try
            save(sfilename, 't', 'y');
        catch ME
            disp('Cannot save');
            disp(sfilename);
        end
    end

    % Carry forward previous simulation results to the next sim
    % in these output variables
    If = y(end, 1);
    Mf = y(end, 2);
    Tf = y(end, 6);

    % Calculate change in magentic energy of sample as field drops a bit
    Eh = y(end, 3).*CONST_Area.*CONST_Length;

    % Calculate energy dumped into dump resistor on switch off and other
    % loses - magnetisation drops a bit in switch off and this is
    % disapated in the ferrofluid
    % y(5) = work lost in resistance
    ERloss = y(end,5);

    figure(h3);
    subplot(2, 1, 1);
    hold on
    plot(t, y(:,1) );
    xlabel('time(s)');
    ylabel('Current(A)');

    figure(h3);
    subplot(2, 1, 2);
    hold on
    plot(t, y(:,2) );
    xlabel('time(s)');
    ylabel('Magnetisation(A/M)');
    hold off

    s = sprintf(...
        '\n\nSwitch off magnetising field\n~~~~~~~~~~~~~~~~~~~~~~~~~~~~~\n');
    disp(s)
    s = sprintf('H field energy returned %0.5g J\n', ERloss);
    disp(s)
    %s = sprintf('Magnetisation energy change %0.5g J\n', Eh);
    %disp(s)
    Emagrem = Emag + Eh;
    %s = sprintf('Magnetisation energy of remnant flux %0.5g J\n', Emagrem);
    %disp(s)
    s = sprintf('Residual current %0.5g A\n', If);
    disp(s)
    s = sprintf('Residual magnetisation %0.5g A/M\n', Mf);
    disp(s)
    %s = sprintf('Final temperature %0.5g K\n', Tf);
    %disp(s)
end
```

```matlab
function Do_sims(Ii, Mi, Ti, Emagff, h1, h2)
    %################################################################
    % Power output code
    %################################################################
    global CONST_perm

    R = [   1e-4 2e-4 5e-4 ...
            1e-3 2e-3 5e-3 ...
            1e-2 2e-2 5e-2 ...
            0.1 0.2 0.5 ...
            1 2 5 ...
            10 20 50 ...
            100 200 500 ...
            1e3 2e3 5e3 ...
            1e4];

    Time = logspace(-4, 4, 150);

    Energy = zeros(1, numel(R));

    for i = 1:numel(R)
        % Model independent flux collapse into electrical load
        % initial current
        % initial magnetisation
        % initial temperature
        % time = 100s, Ii, Mi, Ti, R, Vsupply = 0,
        % Simulate output:-
        % y(1) = current
        % y(2) = flux from M
        % y(3) = specf. mag work = mu0*mu*HdM (total specf. work = HdB)
        % y(4) = total work by power source
        % y(5) = work lost in resistance
        % y(6) = temperature

        sfilename = sprintf(...
    'SIM_DATA/electro_thermo_linear_data_field_MU%0.3g_SIM%0.2g.mat', ...
            CONST_perm, R(i));
        try
            % if we've done the simulation before, the data might exist
            % in the current directory
            load(sfilename);

        catch ME % if no data, run the simulation
            s = sprintf('electro-thermo.m busy, R = %0.2g', R(i));
            [t y] = Simulate_Linear(Time, Ii, Mi, Ti, R(i), 0, s);

            % Now save the data if no data has been saved before
            warning('off', 'MATLAB:MKDIR:DirectoryExists');
            mkdir('SIM_DATA');
            warning('on', 'MATLAB:MKDIR:DirectoryExists');
            try
                save(sfilename, 't', 'y');
            catch ME
                disp('Cannot save');
                disp(sfilename);
            end
        end

        Energy(i) = y(end,5);

        % Plot graphs of Current vs. time, Magnetisation vs. time
        plot_graphs(h2, t, y, R, i);
    end

    % Plot energy output vs. resistance
    figure(h1);
    clf;
    loglog(1./R, Energy, '-b');
    hold on;
    loglog(1./R, Emagff.*ones(size(R)), '-r');
end

function Do_sim_cancel(Ii, Mi, Ti, h1, h4)
    %################################################################
    % Power output code with field cancellation method
    %################################################################
```

```matlab
    % Carry forward previous simulation results (from H_field_off) to this
    % routine in Ii Mi Ti: Current, Magnetisation, Temperature respectively
    %
    % h1 is pre-existing Energy vs. 1/R graph
    % h4 is new current and magnetisation vs. time graph

    R = [   1e-4 2e-4 5e-4 ...
            1e-3 2e-3 5e-3 ...
            1e-2 2e-2 5e-2 ...
            0.1 0.2 0.5 ...
            1 2 5 ...
            10 20 50 ...
            100 200 500 ...
            1e3 2e3 5e3 ...
            1e4];

    s = sprintf(...
        '\n\nDipole-work with remag field cancellation calculation\n\n');
    disp(s)

    s = sprintf('electro-thermo.m busy, remag cancel step');
    Time = logspace(-4, 4, 100);

    Energy = zeros(1, numel(R));

    for i = 1:numel(R)
        % Model independent flux collapse into electrical load
        % initial current
        % initial magnetisation
        % initial temperature
        % time = 100s, Ii, Mi, Ti, R, Vsupply = 0,
        % Simulate output:-
        % y(1) = current
        % y(2) = flux from M
        % y(3) = specf. mag work = mu0*mu*HdM (total specf. work = HdB)
        % y(4) = total work by power source
        % y(5) = work lost in resistance
        % y(6) = temperature

        [t y] = Simulate_Cancel(Time, Ii, Mi, Ti, R(i), s);
        Energy(i) = y(end,5);

        % Plot graphs of Current vs. time, Magnetisation vs. time
        plot_graphs(h4, t, y, R, i);
    end

    % On pre-existing E vs. 1/R graph plot the new output energy
    figure(h1);
    hold on;
    s = [ sprintf('Magnetisation energy (red)\n') ...
        sprintf(...
 'Dipole-work vs. 1/R: R = %0.2g to %0.2g (blue)', R(1), R(end)) ...
        sprintf('\nDipole-work (green)\n') ...
        sprintf('   with re-magnetisation term knocked out') ];

    title(s);
    xlabel('1/R (S)');
    ylabel('Energy (J)');
    loglog(1./R, Energy, '-g');

end

function plot_graphs(h2, t, y, R, i)
    % y(1) = current
    % y(2) = flux from M
    Rpick = [1e-4, 1e-2, 1e0, 1e2, 1e4];

    figure(h2);

    j = find(Rpick >= R(i));
        if numel(j) > 0

            % Plot magnetisation
            subplot(2, 6, j(1)+6 );
            plot(t, y(:,2) );
            xlabel('time(s)');
            ylabel('Magnetisation(A/M)');
```

```matlab
                try
                    max_m = y(1,2); % find maximum mag to scale nicely
                    ind_m = find(y(:,2) < 0.1*max_m);
                    axis( [ 0 t(ind_m(1)) 0 1.05.*max_m ] );
                catch ME
                    disp(' ');
                    disp('My autoscale code has failed, not clever enough');
                    disp('Use plottools to manually scale');
                    disp(' ');
                end
                % Plot current
                subplot(2, 6, j(1) );
                plot(t, y(:,1) );
                s = sprintf('R = %0.2g\n', R(i));
                title(s);
                xlabel('time(s)');
                ylabel('Current(A)');

                try
                    max_i = max(y(:,1)); % find maximum current to scale nicely
                    ind_i = find(y(:,1) >= max_i);

                    % scale x-axis
                    ind_i2 = find( y(ind_i:end, 1) < 0.1*max_i, ind_i);
                    if ind_i < 5
                        axis( [ 0 t(ind_m(1)) 0 1.05.*y(ind_i(end),1) ] );
                    elseif numel(ind_i2) > 1
                        axis( [ 0 t(ind_i + ind_i2(1) ) ...
                                0 1.05.*y(ind_i(end),1) ] );
                    else
                        axis( [ 0 100 0 1.05.*y(ind_i(end),1) ] );
                    end
                catch ME
                    disp(' ');
                    disp('My autoscale code has failed, not clever enough');
                    disp('Use plottools to manually scale');
                    disp(' ');
                end
            end
            %{
            figure(h2);
            hold  on;
                title([...
        sprintf('\nLINEAR DIPOLE-WORK current and magnetisation traces\n')...
                    '    at various resistances']);
            %}
    end

function [t y] = Simulate_Linear(Time, Ii, Mi, Ti, R, Volt, mesg)

    global CONST_MU_0      % Permeability free space
    global CONST_Area
    global CONST_Length
    global CONST_Nturns
    global CONST_kBoltz    % Boltzman's constant
    global CONST_Ms        % Saturation magnetisation at 0K
    global CONST_mom       % magnetic moment of particle
    global CONST_Tneel     % Neel frequency constant
    global CONST_Kcryst    % Crystaline anisotropy constant
    global CONST_Vff       % Single domain particle size
    global CONST_perm      % Permeability

    persistent handle_wb
    persistent ind
    % y(1) = current
    % y(2) = flux from M
    % y(3) = specf. mag work = mu0*mu*HdM (total specf. work = HdB)
    % y(4) = total work by power source
    % y(5) = work lost in resistance
    % y(6) = temperature

    handle_wb = waitbar(0, ' ');
    ind = 1;
    sizeTimeArray = size(Time, 2);
    waitbar(0, handle_wb, mesg);
```

```matlab
    y0 = [Ii Mi 0 0 0 Ti];
    options = odeset('RelTol',1e-6,'AbsTol',1e-6);
    [t y] = ode23s(@flux_lin, Time, y0, options);
    close(handle_wb);

    % nested function 1
    function do_wait_bar(t)
        if (t > Time(ind)) && (ind <= sizeTimeArray)
            waitbar(log(t./Time(1))./ log(Time(end)./Time(1)), ...
                        handle_wb );
            ind = ind + 1;
        end
    end

    % Nested function 2
    function dy = flux_lin(t, y)

        do_wait_bar(t);

        T = y(6);
        Curr = y(1);
        M = y(2);
        H = Curr.*CONST_Nturns./CONST_Length;
        fac = 1 - (M./CONST_Ms).^2; % common factor to do with saturation

        % susceptibility, about 0.6 with params at 290K
        Xchi = CONST_Ms.*CONST_mom./CONST_kBoltz./T;
        % time constant about 0.02 with params at 290K
        tor = CONST_Tneel .* exp(CONST_Kcryst.*CONST_Vff./CONST_kBoltz./T);

        dy = [0; 0; 0; 0; 0;];

        fac2 = (1./tor) .* fac .* ( M - H.*Xchi.*CONST_perm );
        fac3 = fac2 - ( Curr.*R - Volt)...
                            ./CONST_MU_0./CONST_perm ...
                            ./CONST_Nturns./CONST_Area;

        dy(1) = (CONST_Length./CONST_Nturns) .* fac3;

        dy(2) = -fac2;

        % dB = mu0*perm*(dM + dH)
        %dB = CONST_MU_0.*CONST_perm.*(dy(2) + fac3);
        %dy(3) = H.*dB;

        % Total specific magnetic work = HdB = H*mu0*mu*(dM+dH)
        % We want specific magnetising work mu0*mu*HdM
        dy(3) = H.*CONST_MU_0.*CONST_perm.*dy(2);

        dy(4) = Curr .* Volt;

        dy(5) = Curr.^2 .* R; % I^2R

        dy(6) = 0; % temperature change
    end
end


function [t y] = Simulate_Cancel(Time, Ii, Mi, Ti, R, mesg)

    global CONST_MU_0      % Permeability free space
    global CONST_Area
    global CONST_Length
    global CONST_Nturns
    global CONST_kBoltz    % Boltzman's constant
    global CONST_Ms        % Saturation magnetisation at 0K
    global CONST_mom       % magnetic moment of particle
    global CONST_Tneel     % Neel frequency constant
    global CONST_Kcryst    % Crystaline anisotropy constant
    global CONST_Vff       % Single domain particle size
    global CONST_perm      % Permeability

    persistent handle_wb
    persistent ind
    % y(1) = current
    % y(2) = flux from M
    % y(3) = specf. mag work = mu0*mu*HdM (total specf. work = HdB)
```

© Remi Cornwall 2013

```matlab
% y(4) = total work by power source
% y(5) = work lost in resistance
% y(6) = temperature

handle_wb = waitbar(0, ' ');
ind = 1;
sizeTimeArray = size(Time, 2);
waitbar(0, handle_wb, mesg);

y0 = [Ii Mi 0 0 0 Ti];
options = odeset('RelTol',1e-6,'AbsTol',1e-6);
[t y] = ode23s(@flux_cancel, Time, y0, options);
close(handle_wb);

% nested function 1
function do_wait_bar(t)
    if (t > Time(ind)) && (ind <= sizeTimeArray)
        waitbar(log(t./Time(1))./ log(Time(end)./Time(1)), ...
                    handle_wb );
        ind = ind + 1;
    end
end

% Nested function 2
function dy = flux_cancel(t, y)

    do_wait_bar(t);

    T = y(6);
    Curr = y(1);
    M = y(2);
    H = Curr.*CONST_Nturns./CONST_Length;
    fac = 1 - (M./CONST_Ms).^2; % common factor to do with saturation

    % susceptibility, about 0.6 with params at 290K
    Xchi = CONST_Ms.*CONST_mom./CONST_kBoltz./T;
    % time constant about 0.02 with params at 290K
    tor = CONST_Tneel .* exp(CONST_Kcryst.*CONST_Vff./CONST_kBoltz./T);

    dy = [0; 0; 0; 0; 0;];

    %#########################################################
    % Knock out re-magnetising term with 0.*H
    % to simulate a superimposed high frequency signal with
    % a low frequency component that cancels the low frequency
    % remagnetising term. Real ferrofluid will have no
    % dissipation at high frequency and is "transparent".
    % Also the power output circuit can have a low frequency
    % series choke to stop the bias signal being wasted in the
    % output circuit via transformer action.
    %
    % Another possibility is to use a non-linear permeability
    % with a high frequency bias once again such that Perm(i,t)
    % and can be made to drop advantageously on the power
    % output phase to effectively knock out the re-magnetising
    % term again without affecting the second power induction
    % equation. The same considerations on the ferrofluid not
    % responding to high frequencies signals and the choke
    % in the power output circuit applies.
    %#########################################################
    dMdt = (1./tor) .* fac .* ( M - 0.*H.*Xchi.*CONST_perm );
    fac3 = dMdt - ( Curr.*R )...
                    ./CONST_MU_0./CONST_perm ...
                    ./CONST_Nturns./CONST_Area;

    dy(1) = (CONST_Length./CONST_Nturns) .* fac3;

    dy(2) = -fac2;

    % dB = mu0*perm*(dM + dH)
    %dB = CONST_MU_0.*CONST_perm.*(dy(2) + fac3);
    %dy(3) = H.*dB;

    % Total specific magnetic work = HdB = H*mu0*mu*(dM+dH)
    % We want specific magnetising work mu0*mu*HdM
    dy(3) = H.*CONST_MU_0.*CONST_perm.*dy(2);
```

```
    %dy(4) = Curr .* Volt;

    dy(5) = Curr.^2 .* R; % I^2R

    dy(6) = 0; % temperature change
end

end
```

The cancellation method can be implemented physically with a high frequency varying field rather than zeroing the H-field as in the code above, viz. dMdt = … (M - 0.*H.*Xchi.*CONST_perm); Though the code will run very slowly to cater for the wide differences in time scale of the cancellation field and the circuit dynamics; notably in the first code in function "Do_sim_cancel" the time array was logarithmic:

Time = logspace(-4, 4, 100);

And in the second version, it has to be a linear time array:

Time = linspace(0, 5, 2e5);

But the point is proven. The code is below.

```
function dy = flux_cancel(t, y)

    do_wait_bar(t);

    T = y(6);
    Curr = y(1);
    M = y(2);
    H = Curr.*CONST_Nturns./CONST_Length;
    fac = 1 - (M./CONST_Ms).^2; % common factor to do with saturation

    % susceptibility, about 0.6 with params at 290K
    Xchi = CONST_Ms.*CONST_mom./CONST_kBoltz./T;
    % time constant about 0.02 with params at 290K
    tor = CONST_Tneel .* exp(CONST_Kcryst.*CONST_Vff./CONST_kBoltz./T);

    % common factor made up of Lchoke + Lcoil and Lchoke set up
    % to have similar time constant Lchoke/R to 1*tor
    Lfac = 0.*R.*tor + CONST_MU_0.* CONST_perm .* CONST_Area...
                .* CONST_Nturns.^2 ...
                ./ CONST_Length;

    dy = [0; 0; 0; 0; 0;];

    %#########################################################
    %
    % Add on high frequency cancellation field
    %
    %#########################################################
    dMdt = -(1./tor) .* fac .* ( M - H.*(1-Cancel(t)) ...
        .*Xchi.*CONST_perm);

    dy(1) = ((-CONST_MU_0.* CONST_perm .* CONST_Area ...
                .* CONST_Nturns).*dMdt ...
                    -( Curr.*R )) ./Lfac;

    dy(2) = dMdt;

    % dB = mu0*perm*(dM + dH)
    %dy(3) = H.*dB;

    % Total specific magnetic work = HdB = H*mu0*mu*(dM+dH)
    % We want specific magnetising work mu0*mu*HdM
    dy(3) = H.*CONST_MU_0.*CONST_perm.*dy(2);

    %dy(4) = Curr .* Volt;

    dy(5) = Curr.^2 .* R; % I^2R
```

```matlab
        dy(6) = 0; % temperature change
    end


    % Nested function 3
    function field = Cancel(t)
        % Generate square waveform 0-1.5 at frequency "freq"
        freq = 20000; % freq = 100/tor;

        field = 2.0.*(0.5+0.5.*sign(0.5+freq.*t-round(freq.*t+0.5)));
    end

end
```

References

1.   Rosensweig R. E., Resler E.L., *Magnetocaloric Power*. AIAA J., 1964. **2**(8): p. 1418-22.

2.   Rosensweig, R.E., *Ferrohydrodynamics*. Cambridge University Press. 1998.

3.   Gschneidner, K.A., Jr.; Pecharsky, V. K., *Recent developments in magnetocaloric materials*. IOP Reports on Progress in Physics, 2005. **68**(6): p. 1479–1539.

4.   Jackson, J.D., *Classical Electrodynamics*. 2nd ed. 1975: Wiley.

5.   Landau, L., *A Course in Theoretical Physics: Classical Theory of Fields*. Vol. Vol. 2 1982: Butterworth-Heinemann.

6.   Feynman, L., Sands, *The Feynman Lectures on Physics*. Addison-Wesley, Reading, Massachusetts. Vol. Vol.1, Vol. 2 1989. 14.7, 15.1-6, 35.4

7.   J. Romero Gómez, R.Ferreiro.G., A. De Miguel Catoira, M. Romero Gómez, *Magnetocalorific effect: A review of the thermodynamic cycles in magnetic refrigeration.* Renewable and Sustainable Energy Reviews, 2013. **17**: p. 74-82.

8.   Potter M. C., Somerton.C.W., *Thermodynamics for Engineers*. Schaum's Outlines, McGraw-Hill. 1993.

9.   Bozorth, R.M., *Ferromagnetism*. IEEE Press 1978.

10.   Landau, L., *A Course in Theoretical Physics: Statistical Physics*. Vol. Vol. 5. 1996: Butterworth Heinemann.

11.   Rosensweig R. E., Resler E.L., *Regenerative thermomagnetic power.* J. Eng. Power, 1967. **89**: p. 399-406.

12.   Vallejo-Fernandez, O'Grady, Patel, *Mechanisms of hyperthermia in magnetic nanoparticles.* J. Phys. D: Appl. Phys., 2013. **46**.

13.   Fannin, P.C., *A Study of the Complex Susceptibility of Ferrofluids and Rotational Brownian Motion.* Journal of Magnetism and Magnetic Materials, 1987. **65**: p. 279-281

14.   Fannin, P.C., *On the Analysis of Complex Susceptibility Data of Ferrofluids.* Journal of Physics D: Applied Physics, 1988. **21**: p. 1035-1036

15.   Cornwall, R., *A method of generating electricity and refrigeration*, in *Patent US 6725668, CN 00806421 etc*. 1999.

16.   Landau, L., *A Course in Theoretical Physics: Mechanics*. Vol. Vol. 1. 1982: Butterworth Heinemann.

17.   Kittel C., Kroemer H., *Thermal Physics*. W. H. Freeman and Company, San Francisco. Vol. 2nd ed. 1980.

18.   Horowitz P., Hill W., *The Art of Electronics*. Cambridge University Press. 1989.

19.   Nilsson, James W., *Introduction to PSpice for Electric Circuits*. Prentice Hall 2008.

20.   Aharoni, A., *Introduction to the Theory of Ferromagnetism*. Oxford Science Publications 1996.

21.   Landau, L., *A Course in Theoretical Physics: Electrodynamics of Medias*. Vol. Vol. 8. 1984: Butterworth-Heinemann.

22.   SusTech, *Technical report on susceptibility measurement of ferrofluids*. GmbH & Co. KG Darmstadt, Petersenstr. 20, 64287 Darmstadt, Germany.

23.   Kreyzig, E., *Advanced Engineering Mathematics*. Wiley Interscience. 2000.